KOVINE ZLITINE TEHNOLOGIJE

METALS ALLOYS TECHNOLOGIES

LETO 1995 / 3-4

SELECTED PAPERS PRESENTED AT THE SLOVENIAN – HUNGARIAN – CROATIAN – AUSTRIAN
6 JOINT VACUUM CONFERENCE AND 3 MEETING OF THE SLOVENIAN AND CROATIAN VACUUMOLOGISTS

BLED 4–7 APRIL 1995

GUEST EDITORS: F. VODOPIVEC AND M. JENKO

PART II

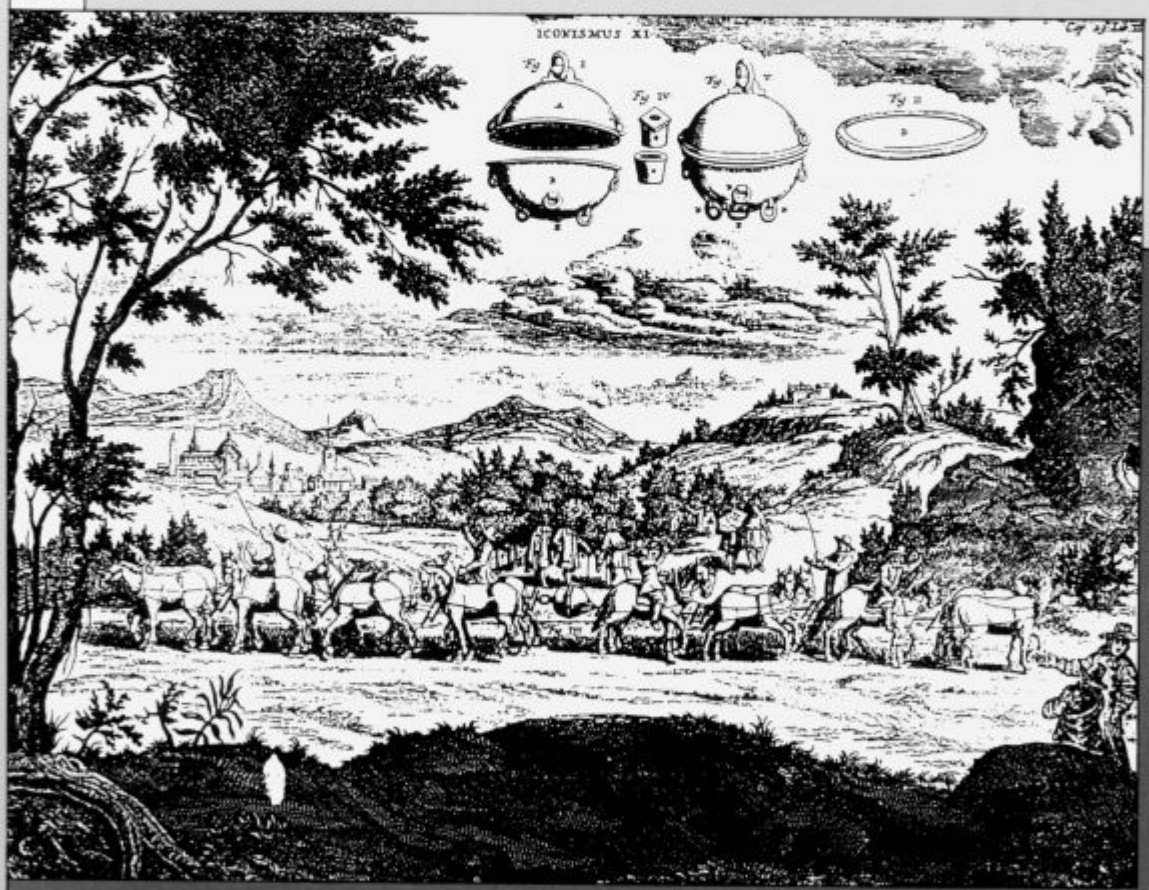

KOVINE ZLITINE TEHNOLOGIJE | LETNIK VOLUME 29 | ŠTEV. NO. 3-4 | STR. P. 361-432 | LJUBLJANA SLOVENIJA | JUL.-SEPT. 1995 | ISSN 1318-0010

Navodilo avtorjem

Prosimo avtorje, da pri pripravi rokopisa za objavo članka dosledno upoštevajo naslednja navodila:
- Članek mora biti izvirno delo, ki ni bilo v dani obliki še nikjer objavljeno. Deli članka so lahko že bili podani kot referat.
- Avtor naj odda članek oz. besedilo napisano na računalnik z urejevalniki besedil:
- WORDSTAR, verzija 4, 5, 6, 7 za DOS
- WORD za DOS ali WINDOWS.

Če avtor besedila ne more dostaviti v prej naštetih oblikah, naj pošlje besedilo urejeno v ASCII formatu.
Prosimo avtorje, da pošljejo disketo z oznako datoteke in računalniškim izpisom te datoteke na papirju. Formule so lahko v datoteki samo naznačene, na izpisu pa ročno izpisane.

Celoten rokopis članka obsega:
- naslov članka (v slovenskem in angleškem jeziku),
- podatke o avtorju,
- povzetek (v slovenskem in angleškem jeziku),
- ključne besede (v slovenskem in angleškem jeziku),
- besedilo članka,
- preglednice, tabele,
- slike (risbe ali fotografije),
- podpise k slikam (v slovenskem in angleškem jeziku),
- pregled literature.

Članek naj bi bil čim krajši in naj ne bi presegal 5–7 tiskanih strani, pregledni članek 12 strani, prispevek s posvetovanj pa 3–5 tiskanih strani.

Obvezna je raba merskih enot, ki jih določa zakon o merskih enotah in merilih, tj. enot mednarodnega sistema SI.

Enačbe se označujejo ob desni strani besedila s tekočo številko v okroglih oklepajih.

Preglednice (tabele) je treba napisati na posebnih listih in ne med besedilom.
V preglednicah naj se – kjer je le mogoče – ne uporabljajo izpisana imena veličin, ampak ustrezni simboli.

Slike (risbe ali fotografije) morajo biti priložene posebej in ne vstavljene (ali nalepljene) med besedilom. Risbe naj bodo izdelane praviloma povečane v merilu 2:1.
Za vse slike po fotografskih posnetkih je potrebno priložiti izvirne fotografije, ki so ostre, kontrastne in primerno velike.

Vsi podpisi k slikam (v slovenskem in angleškem jeziku) naj bodo zbrani na posebnem listu in ne med besedilom.

V pregledu literature naj bo vsak vir oštevilčen s tekočo številko v oglatih oklepajih (ki jih uporabljamo tudi med besedilom, kadar se želimo sklicevati na določeni literarni vir).

Vsak vir mora biti opremljen s podatki, ki omogočajo bralcu, da ga lahko poišče:
knjige: – avtor, naslov knjige, ime založbe in kraj ter leto izdaje (po potrebi tudi določene strani):
H. Ibach and H. Luth, Solid State Physics, Springer, Berlin 1991, p. 245
članki: – avtor, naslov članka, ime revije in kraj izhajanja, letnik, leto, številka ter strani:
H. J. Grabke, Kovine zlitine tehnologije, 27, (1993) 1–2, 9

Avtorji naj rokopisu članka priložijo povzetek v omejenem obsegu do 10 vrstic v slovenskem in angleškem jeziku.

Rokopisu morajo biti dodani tudi podatki o avtorju:
- ime in priimek, akademski naslov in poklic, ime delovne organizacije v kateri dela, naslov stanovanja, telefonska številka, E-mail in številka fax-a.

Uredništvo KZT
- odloča o sprejemu članka za objavo,
- poskrbi za strokovne ocene in morebitne predloge za krajšanje ali izpopolnitev,
- poskrbi za jezikovne korekture.

Rokopisi člankov ostanejo v arhivu uredništva Kovine zlitine tehnologije.

Instructions to Authors

Authors are kindly requested to prepare the manuscripts according to the following instructions:
- The paper must be original, unpublished and properly prepared for printing.
- Manuscripts should be typed with double spacing and wide margins on numbered pages and should be submitted on floppy disk in form of:
- WORDSTAR, version 4, 5, 6, 7 for DOS,
- WORD for DOS or WINDOWS,
- ASCII text without formulae, in which case formulae should be clearly written by hand in the printed copy.

Preparation of Manuscript:
- the paper title (in English and Slovenian Language)*
- author(s) name(s) and affiliation(s)
- the text of the Abstract (in English and Slovenian Language)*
- key words (in English and Slovenian Language)*
- the text of the paper (in English and Slovenian Language)*
- tables (in English Language)
- figures (drawings or photographs)
- captions to figures (in English and Slovenian Language)*
- captions to tables (in English)
- acknowledgement
- references

* The Editorial Board will provide for the translation in Slovenian Language for foreign authors.

The length of published papers should not exceed 5–7 journal pages, of review papers 12 journal pages and of contributed papers 3–5 journal pages.

The international system units (SI) should be used.
Equations should be numbered sequentially on the right-hand side in round brackets.

Tables should be typed on separate sheets at the end of manuscript. They should have a descriptive caption explaining displayed data.

Figures (drawings or photographs) should be numbered and their captions listed together at the end of the manuscript. The drawings for the line figures should be twice the size than in the print. Figures have to be original, sharp and well contrasted, enclosed separately to the text.

References must be typed in a separate reference section at the end of the manuscript, with items refereed too in the text by numerals in square brackets.

References must be presented as follows:
- books: author(s), title, the publisher, location, year, page numbers
  H. Ibach and H. Luth, Solid State Physics, Springer, Berlin 1991, p. 245
- articles: author(s), a journal name, volume, a year, issue number, page
  H. J. Grabke, Kovine zlitine thenologije, 27, (1993), 1–2, 9

The abstract (both in English and in Slovenian Language) should not exceed 200 words.

The title page should contain each author(s) full names, affiliation with full address, E-mail number, telephone and fax number if available.

The Editor
- will decide if the paper is accepted for publication,
- will take care of the refereeing process,
- language corrections.

The manuscripts of papers accepted for publication are not returned.

KOVINE ZLITINE TEHNOLOGIJE

METALS ALLOYS TECHNOLOGIES

KOVINE ZLITINE TEHNOLOGIJE

Izdajatelj (Published for):
Inštitut za kovinske materiale in tehnologije Ljubljana
Soizdajatelji (Associated Publishers):
SŽ ŽJ ACRONI Jesenice, IMPOL Slovenska Bistrica, Kemijski inštitut Ljubljana, Koncern Slovenske Železarne, Metal Ravne, Talum Kidričevo

Izdajanje **KOVINE ZLITINE TEHNOLOGIJE** sofinancira: Ministrstvo za znanost in tehnologijo Republike Slovenije
(Journal **METALS ALLOYS TECHNOLOGIES** is financially supported by Ministrstvo za znanost in tehnologijo Republike Slovenije)

Glavni in odgovorni urednik (Editor-in-chief):
prof. Franc Vodopivec, Inštitut za kovinske materiale in tehnologije Ljubljana, 61000 Ljubljana, Lepi pot 11, Slovenija

Urednik (Editor):
mag. Aleš Lagoja

Tehnični urednik (Technical Editor):
Jana Jamar

Lektorji (Linguistic Advisers):
dr. Jože Gasperič in Jana Jamar (slovenski jezik), prof. dr. Andrej Paulin (angleški jezik)

Uredniški odbor (Editorial Board):
doc. dr. Monika Jenko, prof. Jakob Lamut, prof. Vasilij Prešeren, prof. Jože Vižintin, prof. Stane Pejovnik, dipl. ing. Sudradjat Dai, Jana Jamar

Mednarodni pridruženi člani uredniškega odbora (International Advisory Board):
prof. Hans Jürgen Grabke, Max-Planck-Institut für Eisenforschung, Düsseldorf, Deutschland
prof. Thomas Bell, Faculty of Engineering School of Metallurgy and Materials, The University of Birmingham, Birmingham, UK
prof. Jozef Zrnik, Technicka Univerzita, Hutnicka fakulteta, Košice, Slovakia
prof. Ilija Mamuzić, Sveučilište u Zagrebu, Hrvatska
prof. V. Lupinc, Istituto per la Tecnologia dei Materiali Metallici non Tradizionali, Milano, Italia
prof. Günther Petzov, Max-Planck-Institut für Metallforschung, Stuttgart, Deutschland
prof. Hans-Eckart Oechsner, Universität Darmstadt, Deutschland

Izdajateljski svet (Editorial Advisory Board):
prof. Marin Gabrovšek, prof. Blaženko Koroušić, prof. Ladislav Kosec, prof. Alojz Križman, prof. Tatjana Malavašič, dr. Tomaž Kosmač, prof. Leopold Vehovar, prof. Anton Smolej, dr. Boris Ule, doc. dr. Tomaž Kolenko, dr. Jelena Vojvodič-Gvardjančič

Naslov uredništva (Editorial Address):
KOVINE ZLITINE TEHNOLOGIJE
IMT Ljubljana
Lepi pot 11
61000 Ljubljana, Slovenija
Telefon: +386 61 125 11 61
Telefax: +386 61 213 780
Žiro račun: 50101-603-50316 IMT pri Agencija Ljubljana

Cover: Experiment, first performed in Magdeburg in 1657, von Guericke demonstrated the effect of air pressure on an evacuated cavity formed by two tightly fitted copper hemispheres.
Naslovnica: Magdeburški poskus z dvema polkroglama in evakuiranim vmesnim prostorom, ki ju ni moglo ločiti osem parov konj. Poskus je javno prikazal Otto von Guericke leta 1657.

Oblikovanje ovitka: Ignac Kofol
Stavek: Majda Kuraš
Tisk: Gorenjski tisk, Kranj

Po mnenju Ministrstva za znanost in tehnologijo Republike Slovenije št. 23-335-92 z dne 09. 06. 1992 šteje KOVINE ZLITINE TEHNOLOGIJE med proizvode, za katere se plačuje 5-odstotni davek od prometa proizvodov.

Preface

The 1995 Bled Joint Vacuum Conference continues the tradition of *small family type meetings* of Austrian, Hungarian, Croatian and Slovenian scientists in the field of vacuum physics, techniques and related topics.

Former Austrian-Hungarian Joint Conferences were held in Györ (1979), Brunn am Gebirge (1981) and in Debrecen (1985) where for the first time Yugoslavia was also included, than Portorož (1988) and Vienna (1991).

At the Fourth European Vacuum Conference (EVC-4. Uppsala 1994), the delegates from Austria, Croatia, Hungary and Slovenia expressed the willingness to continue regional cooperation and agreed to organize Slovenian-Hungarian-Croatian-Austrian Sixth Joint Vacuum Conference, with the Slovenian Vacuum Society and Institute of Metals and Technologies, Ljubljana as organizers. Scientists from Czech Republic, Slovak Republic and Poland joined the Conference.

An impressive number of excellent contributions were presented on the Conference, instead of its *small family type*. Papers related to applied surface science, electronic materials, plasma science, surface science, thin films and vacuum science were already published in Journal FIZIKA, 1995, Number 2.

Papers related to vacuum metallurgy are published in the present number of the Journal KOVINE ZLITINE TEHNOLOGIJE – METALS ALLOYS TECHNOLOGIES. Various subjects, such as electron beam welding, laser welding, vacuum brazing, surface treatment by plasma nitriding hard coatings as well as industrial experiences by vacuum manufacturing of stainless steels are included. The authors are affiliated mostly to academic research institutions. In spite of this, results of applied research as well as technological experience from various countries are presented in the papers, which should meet the interest of a large audience.

Editors:

F. Vodopivec and M. Jenko

Nagrajeni mladi raziskovalci za najboljši raziskovalni dosežek predstavljen na 45. Posvetovanju o metalurgiji in kovinskih gradivih in 2. Posvetovanju o materialih na 14. Slovenskem vakuumskem posvetovanju, Portorož, 3.–5. oktober 1994

Darja Steiner Petrovič, dipl. ing. metalurgije, se je na 45. Posvetovanju o metalurgiji in kovinskih gradivih, 2. Posvetovanju o materialih in 14. Slovenskem vakuumskem posvetovanju, predstavila z delom: *Razogljičenje in rekristalizacija neorientirane elektro pločevine.*

Darja Steiner Petrovič se je rodila 18. oktobra 1969 v Ljubljani. Srednjo naravoslovno-matematično šolo je zaključila leta 1988 in nato vpisala študij metalurgije na Univerzi v Ljubljani, FNT – Montanistika, kjer je leta 1993 tudi diplomirala.

Kot mlada raziskovalka je pod mentorstvom doc. dr. Monike Jenko zaposlena na Inštitutu za kovinske materiale in tehnologije v Ljubljani. V času podiplomskega študija se je izpopolnjevala tudi na Inštitutu za fiziko Zagreb, v laboratoriju za fiziko trdne snovi.

Contents

Original Scientific Papers
Vacuum Metallurgy

INŠTITUT ZA KOVINSKE MATERIALE
IN TEHNOLOGIJE p.o.

INSTITUTE OF METALS
AND TECHNOLOGIES p.o.

61000 LJUBLJANA, LEPI POT 11, POB 431,
SLOVENIJA

Telefon: 061/1251-161, Telefax: 061 213-780

VACUUM HEAT TREATMENT LABORATORY

Vacuum Brazing

Universally accepted as the most versatile method of joining metals. Vacuum Brazing is a precision metal joining technique suitable for many component configurations in a wide range of materials.

ADVANTAGES

- Flux free process yields clean, high integrity joints
- Reproducible quality
- Components of dissimilar geometry or material type may be joined
- Uniform heating & cooling rates minimise distortion
- Fluxless brazing alloys ensure strong defect free joints
- Bright surface that dispense with expensive post cleaning operations
- Cost effective

Over five years of Vacuum Brazing expertise at **IMT** has created an unrivalled reputation for excellence and quality.

Our experience in value engineering will often lead to the use of Vacuum Brazing as a cost effective solution to modern technical problems in joining.

INDUSTRIES

- Aerospace
- Mechanical
- Electronics
- Hydraulics
- Pneumatics
- Marine
- Nuclear
- Automotive

QUALITY ASSURANCE

Quality is fundamental to the **IMT** philosophy. The choice of process, all processing operations and process control are continuously monitored by **IMT Quality Control Department**.

The high level of quality resulting from this tightly organised activity is recognised by government authorities, industry and International companies.

Kovine, zlitine, tehnologije / letnik 29 / 1995 / št. 3–4 / strani 369–376

Future Aspects of Electron Beam Welding and Surface Modification

Perspektive varjenja in obdelave površin z elektronskim curkom

Friedel K. P.,[1] Institute of Vacuum Technology, Warsaw, and Institute of Electronic Technology, The Wroclaw Technical University
W. Sielanko, Institute of Vacuum Technology, Warsaw

Some aspects of future electron beam technology are given, especially for welding and modification of metal surfaces. One of the prime advantages of EB welding is the ability to make weld deeper and narrower than one can make using other methods of welding. The weld bead may contain some defects typical for EB welding. The essential requirement for the future equipment development is to avoid or eliminate these defects. Advances in the equipment from this point of view are reviewed.

Key words: electron beam welding, weld defects, equipment for welding

Podane so nekatere perspektivne tehnologije varjenja z elektronskim curkom, posebno za varjenje in obdelavo površin kovinskih materialov. Najpomembnejša prednost varjenja z elektronskim curkom je možnost izdelave ožjih in globjih zvarov v primerjavi z drugimi varilnimi tehnikami. Nizi zvarov lahko vsebujejo napake, ki so tipične za postopek varjenja z elektronskim curkom. Pomembna zahteva za razvoj opreme v bodočnosti je odprava tovrstnih napak.

Ključne besede: varjenje z elektronskim curkom, napake zvarov, oprema za varjenje

1. Introduction

The industrial application of electron beam (EB) welding and surface modification has continually increased since the early 1960's in the number of machines as well as in the number of applications. Throughout this period continuous development of equipment and production engineering has taken place. It is anticipated that EB welding and surface modification will continue to develope extensively in future within the two main domains:
- enhancement of joint quality and reliability as well as process reproducibility,
- thick-section welding and surface hardening of large workpieces with complex shapes at atmospheric pressure.

2. Joint quality and reliability

The main reason for which the EB welding will be able to satisfy the industrial user needs in the future can be summarised as improvement in joint quality and reliability. The joint quality and reliability depends directly upon:
- fusion weld and heat affected zone shape and dimensions and microstructure,
- number and type of defects.

One of the prime advantages of EB welding is the ability to make weld deeper and narrower than one can make using other methods of welding. Unfortunately, the weld of such a shape may contain some defects. The most of them is also encountered in other methods of welding but there are defects typical only for EB welding. The macrodefects of weld caused by EB tend to occur in deep weld both in its central part (cracks, porosity, unmelted lumps etc.), and in weld root (porosity, cold shut, spiking). In case of very high speed of welding, humping and undercut phenomena often occur.

3. Methods of defect prevention

The essential requirement is to avoid or eliminate defects by applying of suitable methods. There are two main groups of such methods[10]:
- material selection methods that rely on improvement in chemical composition either "a priori" or by alloying during the welding,
- system methods which are connected with the possibilities offered by the equipment itself.

The last group of methods can be divided into further three groups:
- methods of defect prevention connected with improvement in the original construction of EB welding machine (e.g. increasing the equipment resistance against electrical breakdown and electromagnetic

[1] Prof. K. P. Friedel,[1] Institute of Vacuum Technology, Warsaw, and Institute of Electronic Technology, The Wroclaw Technical University

interference, etc.). These methods are usually out of range for the equipment operator,
- parametric methods are crucial in improving the joint quality. Certain parameters of an equipment or welding process can be set to make the performance less sensitive to causes of variation and imperfection,
- optional methods that rely on application of special process technology requiring usually the installation of additional optional devices of exactly defined destination.

3.1 Material selection methods

The volume of melted metal during EB welding is small in comparison with other classical welding methods. Besides, the rapid heating and self-quenching in region of welding lead to highly unbalanced changes of microstructure. Additionally the high microstructure diversity within the zone of welding depends frequently on extremaly different welding conditions (e.g. welding of steel plate with a thickness of 5 mm, at welding speed of 30 - 50 mm/s, causes the few milisecond self-quenching in heat affected zone within the range of 800 - 500°C, whrereas at thickness of 150 mm and welding speed of 1,6 mm/s the rate of self-quenching is equal to approximately 50 s[20]. The knowledge of microstructure and particularly of hardness dependence of heat affected zone on weld parameters is by no means less important than the knowledge of bead shape and dimensions dependence on these parameters.

The purity of materials. The basic precondition of high quality joint is the initial purity of materials used. This purity refers not only to surface contamination, but after all to internal impurities, particularly to the contents of gases as well as metallic and nonmetallic alloying constituents. Some impurities like sulfur, phosphorus, arsenic, tin and antimony are very undesirable[24]. Intergranular cracking arises from the grain-boundary segregation of impurity elements[42]. The deeper the weld depth, the higher should be requirements concerning material purity (e.g. at weld depth > 100 mm the contents of oxygen and nitrogen should not exceed 30 and 80 ppm respectively[26].

Deep welding with filler materials. Appropriately selected filler alloy could diminish the risk of hot cracks during the welding of austenitic steels (some alloying components facilitate the development of ferritic microstructure[37]. Insertion of nickel foil into the gap may enable to join the nodular iron[34]. The filler wire is usually fed directly to the vapour channel **(Fig. 1)** either ahead of EB, on the front edge of the channel entrance orifice[5,23], or behind the EB with simultaneous dislocation of wire melting zone alongside the channel[17]. Instead of the filler foil the overlay layer may be used[24,28]. For example, onto the surface of structural steel, contaminated with non-metallic elements, the layer of high quality steel can be overlaid **(Fig. 2)**. This way it is possible to obtain the intermediate layer of filler material of very good adherence to core material and of very good weldability as well.

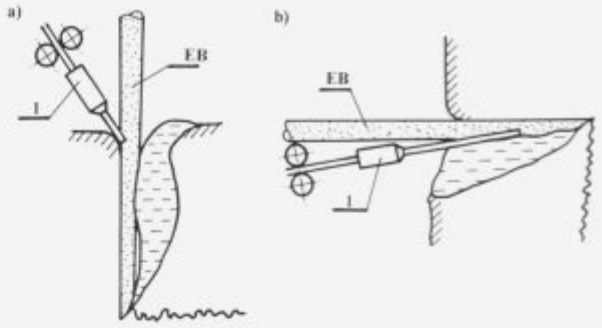

Figure 1: Deep welding with filler wire fed ahead of EB (a) or behind EB. 1 - wire feeder

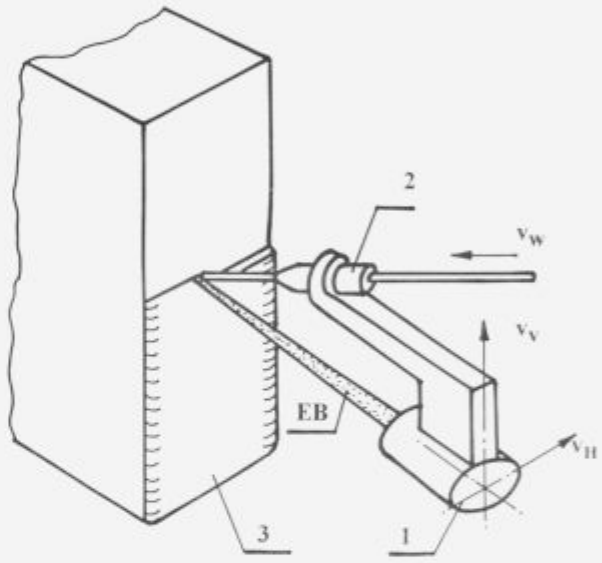

Figure 2: The overlaying of filler material onto the surface of workpiece. 1 - electron gun, 2 - wire feeder, 3 - overlayed layer

New materials for EB welding. There is an urgent need fot not only the entirely new materials but also for improved materials destined for EB welding. These improvements consist usually in lowering the concentration of alloying components undesirable from the joint quality standpoint. It was found that the decrease in Al content in steel favour an acicular ferrite microstructure in EB weld and this has enable the development of new type of steel for EB welding[25]. The reduction of phosphorus content in steel diminishes the intergranular fracture surface area fraction and improves the toughness[42]. New steels designed for EB welding are usualy low-carbon steels of higher toughness owing to such alloying components like Cr, Mn, Mo and Ni[20,21,44]. Besides the properties of many materials are closely related to various manufacturing operations and particulary the thermal treatment. The proper thermal treatment can improve the properties of EB weld[7].

3.2 Parametric methods

It is well known that product or process quality must be properly designed. The Japanese have, through the efforts of Genichi Taguchi[14], built quality methods into the engineering process. This methodology comprises three-phase program involved in the engineering optimization of a product or process: system design, parameter design, tolerance design. The operator of EB welding machine is able to undertake the optimization procedure only by selecting the appropriate process parameter levels. The parameter design phase is crucial also for the improving to the repeatability of a process. It permits to determine the parameter levels such that the process is optimal and present a minimal sensitivity to causes of variation.

The fundamental for parametric method of improvement in joint quality is the knowledge of dependence of weld cross-section shape and defectiveness degree on welding conditions. It is almost impossible to find this dependence theoretically by creating the model of EB-material interactions. Therefore the key stage of such optimization procedure is the properly designed experiment. The most commonly applied design of experiments is the fractional factorial experiment. The main limitation of this method is that no interaction among the parameters studied can be observed. To avoid this disadvantage it is necessary to perform the full factorial experiment.

Fig. 3 shows the example[10] of the relationship between weld depth and focusing parameter (i.e. ratio of the work distance and the position of maximum power density plane of EB) obtained experimentally. The "forbiden zones" of enhanced defectiveness are marked by dotted lines. The larger the work distance the weld becomes more shallow, but at the same time much more sound. To avoid the porosity of the central part of the weld, the EB active zone oughut to be located beneath the workpiece surface rather than onto or above this surface.

Taguchi method can be also used to optimize the electron beam hardening process. This way it is possible to identify the factors which are the most significant and influencial on thickness and hardness of hardened layer and to found the most suitable processing conditions within the range of factor levels that were chosen.

In future many further similar experiments should be performed to establish the allowable zones of all process parameters and to prepare the knowledge representation of both EB welding and surface modification processes. Finally, it seems indispensable to create the expert systems based on such knowledge representation[3].

3.3 Optional methods

The adoption of special optional methods, which enable to weld materials of poor weldability allow to get sound welds without commonly encountered defects, should significantly extend the area of applications of EB welding. These optional methods consist mainly in space-time shaping of EB power density distribution.

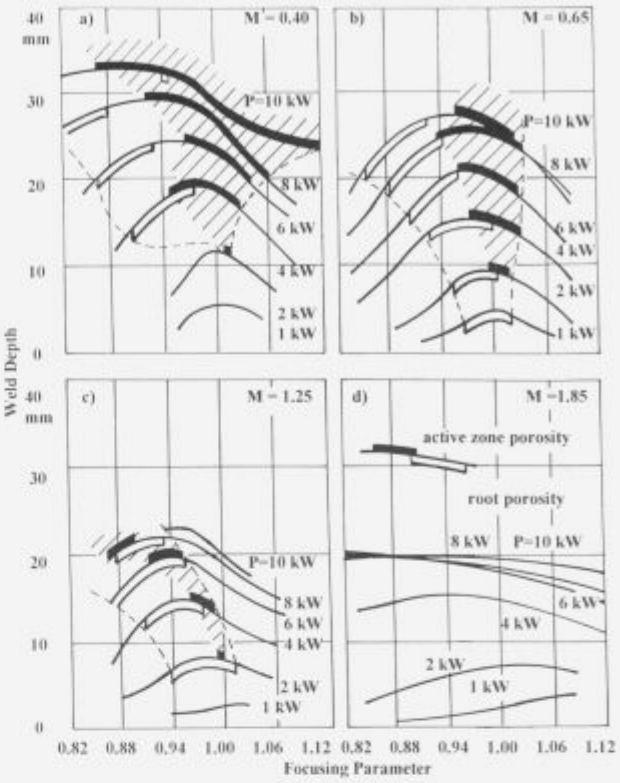

Figure 3: The weld depth vs focusing parameter and zones of defects appearance. M - magnification, P - EB power

Horizontal electron beam. Overhelming majority of EB welds is made by vertical EB. The depth of EB penetration is restricted not only by EB power density but also by disturbances in dynamic equilibrium of vapour channel as well by the highly turbulent flow of molten metal[18]. Therefor, the thick-section welding is usually performed by using horizontal EB **(Fig. 4)** at horizontal or vertical welding direction[4,15,19]. This method enables to stabilize the molten metal flow and keep the vapour channel open during welding. In order to prevent the excessive outflow of molten metal the cover metal strap is usually applied alongside the lower edge of welding gap.

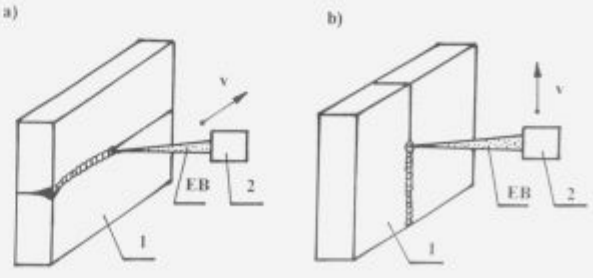

Figure 4: Welding with horizontal EB at horizontal (a) or vertical (b) welding direction. v - welding speed, 1 - workpiece, 2 - electron gun

Modulated electron beam. Deeply penetrating, high-power pulsed EB may be utilized to meet the growing demand for very high quality welding of thick-section workpieces. The main advantage of this welding method consists in lowering the average EB power density and minimizing the melted metal volume. This method of welding is recommended for welding martensitic steels[15,16].

Astigmatic electron beam. The strongly astigmatic EB can be used to improve the weld root defectiveness[18]. This astigmatism is intentionally caused by applying of additional quadrupole lens. Close to the workpiece surface the EB cross-section resemble the elongated ellipse of longer axis parallel to welding direction **(Fig. 5)**. In vicinity of the channel bottom the ellipse longer axis is perpendicular to the welding direction and prevents the creation of spikes. The quadrupole lens is usually connected in feedback loop and is made active only during spike formation, what can be revealed as sudden drop of backscattered electrons current.

Inclined electron beam. The permanent inclination of EB axis in welding plane improves the flow of molten metal and facilitate the degassing of resultant weld bead[24].

Oscillating electron beam. This method consists in very fast deflections of EB during welding. Different types of oscillations are used: parallel or perpendicular to the weld gap, elliptical, circular, "X" type, parabollic and so forth. By selecting the optimum frequency and amplitude, it is possible to obtain a sound weld with a narrow bandshaped bead[6,8,15,23,28,45].

Oscillation of electron beam active zone. In order to deposite the EB energy more uniformly inside the vapour channel the oscillations of EB active zone alongside the channel axis are used. These oscillations rely on applying the additional AC component to DC component of magnetic lens current[8,15].

Doubly-deflected rotating electron beam. The combination of circular oscillations and double deflection of EB **(Fig. 6)** enables to control the position of EB active zone independently of focusing lens[22]. The mutual displacement of EB focus and the waist of EB due to double-deflection serves as a tool for the fine adjustment of EB active zone shape and position.

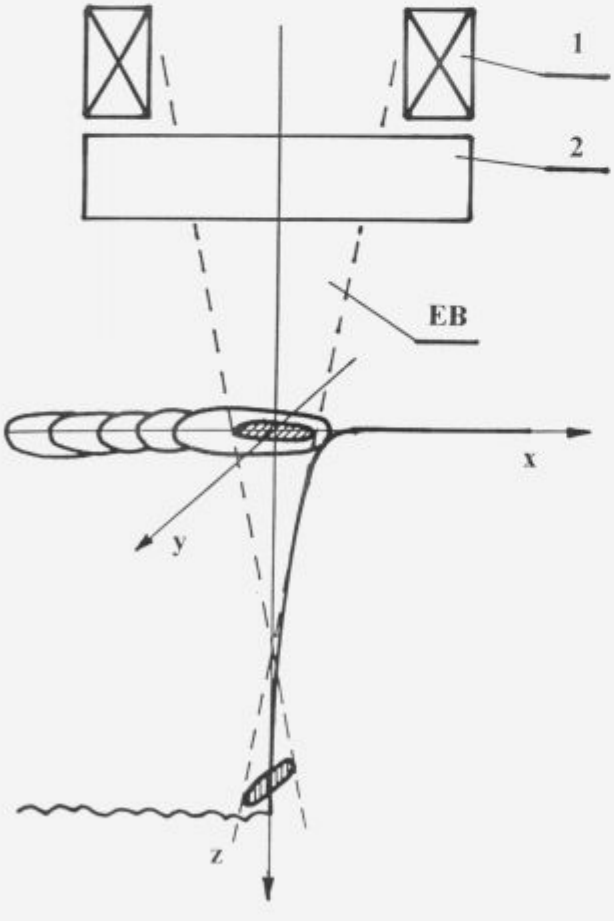

Figure 5: Strongly astigmatic EB. 1 - focusing lens, 2 - quadrupole lens

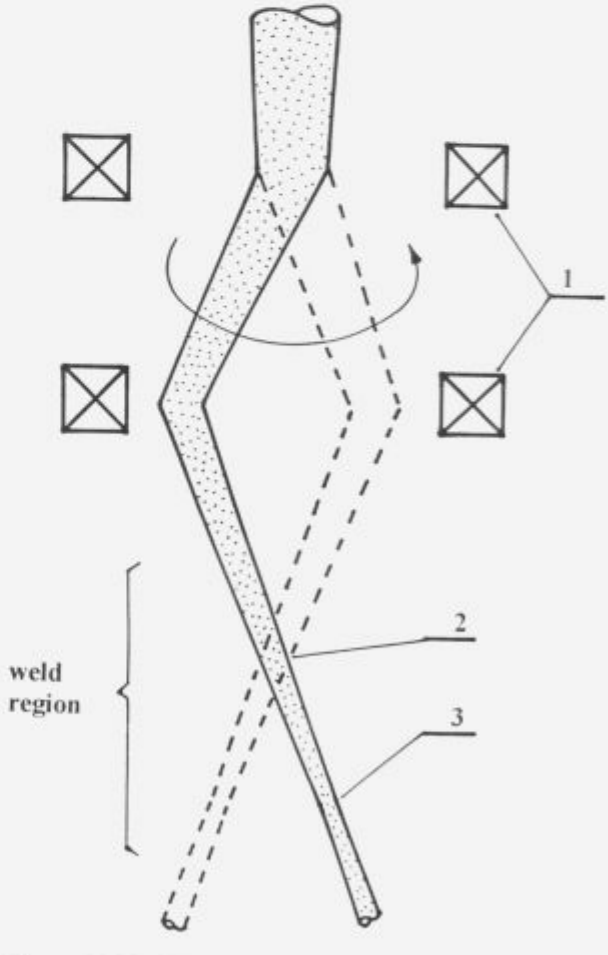

Figure 6: Doubly-deflected rotating EB. 1 - quadrupole deflection system, 2 - waist of EB due to double deflection, 3 - EB focus

Tandem and quasitandem electron beam. Some disadvantages caused by ordinary EB welding, such as humping, spiking and root porosity can be overcome by using tandem or quasitandem EB as shown in **Fig. 7**. This method utilizes two electron beams at the same time. One beam is a conventional vertical EB. The other one is used as the auxiliary sub-beam for the repairment of welding defects. This auxiliary beam may be directed either on the rear wall of vapour channel eliminating this way the defects of active zone[2,38], ot into the channel eliminating the spiking and root porosity. The auxiliary beam may be also directed onto the molten pool, as shown in **Fig. 7b**, changing the flow of molten metal so that it flows smoothly backward[2,40]. This way the humping phenomenon may be suppressed. Some modification of this method consist in splitting the EB into two beams using double deflecting unit **(Fig. 8)**. The power density of both beams can be adjusted by changing the pulse length.

Electron beam current decay in the fade-out region. It was stated[28] that the position of EB active zone has a significant influence on the shape of weld intensity of root defects in the fade-out region. There are many different techniques of defects suppression in the weld fade-out region. The best result may be obtained by proper control of the beam current decay rate. A composite beam current decay curve was designed which allowed to eliminate the voids and diminished root porosity during fade-out **(Fig. 9)**.

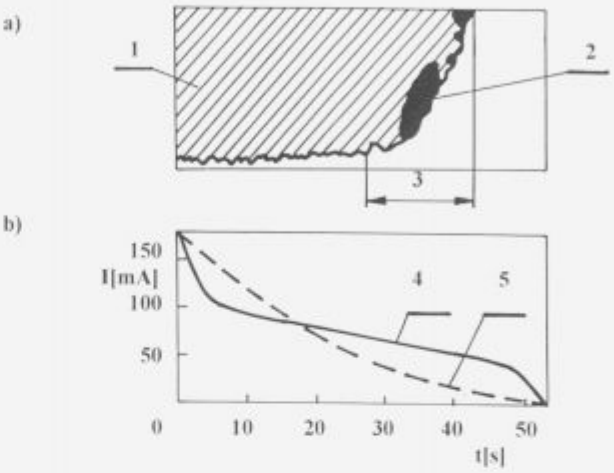

Figure 9: The weld fade-out region. **(a)** - root defects in the fade-out region, **(b)** - a composite beam current decay curve; 1 - weld cross-section, 2 - root porosity, 3 - fade-out region, 4 - optimum EB current decay, 5 - conventional EB current decay

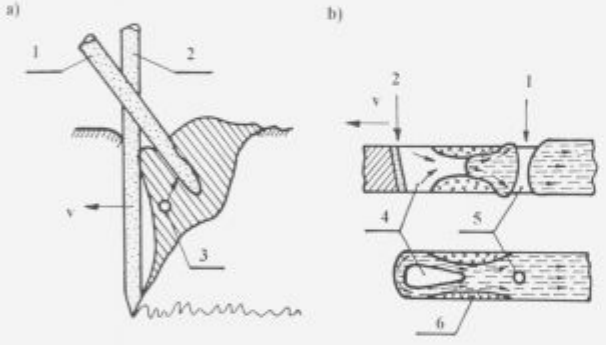

Figure 7: Tandem EB welding. 1 - auxiliary EB, 2 - main EB, 3 - active zone porosity, 4 - main vapour channel, 5 - auxiliary channel, 6 - solidification metal layer, v - welding speed

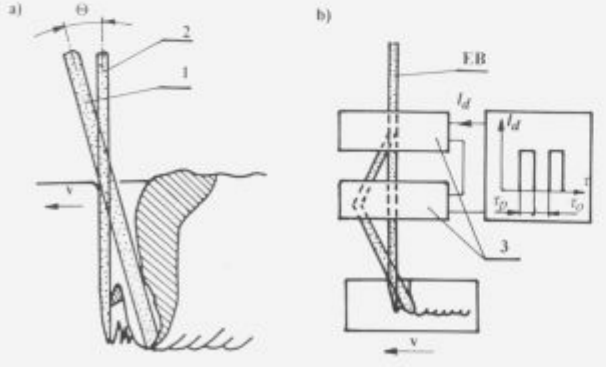

Figure 8: Quasitandem EB welding. **(a)** - reheating of the root zone by auxiliary EB, **(b)** the principle of EB splitting; 1 - auxiliary EB, 2 - main EB, 3 - double-deflection system, v - welding speed, Θ - inclination angle of auxiliary EB

4. Improvements in EB welding machine construction

One of essential requirements in EB welding is to predict and reproduce the weld geometry particularly in case of frequently encountered partial-penetration welds. To satisfy this requirement the continuous improvement in performance of EB welding machines of moderate powers and voltages as well as of higher powers, for thick-section welding, will be necessary.

The overall purpose of equipment developments has been to satisfy the user needs, which can be summarised as improvements in: EB welding machine resistance against electrical breakdown in region of EB formation and against internal and external electromagnetic interference, process control, user friendliness and possibility of main subassemblies monitoring, reliability of power suppliers and CNC systems.

4.1 Vacuum environment

When applied in the heavy industry EB welding technology is faced to the problem of the volume of working chamber which should contain the workpiece to be welded. There are few possibly ways to overcome this problem **(Fig. 10)**: non-vacuum version of EB welding process[27,31,32,36], local vacuum chamber which only contains the seam of workpiece[15,33], movable chamber with local vacuum[15], "air-to-air" type of vacuum chamber[1].

The non-vacuum welding has been in industrial use mostly for automotive applications requiring weld depth of less than 10 mm in a single pass. Recently the non-vacuum beams were generated at an accelerating voltage of 270 kV with sustained power levels of in axcess of 110 kW. The penetration depths of more then 50 mm in steel and 40 mm in copper were achieved[32]. **Fig. 11** illustrates the rapid degradation of electron beam penetration depth over the range 10^{-4} - 10^{3} hPa caused by direct air-scattering. Most EB welding processes are currently performed in partial vacuum conditions, since the vacuum system is cost-effective in this case and the vacuum chamber pump-down time does not limit significantly the production throughput[30].

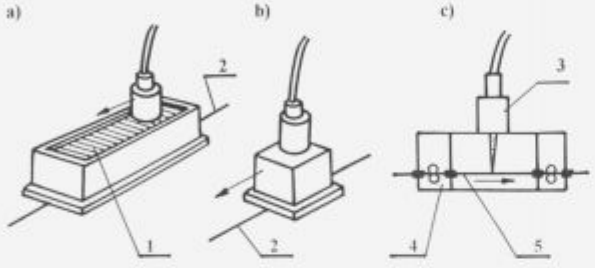

Figure 10: Vacuum chambers: **(a)** local, **(b)** movable, **(c)** "air-to-air"; 1 - sliding louver, 2 - welding gap, 3 - electron gun, 4 - air lock, 5 - continuously welded bimetallic ribbon

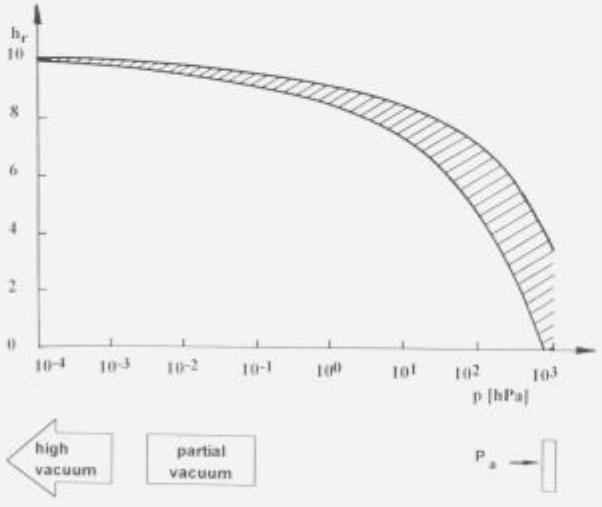

Figure 11: Effect of air pressure in vacuum chamber on penetration depth. h_r - relative welded depth, p_a - atmospheric pressure

4.2 Accelerating voltage and EB power

Contemporary EB welding machines utilize the electron guns of moderate power of 10 - 150 kW which operate in the range of 50 - 200 keV. The reason for increasing EB power and accelerating voltage is to increase the maximum allowable weld depth. However, as could be seen in **Fig. 12**, the penetration range for electrons of above mentioned energies is 10 - 100 μm only[35]. It means that the thermal energy is deposited essentially on the surface of materials. Therefore, the increasing of EB power density over to $\approx 10^{6}$ W/cm^2 does not improve essentially the penetration depth and instead leads to surface vaporization of the workpiece. The dramatic improvement in penetration depth is possible only by increasing the EB energy to ≈10 MeV. At this energy the EB will interact with material in a way fundamentally different from the conventional EB. The electron range is now of the order of 1 cm, what means that material is heated volumetrically. The energy required to melt the material is delivered by several pulses of very high energy EB.

Moreover, at EB energies greater than few MeV the gas-scattering of electrons drops dramatically **(Fig. 13)** causing a significant improvement in penetration of EB through the air. Additionally, if the peak EB current is also increased to approximately 1 kA, the self-pinch phenomenon becomes strong enough to resist the spreading of EB during its propagation through the atmosphere. This type of "pinched" EB enables to weld thick-section workpieces (up to 30 cm) at atmospheric pressures. Besides, such high energy EB can be used also as large-area, nearly instantaneous, volumetric heat source for surface treatment.

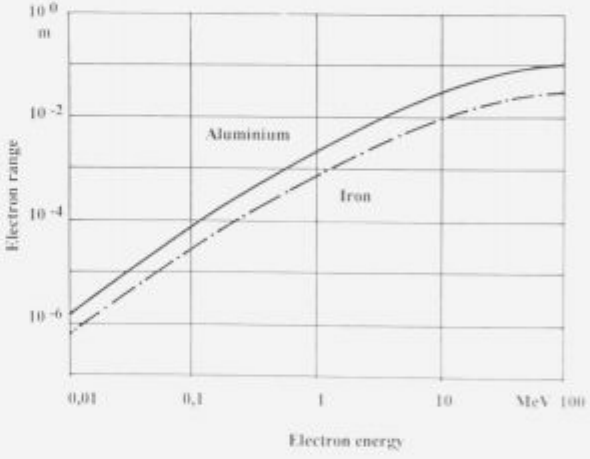

Figure 12: Electron range in iron and aluminium

4.3 Power supplies

The traditional HV transformer rectifiers are still in use. Nevertheless, the adoption of solid state invertors typically of a 5000 Hz base frequency seems to be very promising[9,12,32]. This approach greatly simplifies the design as well as cost of the high voltage transformer and cable terminations. Moreover, these power supplies facilitate the discharge control. It is possible to switch off the power inverter within 20 μs of detection of the current rise[31]. For the traditional EB welding machines which operate at voltages less than 200 kV the standard high voltage DC power supplies are adequate. However, for equipment of higher voltages and powers other high voltage tech-

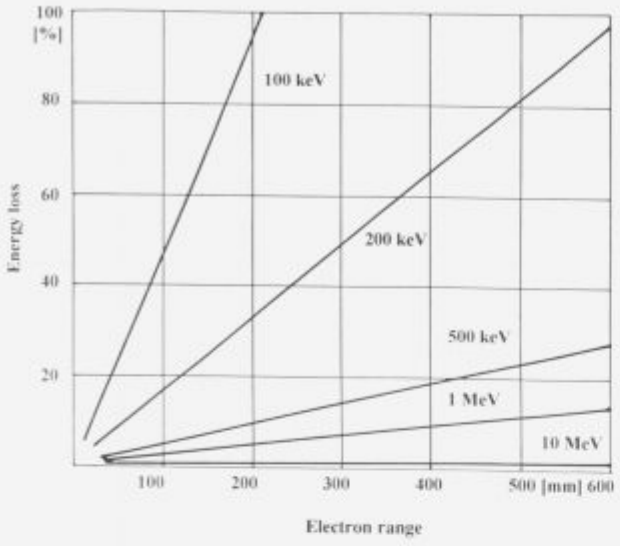

Figure 13: Rate of electron energy loss in air at atmospheric pressure

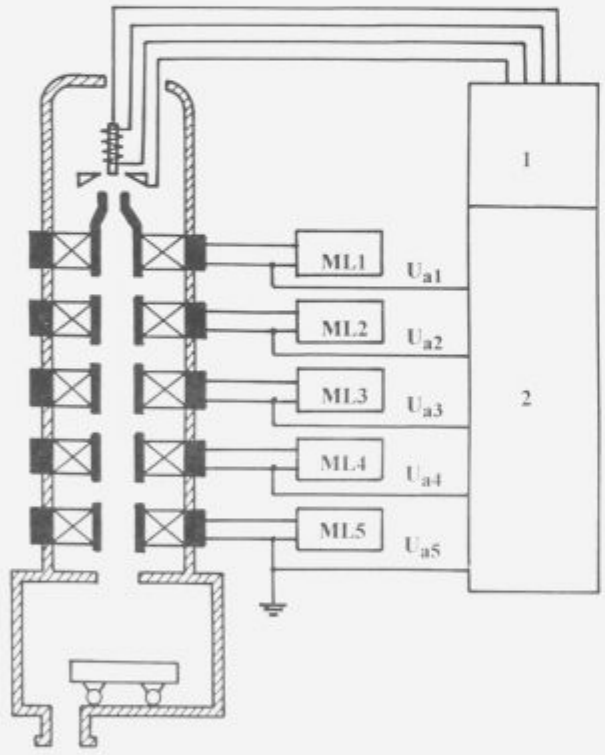

Figure 14: High-voltage accelerating system. ML - power supply for magnetic lens, 1 - electron gun power supply, 2 - EB accelerating power supply

niques are required and non-pulsed power accelerators have been developed[2,41] **(Fig. 14)**. EB currents greater than 0,1 A cause in this type of accelerators serious beam instabilities[39]. Thus, these accelerators are not expected to scale to the higher voltage and power levels at which the pulsed power options is most attractive. In this case the high energy electron beam pulsed accelerators has been developed, designated to accelerating potentials of few MV, beam currents of thousands of amperes, pulse duration of tens to hundreds of nanoseconds, kilojoules of EB energy, and instantaneous power of gigawatts to terrawatts. These accelerators has been developed to a state in which the parameters required for welding and materials treatment can be met with minimal additional development[43].

4.4 Guns and cathodes

Predominantly the conventional triode guns are used, but recently the return to diode gun configuration is also observed[31]. The diode electron gun enables to precise control of EB current over the full operating range without risk of sudden current increase during breakdown. The displacement of EB waist is also reduced. In case of very high energy EB (≈MeV) the diode gans are used. Depending on the application and the type of accelerator, the anode of this gun can be made out of grid or thin foil, or it may have an aperture to allow the EB injection into the beam transport pipe. The cathode of very high current diode gun is often made out of graphite. Very high electric field (1 MV/cm) causes the so called explosive emission. No external heating of the cathode is required[43].

The design of an electron gun by numerical methods taking into account the influence of many various electrical and geometrical parameters takes a lot of time and work but can easily be done employing modern computer technique. The detailed examination of the emittance of the beam and application of mentioned earlier design of experiments have proved to be useful tool in improving the high power electron guns applied in EB welding machines[11,13,14].

5. Conclusions

As described above the development of advanced electron beam technology will be promoted in two main directions. The first consists in the enhancement of joint quality and reliability. Progress in this area will require intensive research of fundamental phenomena, clarifying the welding and surface treatment processes. The adoption of special methods of EB welding and surface treatment as well as implementation of new materials destined for EB welding should significantly extend the scope of applications and performance of the process. The second direction of EB development is connected with the thick-section welding and surface hardening of large workpieces with complex shapes at atmospheric pressure. High energy EB of extremely high power may be utilized to meet the growing demand for high quality welding of thick and large workpieces of refractory and fusible materials at or even above atmospheric pressures and for large area surface treatment of components whose large size and complex shapes make more conventional surface treatments time-consuming and expensive. EB welding

and surface treatment can offer the comprehensive range of versatility and can be still regarded as very competitive with other conventional methods.

6. References

[1] P. Anderl, J. Koy, W. Scheffels, *Proc. 4th CISFFEL* (Cannes 1988), 733
[2] Y. Arata, *ibid.1*, 21
[3] P. Bonnin, M. Aji, *ibid1*, 325
[4] B. Dalmastri, R. Festa, *Weld. Int.*, 10, 1989, 878
[5] I. Decker, C. Oestmann, *Bänder Bleche Rohre*, 30, 1989, 2, 22
[6] K. Depner, F. Eichhorn, W. Janseen, K. Iversen, M. Engberding, *ibid.1*, 301
[7] M. Dijols, J-C. Goussain, G. Colombe, P. Grenier, *Proc. 5th CISFFEL (LaBaule 1993)*, 339
[8] J-L. Doong, J-M. Chi, J-R. Hwang, *Fatig. Fract. Eng. Mat. Struct.*, 13, 1990, 3, 253
[9] C. D. A. Eccleston, *ibid.1*, 795
[10] J. Felba, K. P. Friedel, *Proc. Int. Conf. EBT (Varna 1991)*, 336
[11] J. Felba, K. P. Friedel, W. Sielanko, S. Wójcicki, A. Wymyslowski, *Proc. 4th Int. Conf. EBT (Varna 1994)*, 63
[12] J. D. Ferrario, S. P. Kyselica, G. S. Lawrence, *ibid.1*, 69
[13] K. P. Friedel, J. Felba, *ibid.1*, 77
[14] K. P. Friedel, J. Felba, *ibid.11*, 69
[15] D. Fritz, *IIW Doc. no IV-453-88*, 1988
[16] D. Fritz, *Proc. Int. Conf. "Special Technologie '90" (Pilzen 1990)*, 115
[17] I. M. Frolov, J. G. Kutsan, V. P. Morotchko, V. V. Gumovsky, S. N. Kovbasenko, B. F. Jakushin, *ibid.10*, 172
[18] H. Irie, S. Tsukamoto, *ibid.1*, 123
[19] A. A. Kaidalov, V. J. Lokshin, O. K. Nazarenko, *ibid.16*, 45
[20] A. M. Kosechek, *ibid.16*, 3
[21] A. M. Kosechek, *ibid.16*, 134
[22] S. N. Kovbasenko, K. A. Sukach, M. L. Zhadkevich, J. G. Kutsan, *Svar. Proizv.*, 6, 1988, 5
[23] S. N. Kovbasenko, J. G. Kutsan, B. N. Shipitsyn, *ibid.10*, 318
[24] O. K. Nazarenko, *Mat. Manuf. Process*, 7, 1992, 2, 285
[25] M. Ohara, H. Homma, T. Inoue, *ibid.1*, 227
[26] B. E. Paton, et al., *Weld. Int.*, 6, 1989, 466
[27] V. I. Perevodchikov, S. I. Gusev, M. A. Zavialov, V. F. Martynov, *ibid.7*, 99
[28] C. S. Punshon, *ibid.1*, 287
[29] P. J. Ross, *Taguchi Techniques for Quality Engineering*, McGraw-Hill, New York, 1988
[30] R. Roudier, Ph. Dard, G. Sayegh, *ibid.1*, 767
[31] J. D. Russell, *ibid.7*, 13
[32] A. Sanderson, *ibid.7*, 91
[33] G. Sayegh, *Proc. 4th Int. Symp. IWS (Osaka 1982)*, 127
[34] F. Shibata, *Trans. JWS*, 22, 1991, 2, 18
[35] A. C. Smith, W. M. Fawley, E. E. Nolting, *Proc. HEEB Weld. and Mat. Proc. (Cambridgre, USA, 1992)*, 1
[36] J. Sommeria, A. Metz, *ibid.1*, 813
[37] H-D. Steffens, E-R. Sievers, *Mat. wiss. werkst. Tech.*, 21, 1990, 235
[38] M. Tomie, N. Abe, X-Y. Yao, Y. Arata, *Trans. JWRI*, 17, 1988, 2, 19
[39] M. Tomie, N. Abe, Y. Arata, *Trans. JWRI*, 18, 1989, 1, 31
[40] M. Tomie, N. Abe, Y. Arata, *Trans. JWRI*, 18, 1989, 2, 13
[41] M. Tomie, N. Abe, Y. Arata, *Trans. JWRI*, 19, 1990, 2, 15
[42] Y. Tomita, K. Koyama, K. Tanabe, *ibid.7*, 331
[43] B. N. Turman, M. G. Mazarakis, E. L. Neau, *ibid.35*, 44
[44] J. M. Vitek, S. A. David, *Metall. Trans. A., Phys. Metall. Mat. Sci.*, 11A, 1990, 7, 2021
[45] S. Zolotovsky, *ibid.1*, 147

Kovine, zlitine, tehnologije / letnik 29 / 1995 / št. 3–4 / strani 377–384

Operational Aspects of Experiences in Vacuum Technology by Production of High Quality Stainless and Alloyed Steels

Praktične izkušnje pri uporabi vakuumske tehnologije pri izdelavi visoko kvalitetnih nerjavnih in legiranih jekel

Koroušič B[1]., IMT, Ljubljana, A. Rozman, Metal d.o.o. Ravne, J. Triplat, Acroni d.o.o Jesenice, J. Lamut, Met & Mat. Department, University Ljubljana

Highlights of the technological scheme of manufacturing quality steels as stainless steels in the vacuum by the duplex EAF (electrical arc furnace) + VOD (vacuum oxygen decarburization) process is presented here. Special attention is given to the stage of vacuum oxidation of carbon and chromium and to the use stage of degassing in vacuum. In short feature the VOD computer program is expalained, which enables the effective preparation of the complete technology for VOD - process from 15 to 100 tonnes.

Key words: production of high quality stainless steels by VOD process

Predstavitev tehnološke sheme izdelave kvalitetnih jekel v vakuumu kot so nerjavna jekla po duplex postopku EOP (elektro-obločna peč) + VOD (vakuumsko kisikovo žilavenje). Poseben poudarek je podan na procesno stopnjo vakuumske oksidacije ogljika in kroma ter izkušnje pri uporabi vakuuma. Na kratko bo predstavljen tudi računalniški program oziroma rezultati modeliranja, ki omogočajo hitro in učinkovito pripravo kompletne tehnologije VOD procesa za peči kapacitete 15 do 100 ton.

Ključne besede: izdelava kvalitetnih, nerjavnih jekel po VOD postopku

Introduction

The steel industry faces a number of problems related to an increasing demand for clean steel imposed by the consumer industry as well as increasing costs pressures. For these reasons, the steel industry is in the past reasoning its steelmaking techniques which resulted in a subdivision into two phases, namely:

- *metallurgy in the melter and,*
- *metallurgy in the ladle.*

Accordingly, most of the metallurgical work shifted from the melter to the ladle which became a metallurgical reactor. The great number of techniques developed in the secondary metallurgy is based on the application of complex vacuum systems. Before choosing among these techniques, the steelmaker must be perfectly aware of the objectives to be achieved and the requirements to be satisfied by the steel product and reasonable in price for the customer, while still generating a profit for the steelmaker.

The technology routes for secondary metallurgy are in no way a standardized task, even where the underlying basic processes are identical. The conditions differ too much from shop to shop. The state of technology by production of high quality stainless steels in Slovenia steelworks will be reported in this lexture, highlighting the vacuum processes using a typ case – stainless steel production as an example.

General overview of vacuum processes

The principles of secondary metallurgical processes used the vacuum can be brierfly described as following remarks:

1. Early in the 1950s, the vacuum degassing of molten steel was developed. The purpose was to reduce the hydrogen content in steel and particulary in forging ingots. The best results were achieved by stream degassing during ladle - to – ladle or ladle - to – ingot teeming[1].

2. In 1955 appeared almost simultaneously the **RH** and **DH** processes which led to the development of degassing facilities with much higher throughputs.

3. In 1956 the first argon injection trials were carried out – the method of stirring and heating whilst degassing – to enable large reaction volume necessary and the comparatively high temperature losses incurred led to the development of new advanced metallurgical techniques as: **ASEA-SKF, FINKL, VAD, VOD** combining new inductive stirring, new refracto-

[1] Prof. Dr. Blaženko KOROUŠIČ, IMT, Lepi pot 11, 61000 Ljubljana

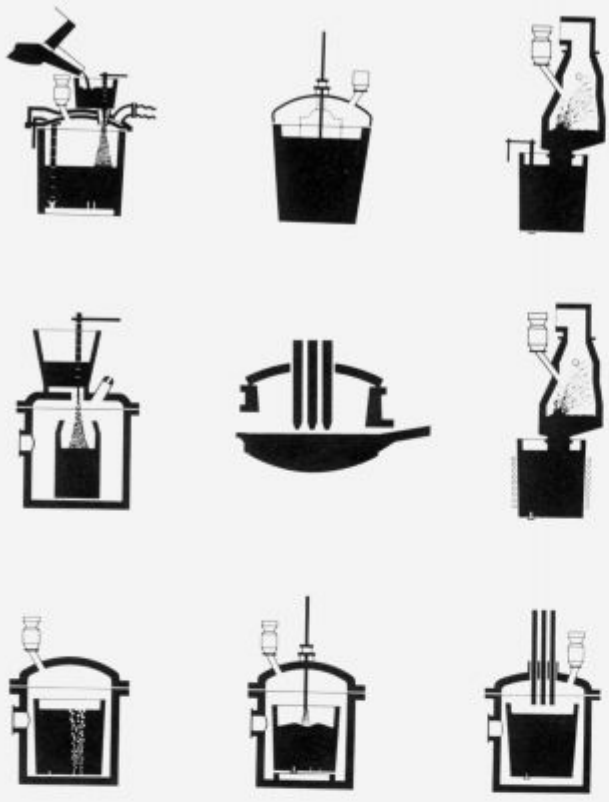

Figure 1: Processing units in the secondary metallurgy
Slika 1: Procesne naprave v ponovčni metalurgiji

ry lining materials, a sliding gate valve and oxygen lancing into the vacuum degassing unit[2-9].

With the industrial application of the above processes, especially vacuum steelmaking equipment passed through several stages of development, see **(Fig. 1)**.

The metallurgical possibilities of vacuum steelmaking have dramatically changed the role of the melting furnace. No longer is it necessary to use a particular type of furnace for the production of particular grades of steel. In other words, all furnace can produce nearly all steels if equiped with a secondary steelmaking facility.

Therefore, the demand for a high availability of the vacuum units is one of the essential factors and the modular concept has proved to be useful in the selection of suitable equipment for each application.

Steel production in Slovenia steelworks was based for more than 120 years on melting in hearth furnaces. During the 1960's and 1970's, the production moved progressively from open heart to electric arc furnace melting.

Vacuum refining began in Steelwork Ravne in 1970 with the installation of the vacuum degassing unit for the removal of hydrogen, particularly for the forging shop. The process did not find a wide application.

Vacuum refining in Ravne began in 1984 with the installation of two VAD/VOD units (20 and 50 tonnes) and some years later also in Jesenice with two 90 tonnes VOD-units with the aim to manufacture more sophisticated steel grades (very low S, O, H, C contents and higher contents in alloys – first of all stainless, dynamo, tool and other high alloyed steels)[10].

1 Some fundamental aspects of metallurgical processes in vacuum

An atmosphere at reduced pressure is one of the purest environments possible. Most of the metallurgical processes are made up of heterogeneous reactions, and the operation in vacuum increases the driving force for interphase mass transfer which is thereby accelerated.

Vacuum processing, compared to air handling, removes the difficulties due to the pick up of oxygen, nitrogen and hydrogen contained in the atmosphere. On the other hand, vacuum processes are concerned with the removal of hydrogen, oxygen, carbon and unwanted non-metallic inclusions from the melt. These benefits are often obtained at the price of same side effects as, for example, the difficulties caused by interaction between melt and refractory linings. Furthermore, just the development of new refractory lining led towards a successful application of vacuum treatment of the molten steel. With introduction of basic linings (magnesite or dolomite) into vacuum ladles began the era of vacuum metallurgical processes.

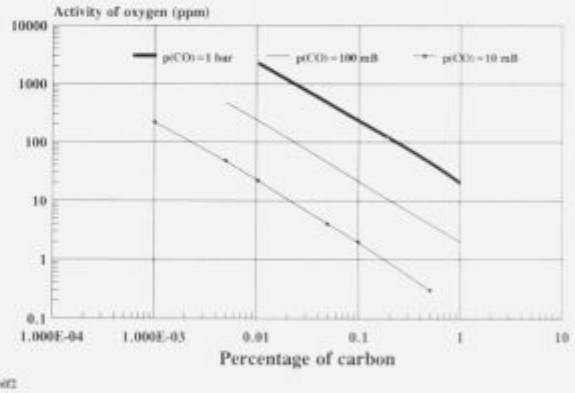

Figure 2: Deoxidation equilibria in liquid iron (1600°C)
Slika 2: Dezoksidacijsko ravnotežje v tekočem železu pri (1600°C)

2 Reactions with carbon and alloying elements

Carbon, probably the most important element in steel, under reduced pressure has a very high affinity towards oxygen, as demonstrated by the following considerations:

For instance, a CO pressure less then 100 Pa is a very effective reaction partner. The principal reaction governing the removal of oxygen by carbon is that producing carbon monoxide:

$$\underline{C} + \underline{O} = CO_g \qquad (1)$$

where:

$\underline{C}$, $\underline{O}$ mean elements C and O are in the melt.

It shows, for instance, that at P_{CO} pressure of 1000 Pa and based strictly on thermodynamic considerations, equilibrium oxygen activity is very low (for the C-content about 0,01 % an oxygen activity of about 20 ppm can be expected).

In the practice this level will be never reached because of the reactions between melt and refractory surface. As will be shown later, the vacuum way of producing stainless steel in VOD-process utilizes low partial pressure of carbon monoxide to the control selective carbon oxydation to prevent the imminent risk of the simultaneously chromium oxidation according to the reaction:

$$2\underline{Cr} + 3\underline{O} = (Cr_2O_3) \qquad (2)$$

where:

( ) means in the slag.

The formation of chromium oxide causes the slag to get crusty. Stirring with argon via the porous plug in the ladle bottom to break the slag layer and keep the metal exposed to vacuum is required.

The selective oxidation of carbon in the molten metal depends on the effective pressure P_{CO}. The fraction of oxygen reacting with carbon appears as CO and CO_2 and the rest as metal oxides (SiO_2, MnO, Cr_2O_3, FeO).

3 Use vacuum by production of the stainless steels

The production of stainless steel represents the specific problem of achieving a very low carbon content together with a high chromium content at the lowest cost. VOD-process **(Vacuum Oxygen Decarburization)** is nowdays the most favourable process for stainless steel production. The VOD – refining is carried out in the teeming ladle which has a basic wear lining and is sufficiently insulated to withstand the aggressive slag at high temperature (over 1700° C) and long heat times (some hours). The conventional way is that the ladle itself with a refractory lined cover constitutes the vacuum chamber or tank degasser of the type VOD-unit (see **Fig. 3**).

Oxygen is supplied at a controlled rate via a consumable refractory lance contained in a vacuum-tight housing on the top of the cover. A water-cooled lance with preferably a laval tuyere is also used. By using the laval tuyere the gas stream is kept concentrated and the distance from the lance tip to the steel surface can be increased to 1200 mm. The process is closely monitored using TV camera mounted on the vacuum cover.

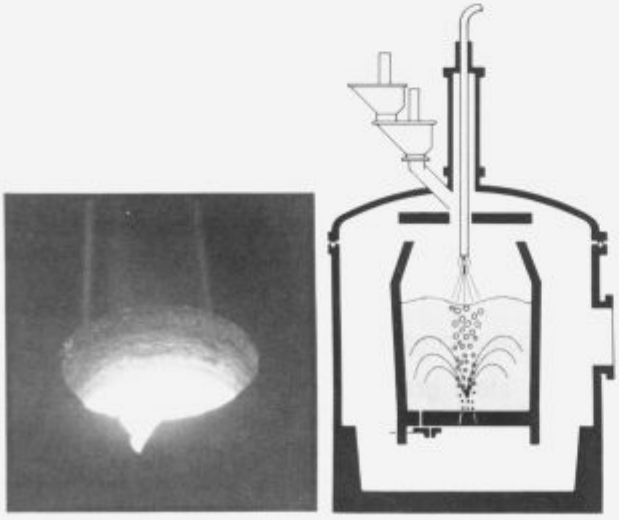

Figure 3: Vacuum oxygen decarburization process (VOD)
Slika 3: Vakuumsko kisikovo žilavenje v VOD procesu

4 Vacuum pumps

For creating vacuum mainly two different types of pumps are in use in the steel industry especially for large units. The most common type is a set of steam ejectors or alternatively a combination of steam ejectors and water ring pumps to save steam consumption, if the cooling water temperature is not too high

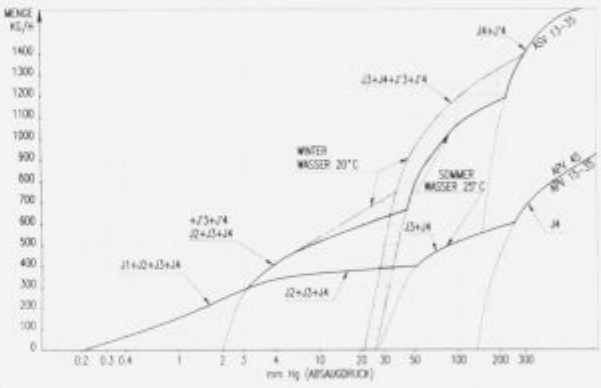

Figure 4: The suction capacity and the chamber pressure for the 30 t VAD/VOD unit in Metal d.o.o. Ravne
Slika 4: Kapaciteta vleka in pritisk v ponovci 30 t. VAD/VOD naprave v Metal d.o.o Ravne

(max. 32° C). The suction capacity at low pressure, i.e. the shape of the pump curve is of special interest for the production engineer. **Fig. 4** shows the pump curve for a 30 tonnes ladle–lid system in Steelwork Metal Ravne. The shape of the curve is very important and had to be flat in the lower pressure regions to prevent the influence of small leakages on the working pressure. To prevent or minimize splashing, the chamber pressure must be kept at constant value for example 90 mbar.

For the heats at Metal Ravne, a 15 tonnes VOD-unit with the oxygen blowing rate about 6 Nm^3 O_2/min, the gas evolution of CO is about 900 kg/h if all oxygen is used for CO-production. For a oxygen yield of 50 % at "end-point" (begin of intensive Cr oxidation) and taking into account the presence of Ar, the *CO + Ar* production will be about 500 kg/h, giving a chamber pressure of 1500 Pa. From practical experiences it is known, that the chamber pressure is a very good

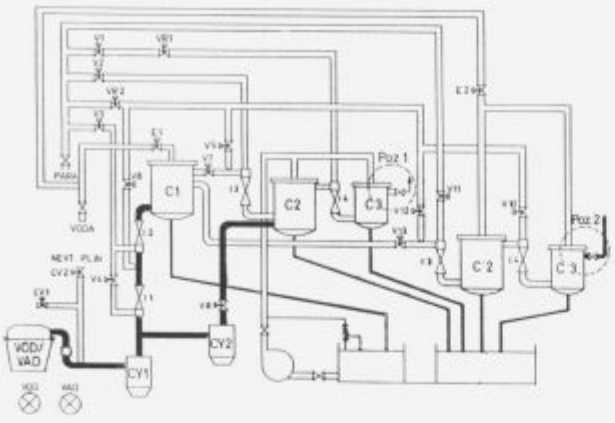

Figure 5: Arrangement of vacuum pump system for the 30 t. VAD/VOD unit
Slika 5: Sistem vakuumskih naprav za 30 t. VAD/VOD napravo

indicator of the boiling reactions and the control of "overboiling" melt which occurr normally at the beginning of the oxygen blowing. To obtain the low working pressures already mentioned the steam ejectors combined with water ring pumps (see example on the **Fig. 5**). As is seen, between the vacuum vessel and the vacuum pump, a gas cleaner/cooler is installed. The cooling is of special importance during the VOD treatment while the gas cleaning always is important for the increased availability of the pumps. The necessary cleaning of the ejectors must be frequent and is difficult.

5 Process control by the production of stainless steels

The vacuum refining process, especially production of stainless steel, present the specific problem of achieving a very high quality at the lowest price. However, from cost and productivity reasons, VOD-process is nowdays a standard way of producing stainless steels in the combination with EAF furnace. The costs of refining treatment, used in the economic assessment depends of the capacity of a unit and use rate, and many other variations of the input prices (the refractory linning, alloys, actual practice, steel grades). In **Table 1** are presented the average total costs for three different capacities of the VOD-units for the production of the steel grade AISI 316L (charge materials, energy consumption, refractory costs, the the vacuum refining treatment, alloys and oxygen + argon).

Table 1: Cost estimate in DM/MELT for the production of the stainless-steel AISI 316L by EAF + VOD route
Tabela 1: Ocena stroškov v DM/talino pri izdelavi nerjavnega jekla AISI 316L po postopku EOP + VOD

VOD-unit	15 tonnes	40 tonnes	90 tonnes
Total (DM)	35.700	90.600	193.950

Comparing the estimated costs reported in **Table 1**, it may be seen that by the production of the stainless-steels, the process control in the plant is of great importance. Technological decisions have to be tacken quickly and exactly since in many cases, for example, the temperature predictions by the smaller VOD-units is very short for manual calculations. The only way to arrive at a result within the time available is to use a computer model. The control of the VOD-process can be divided into two levels:

- Equipment control *(LEVEL 1)*: Including measuring and control of for example the vacuum station, the water-cooled oxygen lance position, alloy-system, etc..
- Process control *(LEVEL 2)*: Including model prediction for oxygen rate, melt temperature and chemical composition during VOD, VCD, slag reduction and finally calculations of alloy and slag additions.

However, from cost and production reasons, very important function has also a third level *(LEVEL 3)* for administration and production planning. A computer model simulation of the **level 2** will be shortly explained.

5.1 General view

The VOD-model for plant process control is developed to serve as an operator guide through the process, assuring an optimum and uniform refining of steel melt in VOD-unit. It will guide and advise the operator through all the different process stages by production of the routine steel grades or operate as an expert system by the introduction of new steel qualities or improvement of the know-how (for example: change oxygen consumable lance with an water cooled oxygen lance).

5.2 Data bank

The data bank contains all the information required for the model simulation for each steel grade according to plant specifications. It contains also all potentially useful data as physical-chemical data for the thermodynamic and kinetic calculations, alloy material characteristics, limited values and so on.

5.3 Process control system

Each steel grade is individually dedicated to a VOD-cycle composed of a number of process steps:

- Oxygen blowing during the VOD-stage,
- Vacuum decarburization,
- Slag reduction,
- Calculation of addition of alloying materials.

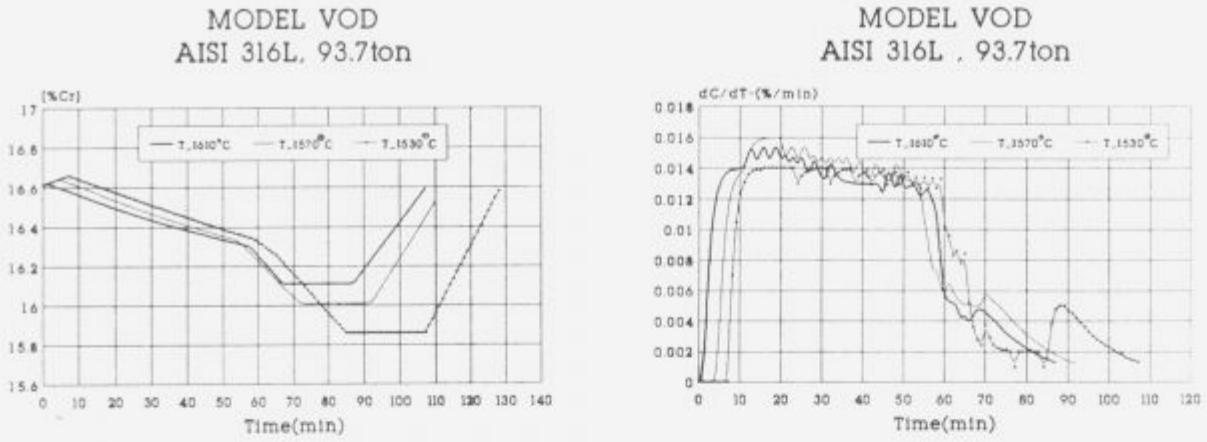

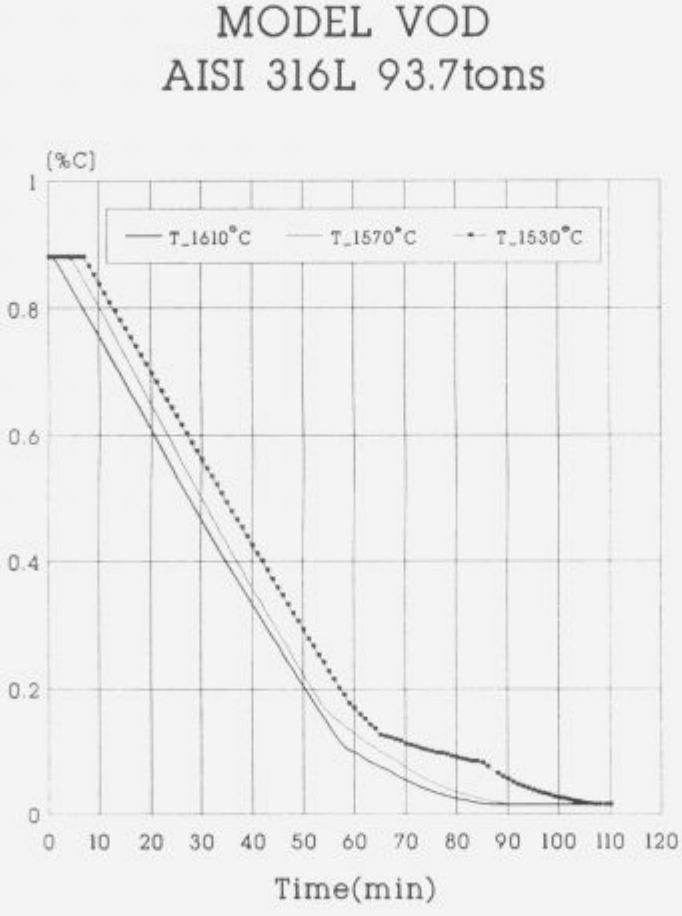

Figure 6: Influence of the initial melt temperature on VOD, VCD and slag reduction processes by the production AISI 316 stainless steel
Slika 6: Vpliv začetne temperature taline na VOD, VCD in redukcijo žlindre pri izdelavi nerjavnega jekla AISI 316

For each process step a number of the influenced input parameters was previously defined, such as: *initial temperature and chemical composition, process time prediction, thermal losses and energy absorbtion during the oxydation period and so on.* **Fig. 6** shows an example the complexity of the influence initial melt temperature on VOD, VCD and slag reduction by the production of the stainless steel AISI 316 in 90 t. VOD-unit.

During the oxygen blowing in VOD, carbon content in melt decreased linearly with the reaction time to about 0.1 % C. Below this carbon content, the oxi-

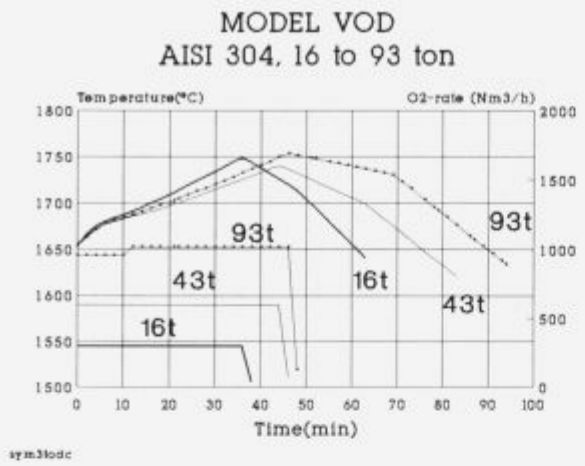

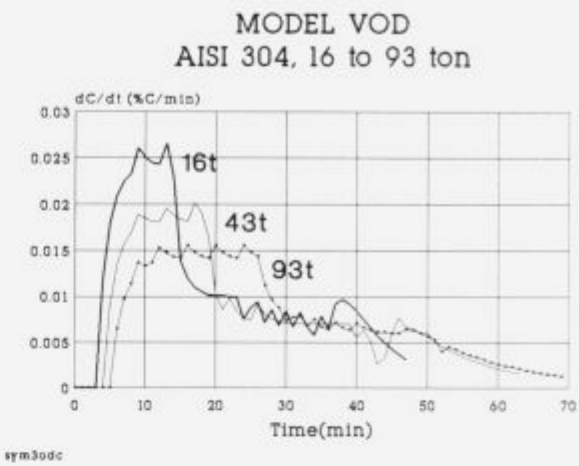

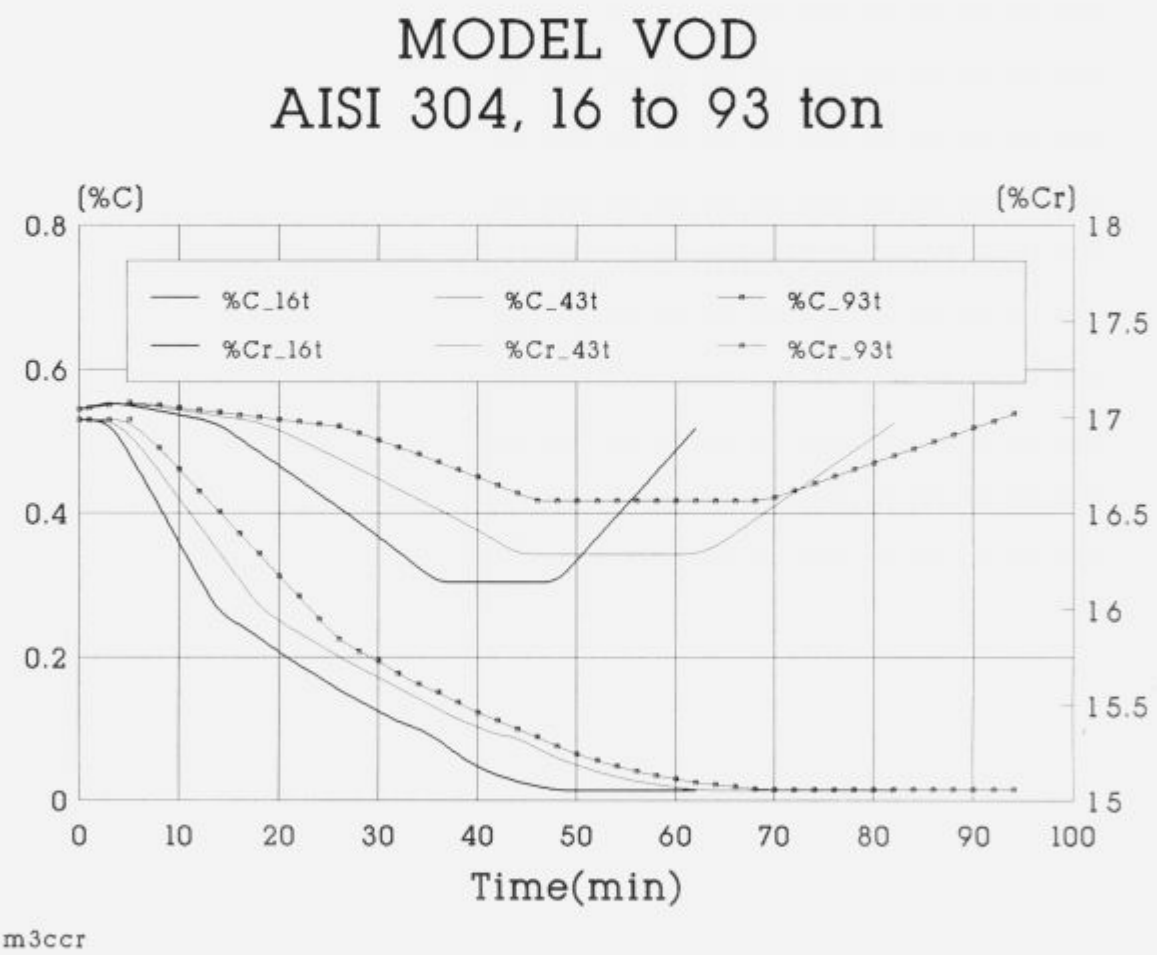

Figure 7: Carbon - Cr oxidation, temperature profile and decarburization rate in austenitic steel AISI 321 for 14.0 ton VOD-unit

Slika 7: Ogljik – krom oksidacija, temperaturni profil in hitrost razogljičenja pri izdelavi nerjavnega jekla AISI 316

dation of chromium was accelerated causes the formation of chromium oxide and slag getting in crusty. A varying starting temperature may have to be compensated by a change in starting analysis in order to reach a correct "carbon end point". Based on the analysis of a simulating model calculation taking into account the thermal losses in the VOD-ladle, an indicative calculation of the VOD-process is done according to principles reported from author[10,11] (see **Fig. 7**).

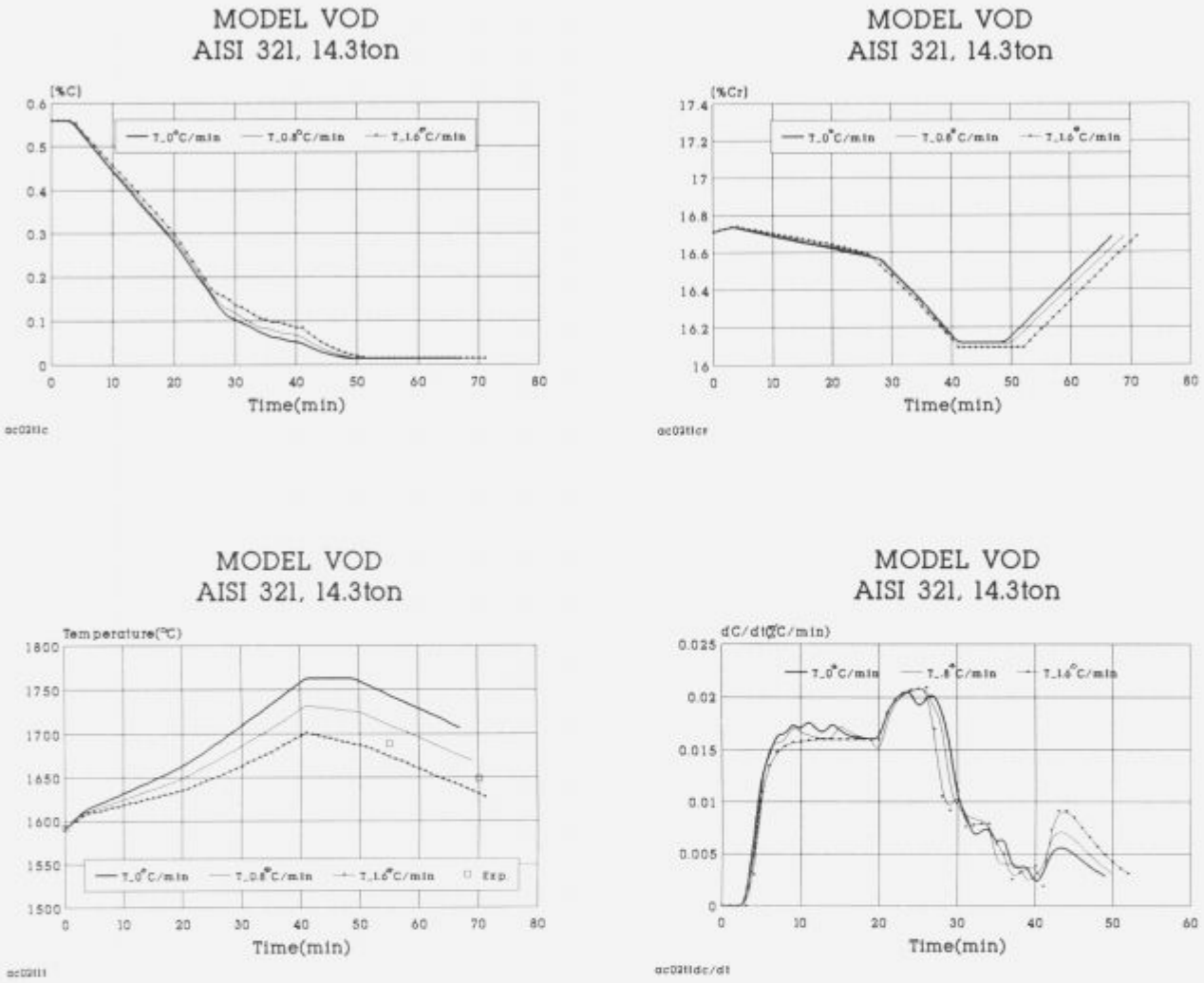

Figure 8: Influence of the unit capacity on metallurgical processes for the same input parameters as in **Fig. 7**
Slika 8: Vpliv velikosti peči na metalurške procese za enake vhodne parametre kot na **sliki 7**

Let us consider the typical example, presented in **Fig. 8** to show influence of the unit size on the metallurgical processes of VOD-technology, for the same input process parameters.

Presently the making of stainless steels and other alloyed steels with a short process time between the process steps is of great importance. As we learnt from this examples, the process modelling, combined with quick-reacting measuring devices helps to improve the vacuum process technology and it is the main purpose of our present and future work. The combination optimal of slag metallurgy and vacuum treatment is not yet accomplished.

References

[1] Tix, A.: Degassing of steel under vacuum-practice for large forging steel (ingots). *Stahl und Eisen*, 76, 1956, 61–68

[2] Eggenhofer, A., Kaiser, G., Bauer, F.: Operating experiences with a vacuum heating plant for 50 tonne heats, *Berg - und Hüttenmanische Monatshefte*, 119, 1974, 338–343

[3] Baitey, W. H.: Finkl VAD steelmaking at BSC River Don Works, *Ironmaking & Steelmaking*, 4, 1977, 209–215

[4] Tiberg, M., Buhre, T., Herlitz, H.: The ASEA-SKF process for the refining of steel, *ASEA-Z.*, 11, 1966, 3, 47–50

[5] Schmidt, M., Etterich, O., Bauer, H., Fleischer, H.J.: Production of high alloy special steels in the basic oxygen

converter (I), Plants and process (II), Metallurgical basis for the oxidation of high-chromium-iron-carbon allos, *Stahl und Eisen*, 88, 1968, 153–168

[6] Bauer, H., Etterich, O., Fleischer, H. J., Otto, J.: The reducing and oxidising vacuum treatment of alloy steel heats, *Stahl und Eisen*, 90, 1970, 725–735

[7] Baum, R., Zorcher, H.: Vacuum oxygen process, *Metals Society Proceedings*, London, May 5–6, 1977, 69–72

[8] Baum, R., Hentrich, R., Yun, Z., Zorcher, H.: The refining of stainless steel in a vacuum-oxygen refining unit, *Stahl und Eisen*, 95, 1975, 8–11

[9] Suzuki, Y., Kuwabara, T.: Secondary steelmaking: review of recent situation in Japan, *Proceedings of the Iron and Steelmaking Conference*, London, May, 1977, 4–13

[10] Koroušič, B.: Use of vacuum in modern metallurgical processes (Uporaba vakuuma v sodobnih jeklarskih procesih), *XI. jugoslovanski vakuumski kongres*, Gozd Martuljek, 17-20. april 1990

[11] Koroušič, B.: VODMET - a general computer program for the simulation of the VOD process for production stainless steel and Ni-based alloys, *The ninth inter. Vacuum Metallurgy Conference on Special Melting*, 1989, April 11–15., San Diego, California, USA

Kovine, zlitine, tehnologije / letnik 29 / 1995 / št. 3–4 / strani 385–390

Electron Beam Welding of Chromium-Nickel Stainless Steel to Duralumin

Varjenje krom nikljevih nerjavnih jekel in duraluminija z elektronskim curkom

Grodzinski A.,[1] J. Senkara, M. Kozlowski, Institute of Vacuum Technology, Warsaw

The paper describes the results of producing and testing joints between duralumin and austenite stainless steel by means of $AgMg_2$ filler metal shims and the electron beam welding method. The structure of the joints was examined using optical microscopy, scanning electron microscopy and electron probe microanalysis. Some mechanical and other properties of the joints, such as microhardness, ultimate tensile strength, impact strength and vacuum tightness were also examined in the relation to welding parameters. The results point out the possibility of application of the joints in vacuum technology.

Key words: electron beam welding, Cr-Ni stainless steels, duralumin, welds, microstructure, mechanical properties

V članku so opisani postopki izdelave in testiranje zvarov med duraluminijem in austenitnim nerjavnim jeklom z uporabo $AgMg_2$ klina in varjenjem z elektronskim curkom. Struktura zvarov je bila določena z optičnim mikroskopom, vrstičnim elektronskim mikroskopom in elektronskim mikroanalizatorjem. Nekatere mehanske lastnosti zvarov kot mikrotrdota, natezna trdnost, udarna žilavost in vakuumska tesnost, so bile izmerjene v povezavi s parametri varjenja. Rezultati kažejo možnost aplikacije zvarov pri vakuumskih tehnologijah.

Ključne besede: varjenje z elektronskim curkom, Cr-Ni nerjavna jekla, duraluminij, zvari, mikrostruktura, mehanske lastnosti

Introduction

Welding of aluminium and its alloys to steels is a difficult but technologically important problem. Direct welding of the two metals is not possible, even using high energy low heat input electron beam (EB) welding methods[1,2].

The main reason for the lack of weldability is based on the metallurgical incompatibility between aluminium and iron. Despite the existence of limited α solid solution of Al in Fe, Fe is almost completely insoluble in Al, and the two metals create several brittle intermetallic compounds[3].

In addition, physical and chemical properties of the metals are significantly different. Large differences in melting temperature, thermal conductivity, and linear thermal expansion coefficients are especially notable. The latter mismatch may cause the generation of cracks in the weldment as a result of high residual stesses during cooling on the one hand, aggravated by the presence of brittle intermetallic compounds on the other. As for welding duralumin to steel, numerous alloying additions complicate the structure of the weld. Difficulties are related to the tendency for hot cracking in such aluminium alloys, a vaporization of some volatile elements (e.g. magnesium), and, last but not least, damage to the precipitates in the heat affected zone. Problems related to the EB welding of heat treatable duralumins are discussed in [4–6].

The aim of the present study was to investigate the welding of chromium-nickel stainless steel to duralumin by means of the EB process using a filler metal shim made of an alloy that is metallurgically compatible with both materials being joined.

[1] Dr. Sc. A. Grodzinski
Institute of Vacuum Technology
44/50 Dluga Street
00–241 Warsaw, Poland

Materials and experimental details

6 mm thick sheets of PA6 alloy (nominal composition $AlCu_4$, 5Mg0,5) and 1H18N9T stainless steel (18–8 type) were used. The chemical compositions of both materials are presented in **Table 1**.

Table 1: Chemical composition of materials

Material	C	Mn	Cr	Ni	Ti	Cu	Mg	Zn	Al	Fe
PA6*	–	0,6	–	0,1	0,1	4,5	0,4	0,1	rem	0,4
1H18N9T**	0,1	1,6	17,3	8,7	0,4	–	–	–	–	rem

* The nearest ASTM equivalent 2024
** The nearest ASTM equivalent 304

The structure of the stainless steel before welding was characterised by a carbon supersatured austenite with small amount of carbides and included approximately 5% of ∂ ferrite. The duralumin alloy was annealed at 500° C for 18h, water-quenched to 5° C, and then naturally aged for 100h. As a result, a uniform, precipitation hardened structure was obtained.

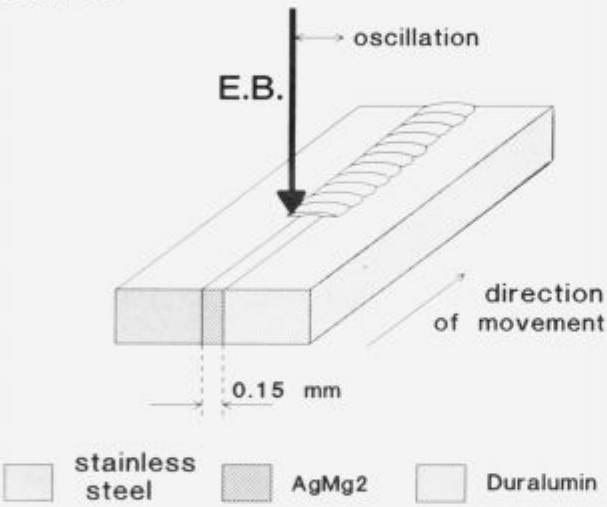

Figure 1: The principal scheme of obtaining of the duralumin-stainless steel joint applied in the work

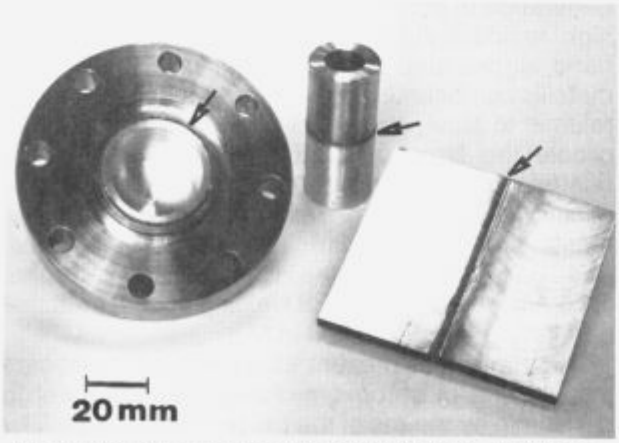

Figure 2: Electron beam welded duralumin – stainless steel joints of different types

After some preliminary study, silver, copper and some of their alloys were chosen as the materials for filler shims. The criteria for the selection was the metallurgical compatibility with each of base metals, a melting point between the fusion temperature of the steel and the duralumin, and a good ductility. The filler metal shims were applied in the form of 0,15 mm thick foil. After the trial experiments, it was clearly seen that AgMg2 alloy is the most perspective and it was used in all further experiments. The arrangement for producing a joint is presented in **Fig. 1**. The joint was produced by means of electron beam welding. A WS 6/25 type EB welder made in the Institute of Vacuum Technology was employed. The constant parameters for welding were: a working pressure of 10^{-2} Pa in the chamber and an accelerating voltage of 30 kV, while the beam current and welding speed were changed over a wide range. In all experiments, the focused beam (spot size diameter of 0,4 mm) was directed onto the edge of the material with the higher melting point (i.e. steel) and oscillated (frequency 1000 Hz, amplitude of 2 mm).

Based on the experimental results obtained, specially prepared joints of different types were manufactured taking advantage of the optimal welding parameters: face-to-face straight-line (butt) joints, sleeve-to-sleeve circumferential joints, and sleeve-to-flange circular joints as presented in **Fig. 2**. Vacuum tightness of these joints was examined by the use of Leybold UL 100 helium mass spectrometer.

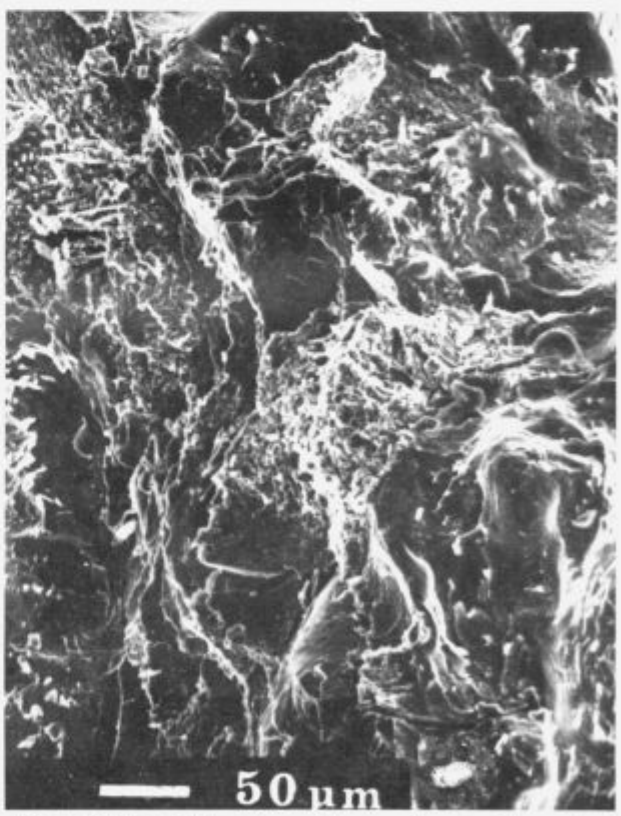

Figure 3: Typical fracture of duralumin – stainless steel joint obtained by presented method

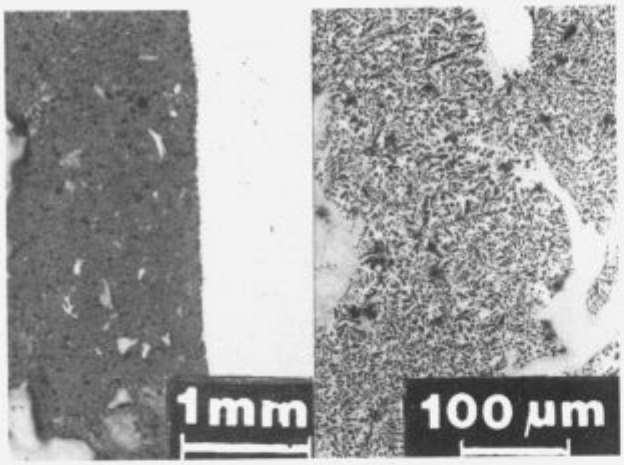

Figure 4: Cross-section of the joint: steel particles dispersed in the weld

Results and discussion

As a result of applying the filler metal shim made of AgMg2 alloy, faultless joints were obtained with good appearance of the weld face and root, and free of macrodefects in the form of cracks after cooling. **Fig. 3** shows the fractographs of such joints which show a ductile character. This fact suggest that no brittle intermetallic compounds appeared.

In **Fig. 4**, the cross-section of a weldment is presented at low magnification. Irregular steel inclusions are seen inside the weld fusion zone which render the joint like a composite material. There is no doubt that this structure was formed as a result of partially melting of the steel substrate, as the EB was directed onto it, leading to transport of liquid steel droplets in the bulk of the bead. The effect is of positive character because mechanical properties of the joints increase as a result of strengthening by these steel particles.

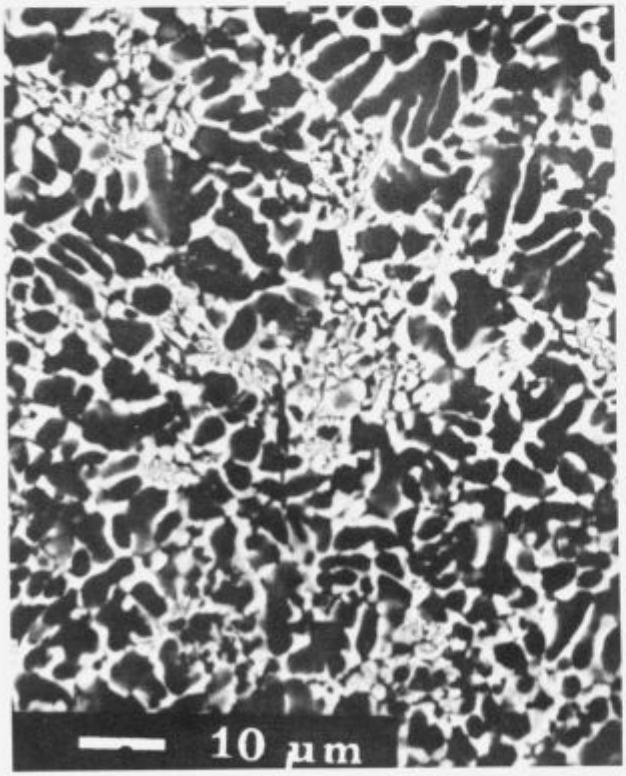

Figure 5: Microstructure in the middle region of the joint

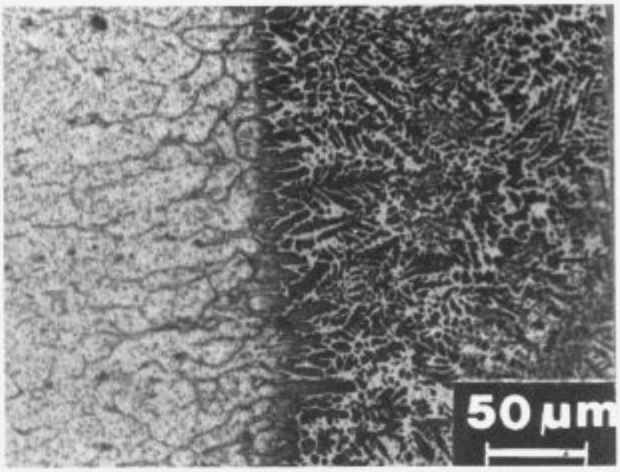

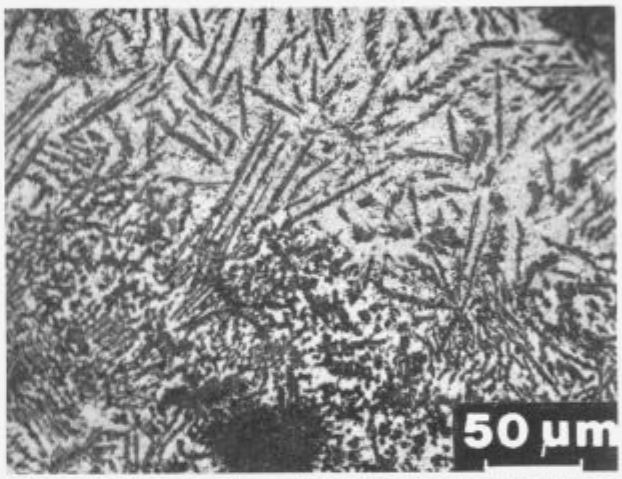

Figure 6: Microstructure of the joint close to fusion lines;
a) duralumin – weld interface,
b) stainless steel – weld interface

The structure in the middle of the weld is shown in **Fig. 5** at higher magnification. It consists of two phases as recognised by XRD and EPMA methods. One of them is the Ag in Al solution (dark phase), while the secondary – solid solution on the basis of Ag_2Al intermetallic compound (light phase). A small copper amount of order of 1% by weight is dissolved in both phases. Nevertheless, no brittle intermetallic phases known from Al-Fe equilibrium diagram have been observed inside the weld and in the vicinity of two fusion lines.

The duralumin-weld and steel-weld interfaces are shown in **Fig. 6 a, b**. Both boundaries are of continuous character and feature no defects. However, some interlayers of different structure situated close-to-interfaces can be observed. The weld near the boundary with steel is of acicular structure whereas in the vicinity with duralumin – dendritic. In the region of fusion line in steel the macroscopic effect of mixing of

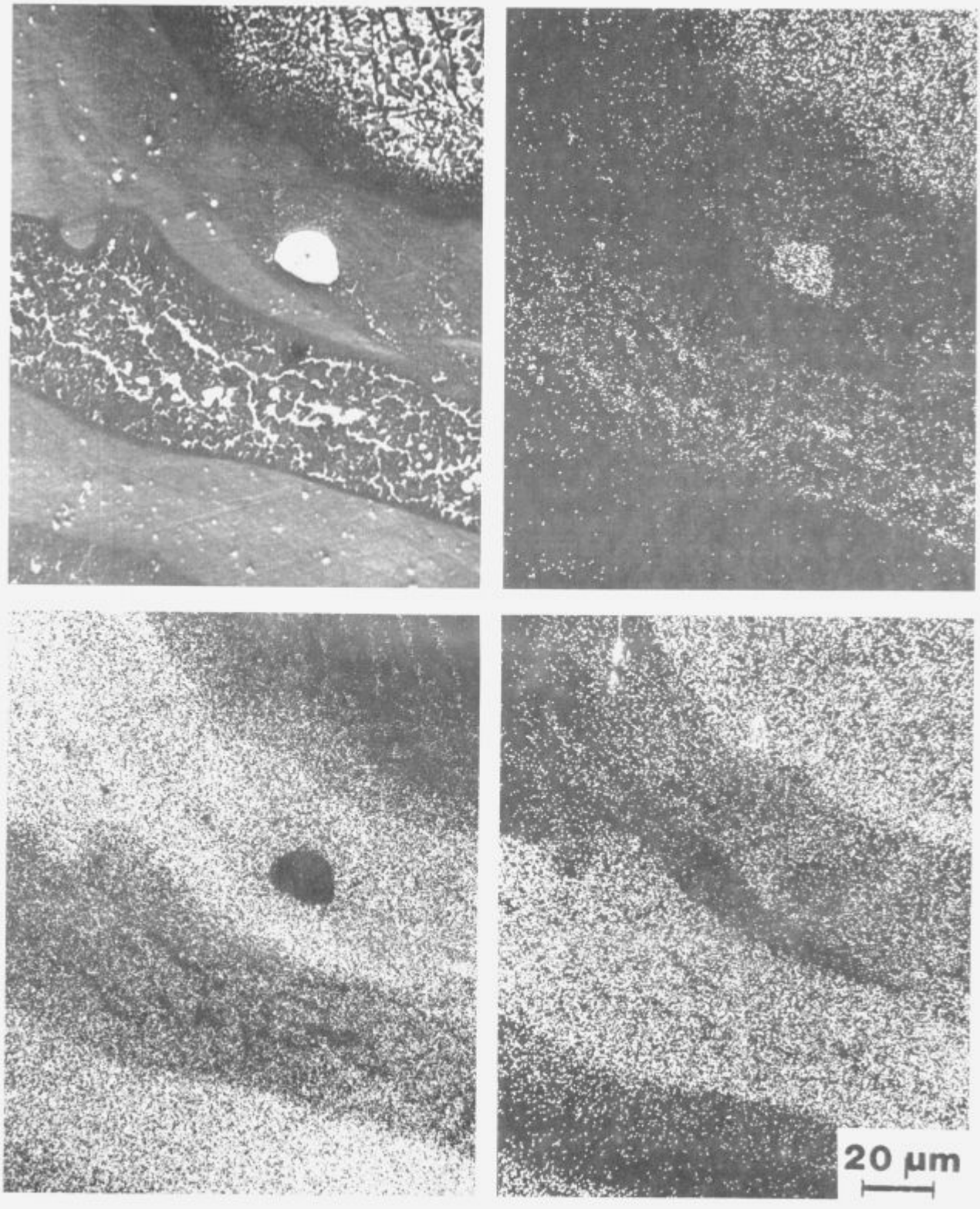

Figure 7: Macroscopical effect of phase intermixing in the vicinity of stainless steel – weld interface:
a) secondary electron image; surface distribution of elements:
b) – Ag,
c) – Fe,
d) – Al

the two materials due to intensive motion of the molten pool followed by fast cooling ratio is remarkable. As the illustration of it may serve **Fig. 7** which presents the mixture of Al-Fe solid solution and multi-phase weld material as well as surface distribution of base elements: aluminium, iron and silver. The "sandwich" character of the joint and visible silver inclusions evidence dynamical, non-equilibrium process of forming of the joint as well as its complicated character. Nevertheless, it should be expected that such constitution of the interface region promotes the decrease of welding stresses.

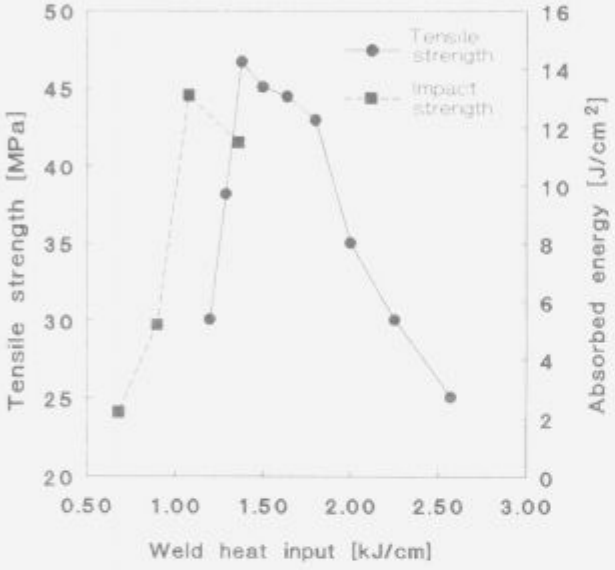

Figure 8: Relationship between ultimate tensile and impact strength of the joint and weld heat input

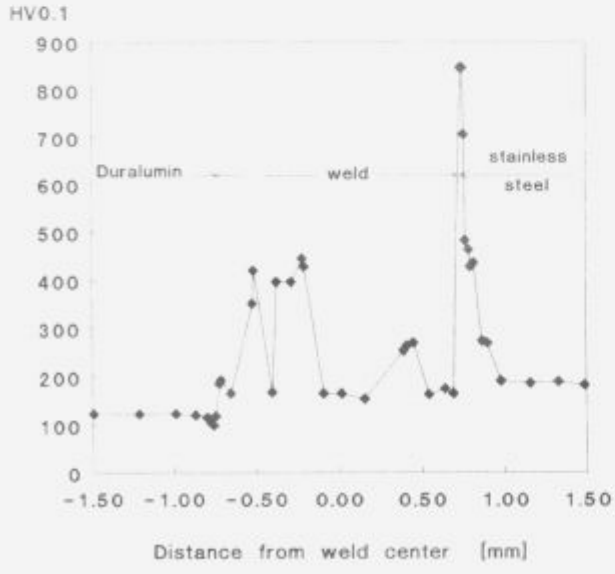

Figure 9: Microhardness distribution in the cross-section of the joint

As the decisive quality tests of stainless steel – duralumin weldments with $AgMg_2$ filler metal shim, the ultimate tensile strength test and impact test were applied. The graphs of the relationship between tensile strength, absorbed energy and weld heat input point out the fact that the best joints are obtained in the energy range of 1,4–1,8 kJ/cm **(Fig. 8)**.

Microhardness (μHV 0,1) profile in the cross-section of EB welded joint is presented in **Fig. 9**. An average microhardness of ca. 150 μHV increases up to 350–450 units in the places where steel inclusions exist. Some decreasing of microhardness in the vicinity of the fusion line in AlCu4,5Mg can be also observed. This area corresponds with the previously determined zone of diminished Mg content. However, microhardness of the material close-to fusion line from the stainless steel side rapidly increases up to the value of 850 μHV. This effect is connected with the separation of chromium carbides and may be considerably diminished by suitable post-weld heat treatment.

A leak detection demonstrates the dependence of the vacuum tightness on the type of joints **(Table 2)**. The butt and also circumferential joints feature satisfactory levels even after multi-time bakeouts whereas circular joints are not sufficient tight. In the last case it is probably connected with the presence of microdefects caused by high thermal stresses resulted in turn from the closed character and big diameter of the joints.

Table 2: Vacuum tightness of different types duralumin – stainless steel joints

Type of the joint	Vacuum tightness (mbar l/s)	Remarks
face-to-face (butt)	$<10^{-10}$	without bakeout
face-to-face (butt)	$<10^{-10}$	with 200°C, 3 x 1h bakeout
sleeve-to sleeve (circumferential)	$<10^{-10}$	without bakeout
sleeve-to-sleeve (circumferential)	$<10^{-10}$	with 200°C, 3 x 1h bakeout
sleeve-to-flange (circular)	$2 \times 10^{-7} \div 7 \times 10^{-9}$	without bakeout

Conclusions

It was stated that it is possible to join AlCu4,5Mg aluminium alloy and 18–8 type chromium-nickel stainless steel using an EB welding method and a filler metal shim in the form of foil made of $AgMg_2$ alloy.

During the welding, macroscopic steel particles are dispersed in the volume of molten pool. A two-phase structure of the weld is formed as a result of solidification, it consists of supersaturated Ag in Al solid solution and the secondary solution on the basis of Ag_2Al intermetallic phase, strengthened by inclusions

of stainless steel. Continuous interlayers without defects are created in the form of solid solutions. On the other hand, Al-Fe intermetallic compounds, characteristic for the phase equilibrium diagram, are not formed. "Composite" constitution and the lack of brittle phases in the weld are decisive factors influencing on the formation of the joint and its strength properties of the joints.

Some weldments obtained by the presented method may be used in construction of low loaded elements in vacuum technology.

References

[1] *Welding Handbook*, 8th ed. (AWS Miami Fl., 1991)

[2] *Electron Beam Welding*. Leybold-Heraeus Catalogue, 1989

[3] T. B. Massalski (ed.), *Binary Alloy Phase Diagrams*, 2nd ed. (ASM Int., 1990)

[4] Y. Arata, M. Ohsumi, Y. Hayakama, *Trans. Jap. Weld. Res. Inst.*, 5, 1976, 1, 19

[5] A. M. Kosecek, A. Bendis, J. Bosansky, P. Gabriska, *Proc. Int. Conf. on Electron Beam Welding Technologies*, Varna-Sofia 1985, 247

[6] A. Grodzinski, J. Senkara, *Przeglad Spawalnictwa*, 45, 1993, 1, 2

Kovine, zlitine, tehnologije / letnik 29 / 1995 / št. 3–4/ strani 391–395

Modification of Steel Surface with Nickel Alloy by an Electron Beam

Modifikacija površine jekla z navarjanjem nikljeve zlitine z elektronskim curkom

Kozlowski M[1]., Institute of Vacuum Technology, Warsaw, Poland, J. Senkara, Warsaw University of Technology, Warsaw, Poland

The paper presents the results of research concerning the production of Ni-base alloy layers on the structural, low-alloyed steel by scanned electron beam (EB) treated as a surface heat source of rectangular power distribution. Under the action of EB, Ni-base alloy powder previously deposited onto the steel surface was melted forming new, thick (0,2 ÷ 0,6 mm), continuous surface layers with satisfactory adhesion to substrate. The beam current was regulated in the range 25 ÷ 100 mA and the exposure time was controlled by a speed of specimen movement in the range 30 ÷ 190 mm min-1. 21 kV accelerating voltage and 10^{-2} Pa pressure in the vacuum chamber were applied in all tests. The structure of layers was investigated using optical microscope, SEM, EPMA and XRD methods. Microhardness measurements, and dependence of thickness of layers and depth of melted zones on process parameters are also presented. The wear resistance is compared between layers obtained by EB and by conventional methods.

Key words: electron beam surfacing

Prikazani so rezultati raziskave izdelave tankih navarjenih plasti na osnovi niklja na konstrukcijsko nizko legirano jeklo z vrstičnim elektronskim curkom, ki smo ga uporabili kot izvor toplotne energije s pravokotno porazdelitvijo moči. Pod vplivom elektronskega curka, se je predhodno nanesena zlitina na osnovi niklja v obliki prahu na površino jekla, raztalila. Nastala je nova zvezna plast, debeline 0.2 do 0.6 mm z zadovoljivo adhezijo na substratu. Tok elektronskega curka je variiral v območju 25 - 100 mA, čas izpostave je bil kontroliran s hitrostjo gibanja vzorca v območju 30 - 190 mm na minuto pri napetosti 21 kV, tlak v delovni komori je bil 10^{-2} Pa. Strukturo plasti smo določili z optičnim mikroskopom, SEM, EPMA in XRD metodami. Podane so tudi meritve mikrotrdote v odvisnosti od debeline plasti in globine talilne cone. Izdelana je primerjava obrabne odpornosti med plastmi navarjenimi z elektronskim curkom in plastmi navarjenimi s konvencionalnimi metodami.

Ključne besede: navarjanje z elektronskim curkom

1 Introduction

One of the advanced surface modification methods is the melting of material layer deposited onto metal surfaces by the use of oscillating electron beam (EB). A little penetration depth of the scanning EB, and specific conditions of solidification and cooling, yield to the formation of surface layers with different structure and properties, in comparison to layers obtained by other conventional methods. High density power of EB allows to produce practically any metallic-base layers (see [1-4], for instance).

The paper presents the results of experimental study carried out to produce, by the method under discussion, hard, anti-wear, heat-resisting Ni-alloy base layers on the low-alloyed, structural steel surface.

2 Materials and experimental procedure

2.1 Preparation of samples

Low-alloyed TStE355 steel (acc. to DIN Standard No 17100-83) was used as a substrate, whereas Ni-alloy in the form of powder, as the layer material. The chemical composition of the both materials used is presented in **Table 1**.

[1] Dr. Sc. Miroslaw KOZLOWSKI, Institute of Vacuum Technology, 44/50 Długa Street, 00-241 Warsaw, Poland

Gas-atomised Ni-alloy powder consisted of spherical particles of 100 ÷ 300 μm in diameter. The phase analysis (XRD) revealed that the solid solution of Cr and Fe in Ni was the dominant phase with a small amount of Ni_3Fe intermetallic compound and silicides. The range of fusion temperature (solidus-liquidus) of the alloy, determined by differential thermal analysis (DTA), was 1299 ÷ 1318 K.

Table 1: Chemical composition of stellite powder and base steel

Stellite powder	Base steel
C - 0,3 %	C - max 0,2 %
B - 2,2 %	Mn - 1,00÷1,15 %
Si- 3,8 %	Si - max 0,04 %
Fe- 2,5 %	P - max 0,04 %
Cr- 7,0 %	S- max 0,04 %
Ni- balance	Cr - max 0,3 %
	Ni - max 0,3 %
	Cu - max 0,3 %

The steel was cut into 50 x 40 x 10 mm plates, ground and degreased. The plate surfaces were coated with a paste consisting of Ni-alloy powder, and then the deposited layer was dried to evaporate the organic paste carrier. The spread layer about 0,5 mm thick, had a satisfactory adhesion to substrates and sufficient for sample manipulation. Such prepared layers were melted by the oscillating EB.

2.2 Melting of surface layers

The specimens were moved under the scanning EB and a melted material path was produced on the surface. The liquid wetted the substrates which in some variants were also partially melted. The principle of the method is presented in **Fig. 1a**. The oscillating EB created a moving, rectangular type melted zone **(Fig. 1b)**.

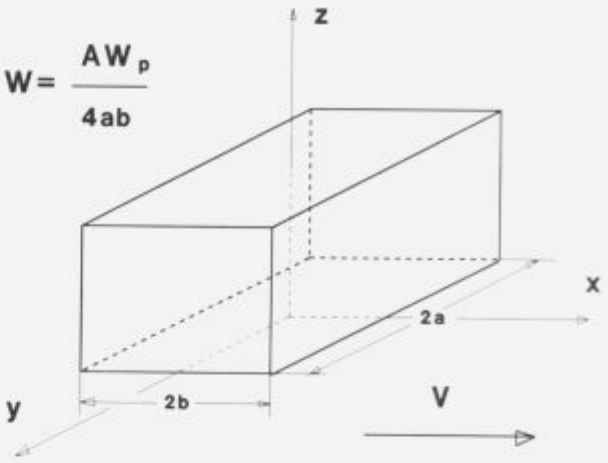

Figure 1b: Surface heat source with rectangular distribution of power (1)

A 6 kW/25 kV electron beam welder, developed in the Institute of Vacuum Technology, additionally equipped with a dynamic deflection coil system, was employed. EB was deflected with frequencies of 15,625 kHz and 50 Hz, respectively, in two perpendicular directions. All experiments were carried out by the oscillation amplitude of 10 mm, focused beam (spot size at the surface of 0,5 mm) and the 21 kV accelerating voltage. The pressure in the vacuum chamber remained below 10^{-2} Pa. The power of heat source was regulated by the beam current in the range of 25 ÷ 100 mA, and exposure time - by a speed of specimens movement from 30 to 190 mm min^{-1}.

2.3 Examination of layers

Structural tests included X-ray phase analysis (XRD) of layer surface as well as investigations of cross-section of samples by optical and scanning electron microscopy (SEM). Electron probe micro-

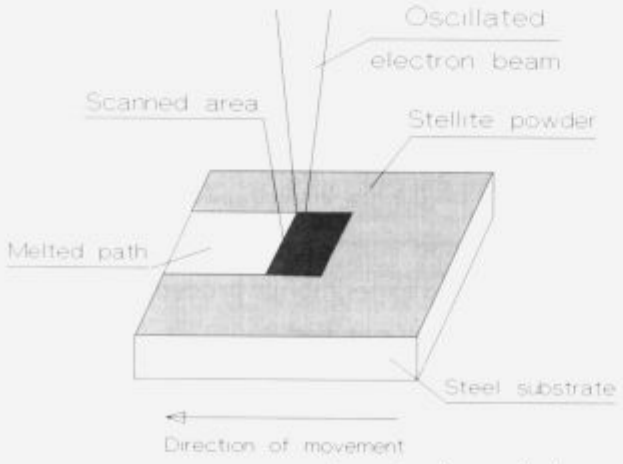

Figure 1a: Scheme of layer formation by an electron beam method

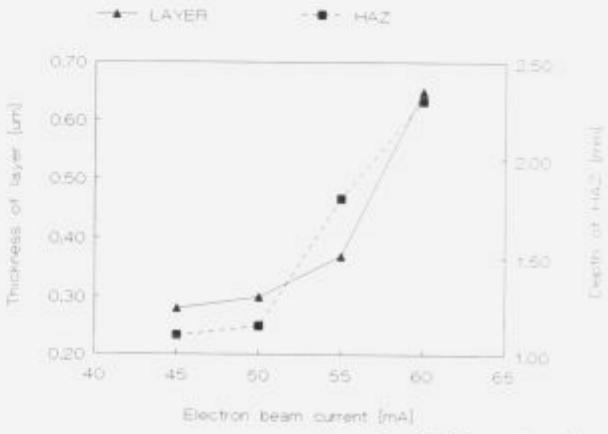

Figure 2: Layer thickness and depth of HAZ as a function of electron beam current

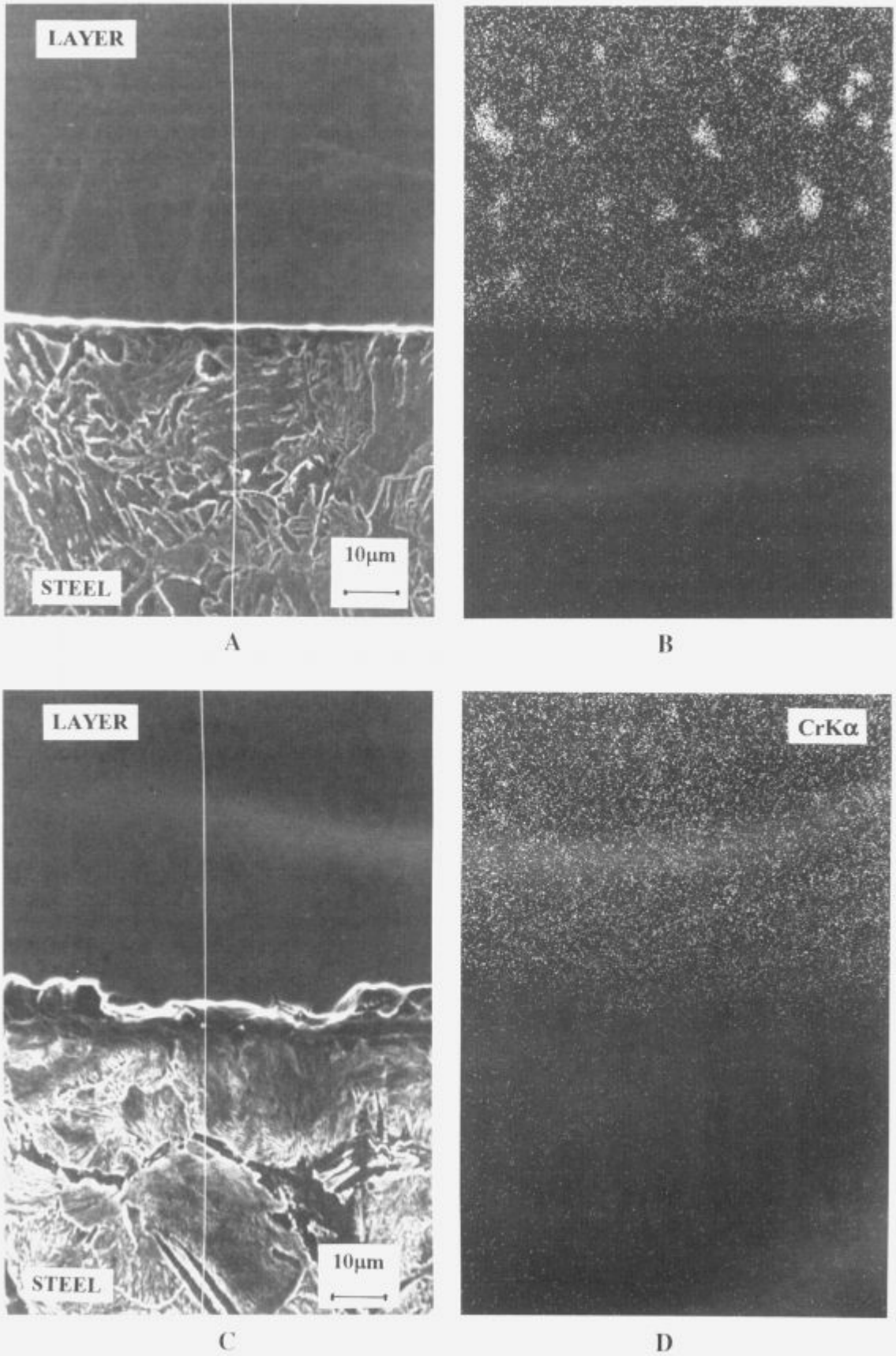

Figure 3: SEM microstructure close-to layer-steel interface and maps of Cr distribution in samples obtained by 45 mA **(a, b)** and 60 mA **(c, d)**

analysis (EPMA) was also used fot the determination of the elements distribution and concentration.

Mechanical testing consisted of Vickers hardness measurement of layer surfaces, and microhardness determination in the interface region with the 100 g load (HV 0,1). The structural observations and hardness results were related to the process parameters.

The wear resistance of samples was determined in the Steyer device according to ISO/TR Standard No 7144. The wear test pieces were produced by cutting and grinding 3 mm diameter and 10 mm length cylinders with Ni-alloy modified faces, from previously obtained plate specimens. The test samples were pressed with a 6,3 N/mm^2 load against the tool steel friction disk rotating at a speed of 250 r.p.m.. For comparison wear test on identical samples were carried out using the same materials, by oxyacetylene hardfacing, plasma transferred-arc hardfacing and plasma spraying.

3 Results and discussion

The diffraction pattern of surface layers are quite similar to the initial Ni-alloy powder spectrum. The only difference is connected with the diminution of line intensity of the Ni_3Fe phase, which was partially dissolved under the action of EB.

The relationships between thickness of produced layers, the depth of heat affected zone (HAZ), and beam current is presented in **Fig. 2**. With the increase of EB power density the substrate begins to melt and the liquid Fe is transferred into the layer. Hence the thickness of the layer represents the balance between the increasing amount of liquid on the one hand, and the higher evaporation rate on the other. The depth of HAZ increases with increasing beam power.

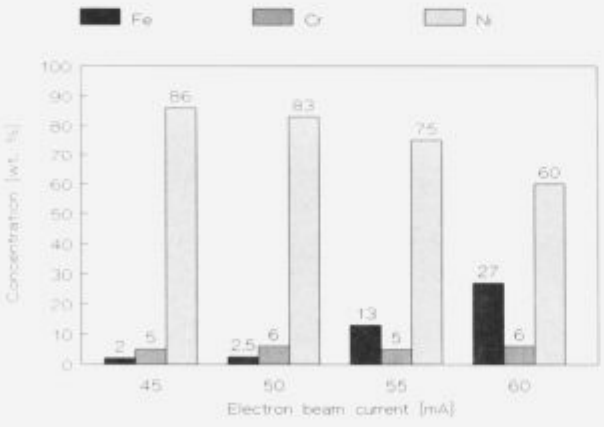

Figure 4: Concentration of main elements in layers as a function of EB current

Significant segregation of chromium was observed in layers obtained by relatively low beam current because this element had no sufficient time to dissolve. This segregation decreased with the increase of the heat delivered. It is clearly seen in **Fig. 3** which shows the structures in the vicinity of interfaces and the maps of chromium distribution for the two layers obtained with the same exposure time and different beam currents. The increase of EB power yielded to the partially melting of substrate and the formation of a liquid Ni-Fe-Cr solution by mixing. As a results of the process, the increase of Fe concentration in the layers from initial 2 wt.% in the powder up to 27 wt.% was observed **(Fig. 4)**.

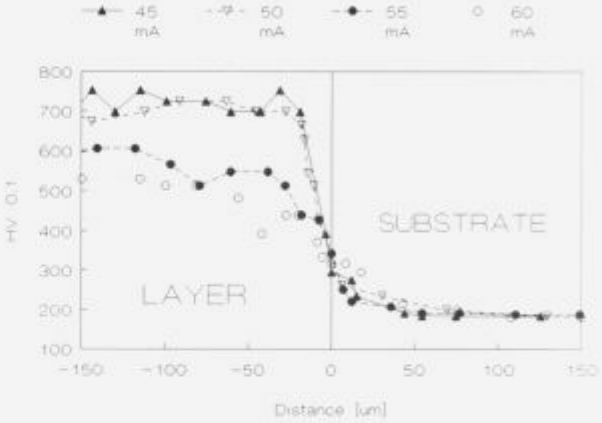

Figure 5: Microhardness distributions across the layer-substrate interface

The structure of layers was dendritic. The microstructure in HAZ was of perlite, bainite and martensite as well as cracks and separations inside the HAZ, in layers and at interfaces were not observed.

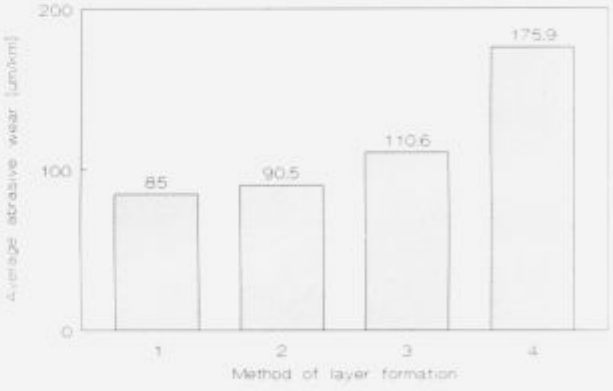

Figure 6: Abrasive wear of layers formed by different welding techniques: 1-EB, 2-Plasma hardfacing, 3-Oxyacetylene flame hardfacing, 4-Plasma spraying

A close relationship is visible between the supplied energy density, which is the product of beam power density and exposure time, and the layer hardness **(Fig. 5)**. Both surface hardness and microhardness at the cross-sections, decreased with the increase of heat delivered due to dissolution of Fe in the layer. For low beam currents only little amount of substrate was melted and the layers were relatively thin (0.2 ÷ 0.3 mm) and hard (HV 0,1 > 700 units).

Due to the action of high power density EB, deep melting of the substrates occured. The layers became thick (0,6 ÷ 0,7 mm) and significantly less hard (HV 0,1 < 500 units).

The results of comparative wear tests are presented in graphical form in **Fig. 6**. An average linear wear of 3 samples produced by each method was a measure of abrasion as function of a friction path. Layers obtained by oscillating EB method were extremely abrasion resistant.

4 Conclusions

1. The application of oscillating EB method allow to produce thick, hard, wear-resistant, Ni-base surface layers with satisfactory adhesion to the low-alloyed structural steel.

2. It is possible to control the appearance, structure and properties of the modified surface by process parameters:

– the thickness of layers and width of HAZ rise with the increase of EB power,

– the depth of melted substrate zone rises in a similar way, which leads to the dilution of Ni-base alloy by Fe and the disappearance of Cr segregation,

– the hardness of layer decreases due to formation of Ni-Fe-Cr solution.

3. The surface layer obtained by the presented method by optimal parameters (21 kV accelerating voltage, 45 mm/min. movement speed, 45 mA beam current) showed a better wear resistance in comparison to samples produced by conventional methods.

The financial support by the State Committee for Scientific Research is greatly acknowledged.

5 References

[1] Y. Arata, *Plasma, electron and laser beam technology*, Am. Soc. of Metals, Metals Park, OH, 1986

[2] M. Tomie, N. Abe, M. Yamada, S. Noguchi, *Trans. JWRI*, 19, (1990), 1

[3] J. Senkara, *J. Mater. Sci. Lett.*, 10, (1991), 1078

[4] Y. Q. Yan, J. Senkara, W. Wlosinski, *Surf. Coat. Technol.*, 48, (1991), 211-217

INŠTITUT ZA KOVINSKE MATERIALE
IN TEHNOLOGIJE p.o.

INSTITUTE OF METALS
AND TECHNOLOGIES p.o.

61000 LJUBLJANA, LEPI POT 11, POB 431,
SLOVENIJA

Telefon: 061/1251-161, Telefax: 061 213-780

VACUUM HEAT TREATMENT LABORATORY

Vacuum Heat Treatment

Vacuum Heat Treatment is recognised as a high quality cost effective and ultra clean method for processing a wide range of components and materials currently in use in today's industry. The range of our equipment enables us to heat treat most sizes of load, from small batches to work up to 350 mm diameter, 910 mm high, and weight up to 380 kg.

ADVANTAGES

- Clean, bright surface finish
- Minimal distortion
- Minimal post treatment operations, e.g., grinding or polishing

Five years of continual investment has ensured that **VHTL** maintains it position as market leader in the field of high quality sub-contract metal processing.

We operate the latest generation of IPSEN VTTC furnace capable of processing components up to 350 mm in diameter, which in addition to our high pressure, rapid quenching facilities increases the range of materials suitable for Vacuum Heat Treatment.

TYPICAL APPLICATIONS

- Bright Annealing
- Bright Stress Relieving
- Hardening/Tempering
- Brazing/Hardening/Tempering
- Solution Treatment
- Demagnetisation
- Degassing
- Diffusion Treatments
- Sintering

QUALITY ASSURANCE

Quality is fundamental to the **IMT** philosophy. The choice of process, all processing operations and process control are continuously monitored by IMT Quality Control Department.

The high level of quality resulting from this tightly organised activity has been acknowledged by government authorities. industry and International companies.

Kovine, zlitine, tehnologije / letnik 29 / 1995 / št. 3–4 / strani 397–404

Influence of Fracture Toughness on Vacuum Hardened HSS

Vpliv lomne žilavosti na vakuumsko toplotno obdelano hitrorezno jeklo

Leskovšek V.,[1] B. Ule, A. Rodič, IMT Ljubljana

Fractures, macro-chipping and micro-chipping are all effects by which cutting edges are destroyed. The ability of a steel to resist these phenomena is known as its toughness. HSS, however, possess an appreciable ductility, although the notched or even unnotched specimens tested in the pendulum test are not sensitive enough to discriminate between high and low levels of toughness. Therefore, it becomes important to use a method of testing which can detect small variations in ductility. To establish the fracture toughness, the round-notched tensile specimens with a fatigue crack at the notch root was used. Fatiguing was done in as soft annealed condition. After that, the vacuum heat treatment for the achievement of optimal working properties was carried out and the final testing was performed. Our experiments confirm that the correlation based on the round-notched tension test can be successfully used to calculate the critical fracture toughness. On the basis of the above-mentioned experimental results, we were able to compose a diagram which simultaneously scoops the technological parameters of vacuum heat-treatment, the mechanical properties and the micro structure of vacuum heat-treated HSS M2.

Key words: fine blanking tool, fracture toughness, hardness, vacuum heat treatment

Lomi, makrookruški in mikrookruški so vzrok propadanja rezilnih robov. Sposobnost jekla, da se upira tem pojavom, pa je poznana kot žilavost. Hitrorezno jeklo ima upoštevanja vredno duktilnost, četudi preizkušanci z zarezo ali celo celo brez zareze pri Charpyjevem preizkusu niso dovolj selektivni, da bi nam omogočali določitev krhke oz. žilave narave loma. Za krhke materiale, med katere spada hitrorezno jeklo, je pomembno, da izberemo metodo preizkušanja, ki zazna že majhne spremembe duktilnosti jekla ter je selektivna in reproduktivna. Poleg standardnega načina merjenja lomne žilavosti na preizkušancih, ki so dovolj debeli, da je izpolnjen pogoj ravninskega deformacijskega stanja, uporabljamo tudi nestandardni način merjenja lomne žilavosti, s cilindričnimi nateznimi preizkušanci z zarezo po obodu. Problemi pri ustvarjanju razpoke v korenu zareze, so nas navedli na idejo, da metodo za določevanje lomne žilavosti s pomočjo cilindričnih preizkušancev z zarezo po obodu modificiramo. Doseženi rezultati so pokazali, da je modificirana metoda tudi dovolj selektivna. Osnovni namen modifikacije je, ustvariti razpoko kontrolirane globine v korenu zareze na mehko žarjenih cilindričnih preizkušancih z zarezo po obodu. Predpulzirane cilindrične preizkušance zatem vakuumsko toplotno obdelamo, temu pa sledi natezni preizkus. Na osnovi rezultatov dobljenih s pomočjo modificirane metode, smo uspeli na istem diagramu zajeti mehanske lastnosti, tehnološke parametre vakuumske toplotne obdelave in mikrostrukturo vakuumsko toplotno obdelanih preizkušancev iz hitroreznega jekla M2.

Ključne besede: orodje za precizno štancanje, lomna žilavost, trdota, vakuumska toplotna obdelava

1. Introduction

A carefully selected vacuum heat treatment process improves the basic characteristics of HSS M2. The required working hardness and fracture toughness of HSS is determined mainly by the hardening and tempering temperatures, depending on the alloying1. With the optimal vacuum heat treatment process, the best possible combination of fracture toughness and hardness, and therefore, wear resistance, is reached.

The design calculations of HSS tools must consider the material strength, with a special emphasis on fracture toughness, because of the danger of brittle tool fracture. Fracture toughness is defined as the ability of a material under stress to resist the propagation of a sharp crack. To establish the fracture toughness of HSS in hardened and tempered conditions, a non-standard testing method with small-scale specimens was developed. This method involves the introduction of a sharp crack at the notch root, in our case, by pulsating round-notched tension specimens, thermal treatment and tensile testing. A high level of hardness makes round specimens

[1] Vojteh LESKOVŠEK, dipl. inž., IMT, Lepi pot 11, 61000 Ljubljana

greatly sensitive to notches, so the test can fail due to unsuccessful pulsating. When successful prepulsating, a fatigue crack is performed at the notch root of the specimen. The method was modified with the formation of a circumferential crack of defined depth at the root of the machined notch on soft annealing specimens, than a tensile test was performed after vacuum heat treatment. Our experiments confirm that the measurements based on the modified round-notched tension test can be successfully used to determine the fracture toughness.

2. Basic characteristics of high speed tool steel M2

Due to the higher wear resistance of HSS, they are nowadays used also for fine blanking, cold working and deep drawing tools, especially in long series. Tool steels must withstand compressive stresses and abrasive or adhesive wear, while have a sufficient toughness to resist chipping and failure. HSS have better resistance to wear in comparison to cold work tool steels because of the increased hardness of the matrix, and of the carbide phase.

The carbide phase in the matrix of HSS increases the wear resistance which is relative to the total volume of carbides, and also to their hardness. The wear resistance in HSS is mainly determined by vanadium carbides which have a micro-hardness of 2200 to 2400 HV[2,3], **(Fig. 1).**

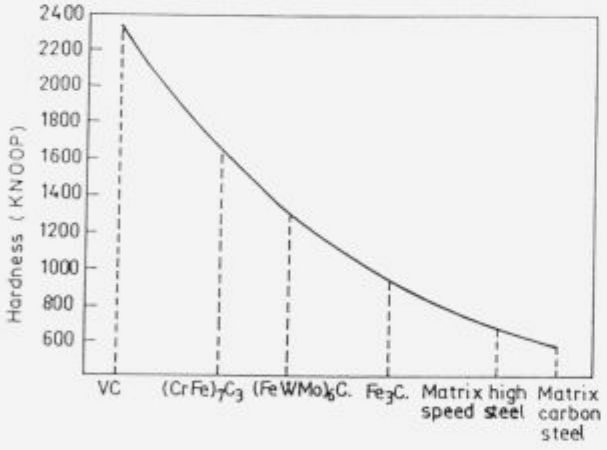

Figure 1: The comparative hardness of carbides found in tool steels2

Slika 1: Primerjalne vrednosti trdot karbidov, ki jih najdemo v hitroreznih jeklih

However, it must not be forgotten that HSS have a greater hot hardness. Even if the work pieces are place into the tools while cold, the working tool surfaces become hot.

Fractures, macro-chipping and micro-chipping can destroy the cutting edges. The ability of a steel to resist these phenomena is known as toughness. The toughness that can be achieved by HSS is limited by the defects in the steel (carbide segregations and bands inclusions etc.). When the steel is subjected to a load, stress concentrations can appear around the defects and cause a tool fracture, unless the stress concentrations are relieved by a local plastic flow on the micro scale. The ability of the matrix to undergo plastic flow can be altered within wide limits by varying the hardness. Thus, the defects in the steel determine the maximum toughness which can be achieved. On the other hand, the heat treatment determines the toughness degree actually achieved within the limits set by the defects.

Vacuum heat treatment is one of the most important operations in the manufacturing of tools. Therefore, when HSS are used for cold working processes, the situation is met by choosing low hardening temperatures and tempering temperatures below the peak secondary hardening temperature, to improve fracture toughness, cutting edge strength, wear resistance and dimensional stability. It is possible to exert a positive influence on all the parameters by vacuum heat treatment which is carefully selected to suit the HSS is determined by a choice of variable tempering temperatures, it is often impossible to optimise the mechanical properties, e.g. fracture toughness. A general recommendation for tools that require good impact strength, such as fine blanking tools, is that they should be hardened from temperatures as low as 1050°C[1]. By this treatment, resistance to tempering is diminished. For tools subjected to high pressures in service, a previous tempering at about 600°C[1] is recommended.

3. Experimental procedure

3.1 Material and treatment parameters

The test material selected was a conventional high-speed steel (HSS) of the AISI M2 type of the same melt. The chemical composition of the steel examined is listed in **Table 1**.

Table 1: Chemical composition of HSS examined (in wt.-%)

Material	C	Si	Mn	Cr	Mo	W	V	Co
AISI M2	0.87	0.29	0.30	3.77	4.90	6.24	1.81	0.53

Cylindrical round-notched tensile specimens with a diameter of 10 mm were machined from soft annealed bars with a Brinell hardness of 255. Specimens were fatigued to produce a sharp circumferential crack at the notch root, then austenitized in a vacuum furnace at temperatures of 1050°C, 1100°C, 1150°C and 1230°C respectively, quenched in a flow of gaseous nitrogen at a pressure of 5 bar abs. and double tempered one hour at temperatures 510°C, 540°C, 570°C and 600°C respectively.

3.2 Mechanical tests

The geometry of cylindrical round-notched precracked tensile specimens, prepared according Dieter's recommendation[4] is shown in **Fig. 2**.

Our previous investigations[5,6] confirmed that such small-scale specimens can be successfully used for the analysis of the relationship between the microstructural variations and the fracture toughness of the investigated steels. Accordingly to Grossmann's concept of hardenability, the formation of the uniform microstructure along the crack front is possible because of, the axial symmetry of the cylindrical specimens, in comparison with the conventional CT-specimens, where this condition is not fulfilled.

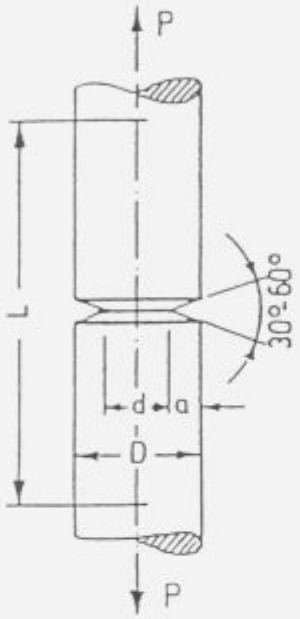

Figure 2: The geometry of a cylindrical round-notched and precracked tensile specimen

Slika 2: Nestandardni cilindrični natezni preizkušanec za merjenje lomne žilavosti z zarezo po obodu ter utrujenostno razpoko v korenu zareze

For a round-notched precracked specimen, the stress intensity factor is given by Dieter[4] as

$$KI = \frac{P}{D^{3/2}} (-1.27 + 1.72\ D/d) \qquad (1)$$

where d is the radius of the uncracked ligament after fatiguing, P is the applied fracture load, and D is the outer diameter of the cylindrical specimen. In the experiments, it is essential for the outer diameter of the specimen in order to obtain a state of plain strain at fracture.

In order to apply linear-elastic fracture mechanical concepts, the size of the plastic zone at the crack tip must be small compared with the nominal dimensions of the specimen. The size requirement for a valid KIC test is given by Shen Wei et. al.[7] as

$$D \geq 1.5\ (K_{IC}/\sigma_{ys}) \qquad (2)$$

where σ_{ys} is the yield stress of the investigated steel. This requirement (2) was fulfilled on all our measurements. The fracture surface of the cylindrical round-notched and precracked specimens was examined in SEM at low magnification. As is shown in Fig. 3, the fatigue crack propagation area was sharply separated from the circular central part of the fast fracture area, so that the diameter d of this area was easily measured.

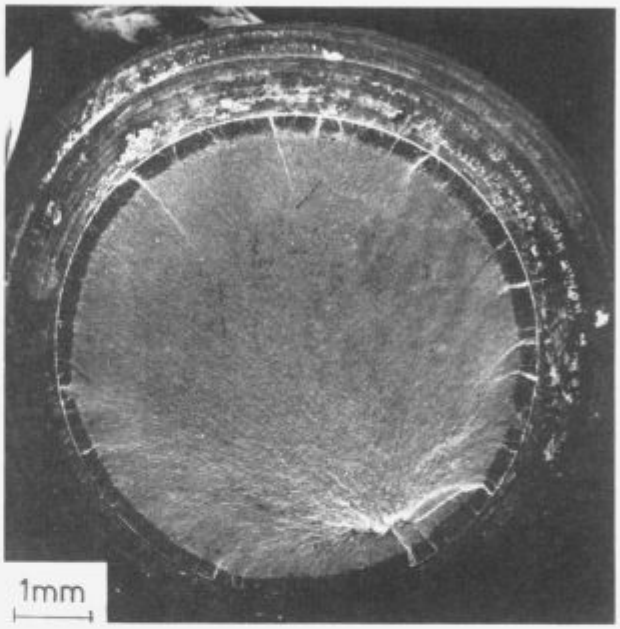

Figure 3: Fracture surface of cylindrical round-notched and precracked tensile specimen with the circumferential fatigue crack propagation area sharply separated from the circular central fast-fractured area

Slika 3: Prelomna površina cilindričnega nateznega preizkušanca z obodno zarezo, s kolobarjastim področjem propagacije utrujenostne razpoke, ki je ostro ločeno od osrednjega, naglo zlomljenega dela. Premer (d) naglo zlomljene prelomne površine lahko izmerimo z optičnim mikroskopom

4. Results and discussion

4.1 Microstructural characterisation

The microstructure develops in dependence on the hardening temperature, as well as the austenite grain size and the residual austenite content of the initial samples. Metallographic examination of specimens show that the austenite grain size of all specimens which were gas quenched from the austenitization temperature 1050 to 1230°C was 21 to 8 SG, **(Fig. 4)**.

The content of residual austenite in as quenched condition was determined by X-ray diffraction. The absolute accuracy of the determination of the residual austenite contents was ± 1 vol%. The HSS AISI M2 steel is fine-grained, right up to high hardening temperatures, and exhibits a residual austenite contents between 21 and 30 vol%.

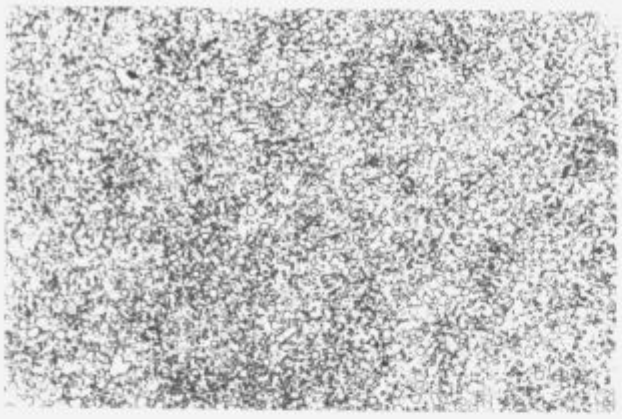

The microstructure after hardening at 1050° C, SG 21. Mag. 500x.

Mikrostruktura po kaljenju s temperature 1050° C, SG 21. pov. 500x.

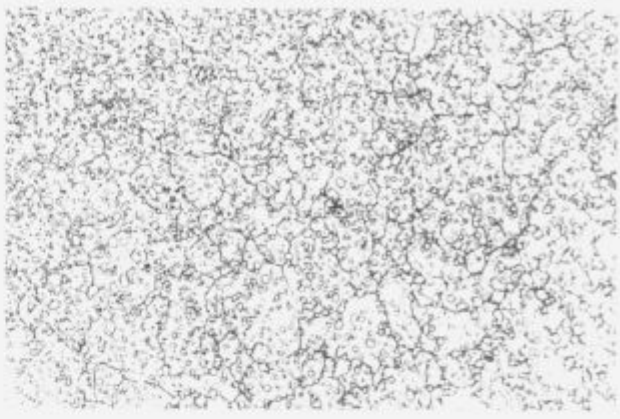

The microstructure after hardening at 1100° C, SG 18. Mag. 500x.

Mikrostruktura po kaljenju s temperature 1100° C, SG 18. pov. 500x.

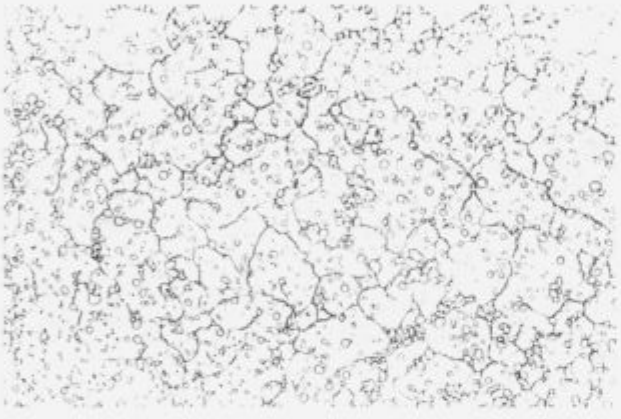

The microstructure after hardening at 1150° C, SG 13. Mag. 500x.

Mikrostruktura po kaljenju s temperature 1150° C, SG 13. pov. 500x.

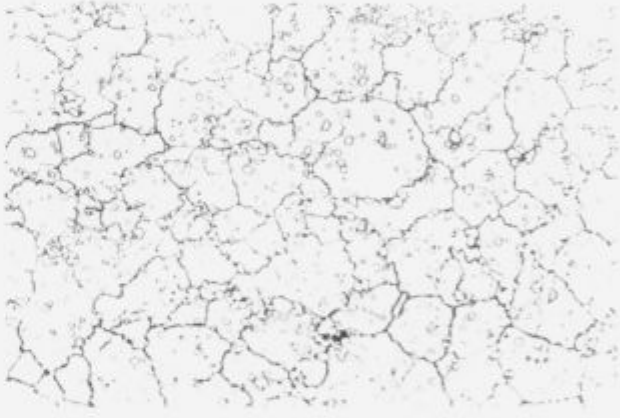

The microstructure after hardening at 1230° C, SG 8. Mag. 500x.

Mikrostruktura po kaljenju s temperature 1230° C, SG 8. pov. 500x.

Figure 4: Microstructures with a different austenite grain size from vacuum hardened specimens from M2 steel

Slika 4: Mikrostruktura in velikost austenitnih zrn, vakuumsko kaljenih vzorcev z različnih temperatur austenitizacije

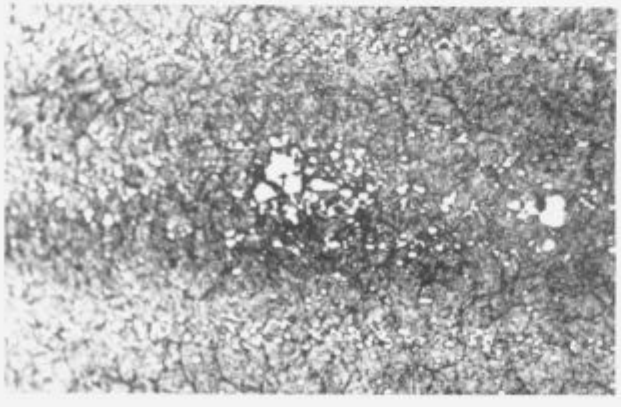

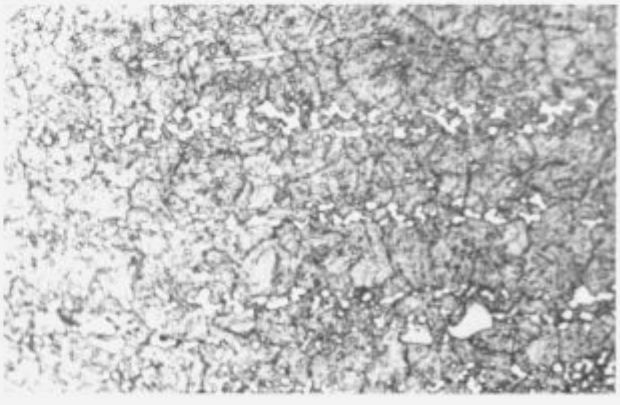

Figure 5: The microstructure shows carbides and tempered martensite with an austenite grain size of 13 SG (T_A:1150° C) and 8 SG (T_A:1230° C)

Slika 5: Mikrostruktura karbidov in popuščanega martenzita z velikostjo avstenitnih zrn SG 13 (T_A:1150° C) in SG 8 (T_A:1230° C)

The carbide particles in all the specimens were alike in size and position, which was due to their origin: all the specimens issued from the same metallurgical melt which was submitted to the same hot plastic transformation. The carbides looked like strips, and had a size of 1-20 μm, **(Fig. 5)**. The residual austenite contents are, with reference to tempering parameters, below 1 vol% in all samples. After metallographic etching, a stronger marking of the austenitic grain boundary could be noticed. L. Calliari

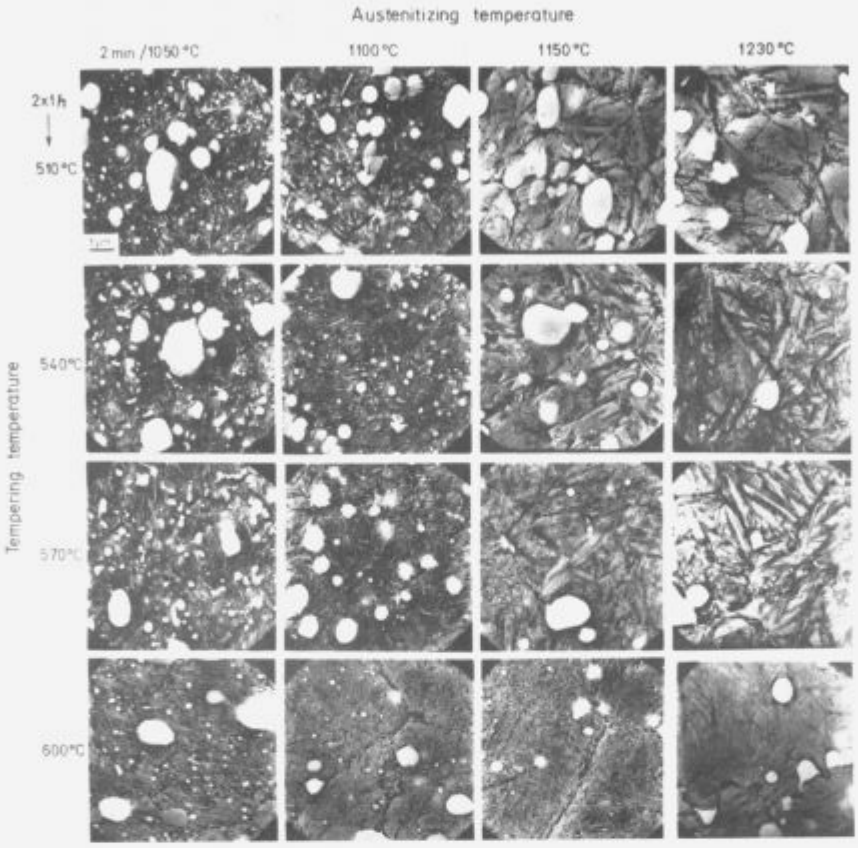

Figure 6: The microstructure of vacuum-hardened and tempered specimens examined by SEM
Slika 6: Mikrostruktura vakuumsko kaljenih in popuščenih vzorcev, posnetih na SEM pri 10 000 kratni povečavi

Table 2: Vacuum heat treatment parameters and mechanical properties of prepulsating round-notched tesion specimens

Vacuum heat treatment			Hardness	Fracture toughness
Spec. No.	Hardening(°C) 2 min.	Tempering(°C) 2 x 1h	HRc	K_{IC} ($MNm^{-3/2}$)
01-02	1050	510	60.0	18.78
03-04	1050	540	60.5	18.26
05-06	1050	570	58.7	15.80
07-08	1050	600	52.8	16.43
09-10	1100	510	61.8	17.28
11-12	1100	540	62.2	15.69
13-14	1100	570	61.3	15.49
15-16	1100	600	55.0	16.99
17-18	1150	510	60.7	18.26
19-20	1150	540	63.3	13.14
21-22	1150	570	63.2	14.70
23-24	1150	600	57.8	15.63
25	1230	510	62.5	17.77
26	1230	540	65.0	10.55
27	1230	570	65.5	12.08
28	1230	600	63.0	12.95

et al.[8], compared vacuum and conventional heat-treated samples of AISI M2, and found that the results of over 100 tests did not point out noticeable differences among the samples treated with the two different procedures. Neither systematic data nor relationship with the treatment parameters are yet available on this subject.

The microstructure of the specimens examined by SEM at a higher magnification **(Fig. 6)** confirmed a carbide precipitation on the austenite grain boundaries for HSS M2 at different austenitizing and tempering temperatures. The quantity of fine carbide particles decreased with the increase of austenitizing temperatures. In addition, it was also noticed that at higher austenitizing temperatures, particularly at 1230°C (last column in **Fig. 6**), the larger carbide particles in contacts of austenite grains seemed to covering the boundaries of the neighboring grains because of variable surface tension on the matrix-carbides boundary. The microstructure of the specimens was of martensite type. The eventual presence of small quantities of retained austenite (1 to 5 vol%)[8] examined by optical microscopy, were too small to estimate without fail in such a heterogeneous microstructure. This phenomena can be attributed to the fact that the heating rate was lower in the vacuum furnace than in the salt bath. By heating the prepulsating round-notched tension specimens between 1050°C and 1230°C, diffusion processes in the vacuum furnace took longer than in the salt bath, which can possibly explain why, after metallographic etching, a more intensive marking of the austenitic grain boundary can also be noticed.

4.2 Mechanical tests

Experiments[9] were performed on 28 prepulsating round-notched tension specimens, **(Table 2)**, heat-treated in an IPSEN VTTC-324 R single chamber vacuum furnace with uniform high pressure gas quenching.

In the following, the assumption is made that the values K_{IC} are determined by the above-mentioned method. The obtained values of K_{IC} are very similar to those obtained by G. Hoyl[10], who determined the fracture toughness K_{IC} for HSS M2 steel, e.g. 18,3 $MNm^{-3/2}$ for sample austenitized 4 minutes at 1220°C and tempered 1 hour at 510°C, by conventional methods. Below a hardness level of about 50 HRc, fracture toughness is dependent only on the hardness of the sample[10]. At higher levels of hardness, the fracture toughness for M2 varies inversely with the austenitizing temperature, as shown in **Fig. 7**. G.Hoyl[10] discovered that above a hardness level of 60 HRc, fracture toughness is insensitive to most metallurgical factors.

The effects of tempering between 510 and 600°C on fracture toughness are shown for M2 in the same figure. As expected, there is a minimum of toughness values corresponding to the hardness peak. The net effect of tempering is attributed to a combination of stress relief and a reduction in ductility due to the secondary hardening effect.

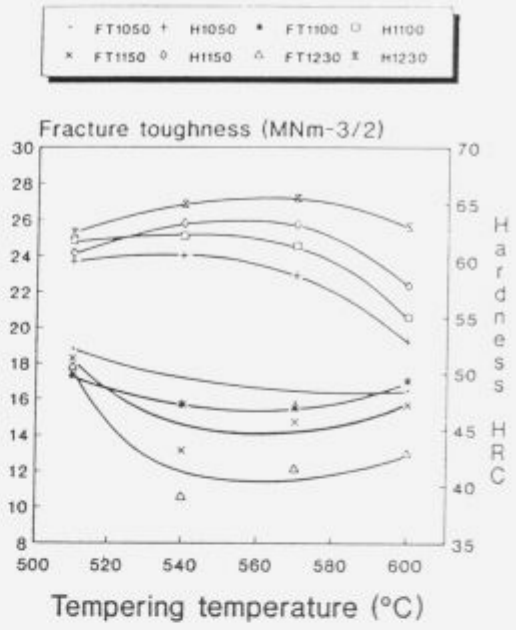

Figure 7: The effect of austenitizing and tempering temperature on fracture toughness and hardness of M2 steel (FT-fracture toughness; H-hardness)

Slika 7: Vpliv temperature austenitizacije in popuščanja na lomno žilavost KIC in trdoto, vakuumsko toplotno obdelanega hitroreznega jekla M2 (FT-lomna žilavost, H-trdota)

In examining the evolution of tempering[10], it was found that there was a peak value of fracture toughness for low tempering temperatures, (below 500°C). The obtained values are similar to those obtained in tempering at the conventional temperature, 25°C above the peak of the secondary hardening temperature. This is considered as advantageous, but as the effect is due to retained austenite that could transform later, the under-tempered tools could be susceptible to dimensional instability in service, which is unacceptable for fine blanking tools.

On the basis of the experimental results, it was possible to draw the diagram shown in **Fig. 8** where the technological parameters of the vacuum heat-treatment, mechanical properties and microstructure of the vacuum heat treated specimens are simultaneously combined.

From the diagram in **Fig. 8**, it is also evident that the fracture toughness for the tempering temperatures 540°C, 570°C and 600°C, respectively, increases with the decrease of hardening temperature in agreement with observations in reference 10. On the other hand, for the tempering temperature of 510°C, it was found that the fracture toughness values were very close, though slightly higher than for 600°C, irrespective of the hardening temperatures. On the basis of the curves in **Fig. 8**, it can be reliably assumed that the HSS M2 hardened from low austenitizing temperatures and tempered at 510°C can achieve the optimal combination of hardness and fracture toughness.

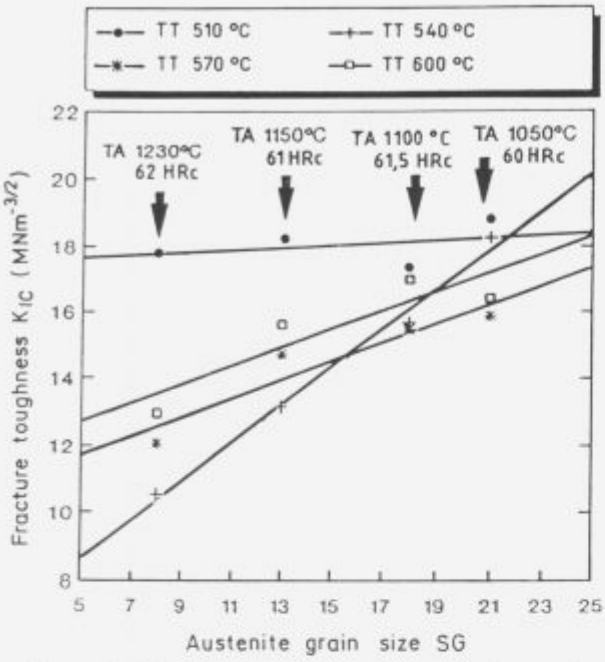

Figure 8: The influence of austenite grain size on the fracture toughness of HSS AISI M2, (TT-tempering temperature, TA-hardening temperature, HRc-hardness at 510° C)

Slika 8: Vpliv velikosti austenitnega zrna na lomno žilavost hitroreznega AISI M2, (TT-temperatura popuščanja, TA-temperatura kaljenja, HRc-trdota po pop. na temperaturi 510° C)

The relationship between fracture toughness and austenite grain size, f.i. SG grade 8, shows us that at the tempering temperatures between 510 and 600° C, the obtained values K_{IC} are from 17,77 to 10,55 $MNm^{-3/2}$ and the difference is quite important in practice. Different fracture toughness at equal austenite grain size or the nearly constant fracture toughness of HSS M2 hardened from different austenitizing temperatures, f.i. from 1050 to 1230° C, and double tempered at 510° C, is in accordance with the hypothesis that the austenite grain size is not the dominant parameter effecting the fracture toughness of HSS M2.

The result of the present investigation is useful for the optimisation of vacuum heat treatment for different HSS tools submitted to tensile impact stress during use where an optimal combination of hardness and fracture toughness are decisive.

4.3 Tool life tests

Long production runs have underlined the importance of an improved fine blanking tool life, **(Fig. 9)**.

On the basis of the experimental results shown in **Fig. 8**, it was found that the optimum vacuum heat treatment of fine blanking HSS M2 tools needs at least two preheating stages (650 and 850° C respectively), a variable hardening temperatures (usually 1050 to 1150° C) and double tempering at the same temperature (510° C/1hour).

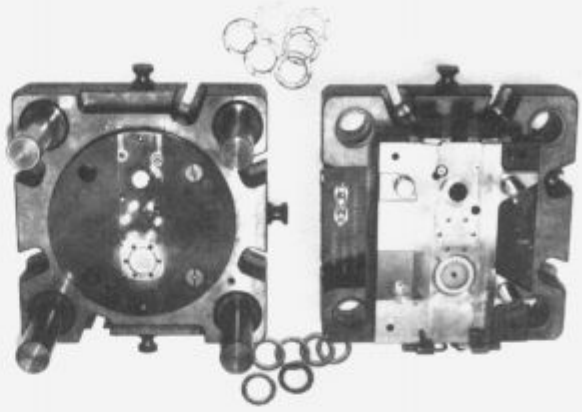

Figure 9: Fine blanking tool for a ratchet wheel

Slika 9: Orodje za precizno štancanje zobnika varnostnega pasu

The life of a fine blanking tool varies considerably depending on the size and design of the blank, the type of blanking steel, and care and maintenance. To establish tool life, we selected three tools for a fine blanking ratchet wheel. The punches and dies were from HSS AISI M2. Blanks with a material gauge of 4 mm were from AISI C 1045 blanking steel in a spheroidized-annealed condition. The punches and dies were stress-relieved at 650° C 4 hours and vacuum heat-treated in a single chamber vacuum furnace with uniform high pressure gas quenching. Depending on the alloying and the condition of austenitization (1100° C/2min), the final hardness of 61.5 HRc and the final fracture toughness of 17.28 $MNm^{-3/2}$ was reached after double tempering at 510° C for 1 hour **(Fig. 8)**. The vacuum heat-treated punches and dies were tested on a 250t triple-action hydraulic press and compared with the fine blanking tools for fine blanking ratchet wheels conventionally heat-treated in a salt bath as follows: stress relieved at 650° C/4hour, preheated at 450° C, 650° C and 850° C respectively, austenitized at 1100° C/2min and control-quenched to 550° C in 5 min, held isothermally at 550° C for 10 min and cooled to 80° C with air, followed by double tempering at 600° C/1 hour. The final hardness of the tools achieved after double tempering at 600° C/1 hour, was 58 to 59 HRc, depending on the alloying.

The basic trial parameters (such as the cutting force, strikes per time unit, temperature, greasing etc.) were constant during the experiments, and did not affect the final results. The differences observed in fine blanking tools could only originate in the punches and dies themselves. 15.000 ratchet wheels were made with each tool and edges examined in a binocular microscope to estimate the damage. Minor defects were observed on the vacuum heat-treated punches and dies and those conventionally heat-treated in a salt bath.

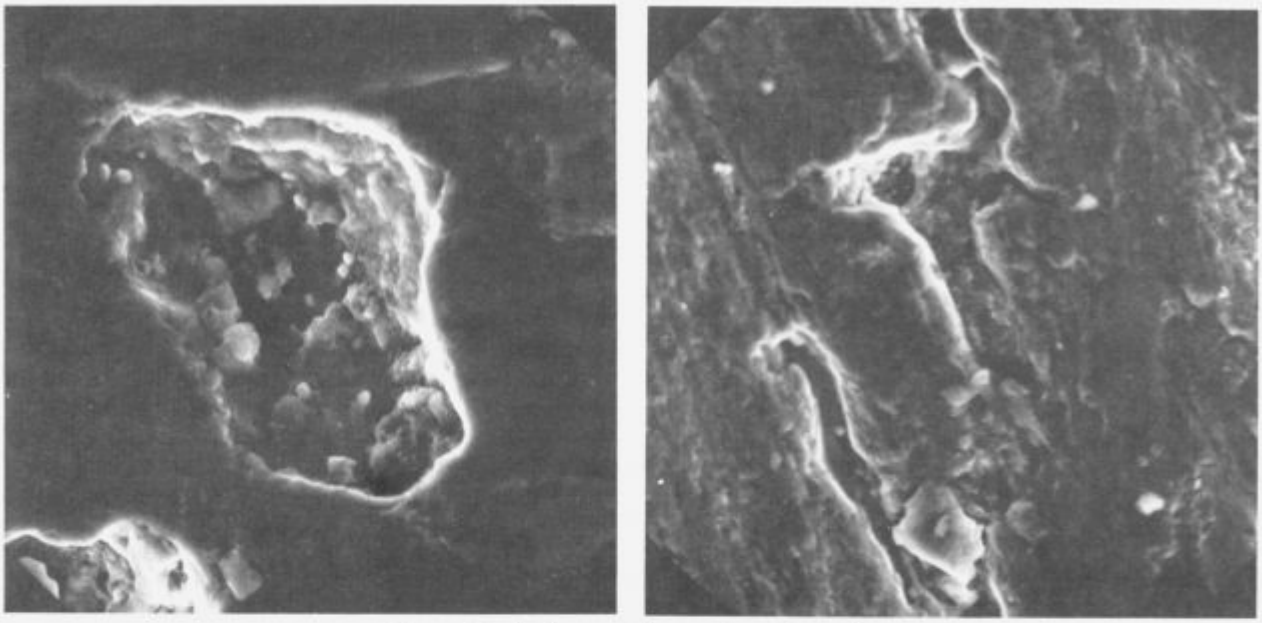

Figure 10: Defects on the punch cutting edge
Slika 10: Poškodbe na rezilnem robu pestiča

The wear of the punches and dies increases with the operation time. SEM observations show that the starting wear of the cutting edges of the punches and dies could not be easily determined. The material showed not only surface fatigue, but also adhesion and abrasion, **(Fig. 10)**.

The experiments showed that higher working hardness (61.5 HRc) and improved fracture toughness of vacuum heat-treated punches and dies - particularly those double-tempered at 510°C - had significant effect on the defects on the cutting edges. Compared to conventionally heat treated tools tempered at 600°C was the vacuum heat-treated tool life by 15 to 20%, greater. During the tool tests, no effects were found that could be related to the in service dimensional instability due to the later-transformed retained austenite. Namely, X-ray structural analyses showed that the content of retained austenite did not exceed 1 vol% in all the specimens.

5. Conclusions

The exact significance of fracture toughness as it affects HSS properties and service behavior is not thoroughly understood, and there are differences in behavior between grades and process routes. However, the modified method for the establishment of fracture toughness improved by IMT, appeared to be a successful method for establishing the fracture toughness of HSS.

The measurements of wear in the cutting edges of punches and dies show that double tempering at 510°C/1h after vacuum heat treatment prolongs the life of fine blanking tools for ratchet wheels by 15 to 20%, compared to conventionally heat-treated tools which were hardened at the same austenitizing temperature and tempered twice at 600°C. It seams that it is not the type of process which substantially affects the tool life, but first of all, the proper choice of hardening and tempering temperatures.

The wear resistance of punches and dies cannot only be described as a material property, but as a property of a complex tribological system. Yet, it is proven that the wear resistance depends, above all, on the microstructure of the tool material and on its physical and chemical properties.

The presented results, obtained by the evaluation of daily confirmed data, justify the use of modern vacuum heat-treatment technology and the use of the newest high-performance HSS steels to achieve great improvements in tool lives and overall economy.

6. References

[1] K. E. Thelning: *Steel and its Heat Treatment*, Bofors Handbook, 1975, 313 - 319
[2] R. Wilson: *Metallurgy and Heat Treatment of Tool Steels*, McGraw-Hill Book Company UK, 1975, 69
[3] H. Czichos: *Tribology*, Elsevier Scientific Publishishing Company Amsterdam, 1978
[4] G. E. Dieter,: *Mechanical Metallurgy*, McGraw-Hill, 1986, 358
[5] B. Ule, D. Kmetič, A. Rodič: *Rudarsko-Metalurški zbornik*, 1989, 3, 509-519
[6] V. Leskovšek, B. Ule, A. Rodič, D. Lazar: *Vacuum*, 43, 1992, 5-7, 713-716
[7] Shen Wei et.al.: *Engineering Fracture Mechanics*, 16, 1982, 1, 69-92
[8] L. Calliari, A. Molinari, E. Ramous, G. Torbol, G. Wolf: *Vacuum and Conventional Treatment of Tool Steels*, Instituto per la Ricerca Scientifica e Technologica 38050 Povo (Trento) Italy, 49-57
[9] V. Leskovšek, B. Ule, A. Rodič: *Metals Alloys Technologies*, 27, 1993, 1-2, 195-204
[10] G. Hoyle, *High Speed Steels*, Butterworth & Co. Ltd, 1988, 143-146

Kovine, zlitine, tehnologije / letnik 29 / 1995 / št. 3–4 / strani 405–412

Characteristics of Cemented Carbide Particles/Structural Steel Vacuum Brazing Joint

Značilnosti vakuumskega spoja zrn karbidne trdine s konstrukcijskim jeklom

Šuštaršič B., V. Leskovšek, A. Rodič, IMT, Ljubljana

The strength of the vacuum brazing joint between cemented carbide particles and the structural steel base depends on microstructural characteristics of the hard metal/braze interface formed during vacuum brazing. These are determined by the selected brazing agent, the structural steel base, as well as the vacuum brazing procedure. The R&D work concerning the procedure of manufacturing these types of grinding tools is introduced, with a strong emphasis on the characteristics of the brazing agent used, the vacuum brazing procedure, as well as the resulting microstructural characteristics of the brazing joint between the hard metal particles and the structural steel base.

Key words: vacuum brazing, cemented carbide particles, structural steels, Cu-based brazing alloy-powders, microstructural features

Trdnost vakuumskega spoja zrn karbidne trdine s konstrukcijskim jeklom je odvisna predvsem od mikrostrukture mejne plasti kovinska osnova/karbidna trdina, nastale med vakuumskim trdim spajkanjem. Le-ta pa je odvisna od izbrane kovinske osnove (konstrukcijskega jekla), vrste karbidne trdine in tehnoloških parametrov spajkanja. V pričujočem prispevku je predstavljeno razvojno raziskovalno delo vezano na postopek izdelave brusnih plošč, ki so sestavljene iz jeklenih plošč na katere so nanešena groba zrna karbidne trdine. Poudarek je na opisu mikrostrukturnih značilnostih nastalega spoja v odvisnosti od uporabljene spajke, karbidne trdine in jekla, kakor tudi pogojev vakuumskega spajkanja.

Ključne besede: vakuumsko trdo spajkanje, zrna karbidne trdine, konstrukcijska jekla, spajke na osnovi Cu, mikrostrukturne značilnosti

1. Introduction

Tungsten carbides with Co matrix (WC-Co) are old and well-known composites, referred to as cemented carbides or hard metals. They are also well-known under the trade mark name WIDIA. The most important application of cemented carbides is in the production of machining tools, as well as in the production of wear resistant parts or layers in many fields of application. Waste cemented carbide parts of worn tools (inserts, knives, drills, cutters, saws, punches, etc.) can be ground and the resulting relatively rough and sharp edged particles of the WC-Co composite can be used for the manufacturing of grinding wheels which are fast and simply mounted on the electric drill. The cemented carbide particles are uniformly deposited on a clean surface of a steel base (grinding wheel) and the diffusion bonding of particles with the steel base can be obtained by different methods of brazing. The most convenient brazing method is vacuum brazing.

In wood, stone-cutting and leather industry, as well as in rubber industry, it is often necessary (by a fast and simple procedure) either to clean or to rub off the surface of the semi-finished products during individual steps of the manufacturing procedure. Stock-farming is gradually substituting for the hard and time-consuming trimming of hoofs by manual grinding. These kinds of grinding wheels are also appropriate tools for housework applications. Currently, this type of grinding tools is also increasingly in demand on the Slovenian market. The researchers of the Institute of Metals and Technologies in Ljubljana, Slovenia, have many years of experience in different R&D fields concerning wear resistant materials (metal powder manufacturing, heat treatment, vacuum brazing, material development, investigations and testing, etc.). Therefore, a decision was made at the IMT Ljubljana to develop a procedure of manufacturing these types of grinding tools.

For the brazing of sintered cemented carbides (WC-Co composites), either with tool or structural steel base as a brazing agent, technically pure copper (usually OFHC Cu 99.9 mass %) powder is commonly used[1,2,3]. The joining of WC-Co composites and steel base with pure Cu and the diffusion processes occurring in this connection, as well as the formation of different phases at the interface hard

Mag. Borivoj ŠUŠTARŠIČ, dipl. inž., IMT, Lepi pot 11, 61000 Ljubljana

metal/braze and braze/steel base was the subject of several previous investigations[1-4]. The common statement of these is that, during brazing at the hard metal/braze interface, thin Co and Fe rich layer of an intermetallic compound is formed. Voids are also generated in the border zone of the hard metal which greatly reduce the strength of the joint.

Commercial producers[5,6] of Cu based brazing agents often recommend Cu-Ni based powders as a proper material for the brazing of cemented carbides/steels couples. Simultaneously, our own powder preparation experiments[7] show that by the water atomization of Cu-2%Ni alloy, a nearly spherical powder with relatively high apparent density and flowability, as well as a proper particle size distribution with the mean particle size between 40 in 70 μm can be obtained. Thus by the optimization of process parameters of water atomization[7,8,9] (especially of water pressure, tundish nozzle diameter and superheat) it can be concluded that the manufacturing of brazing powder with required morphological properties is possible.

Water atomization experiments show[7] that Cu-2%Ni alloy powder has even slightly better morphological properties in comparison to pure Cu based water atomized powder. In spite of the fact that water atomized powders have a relatively high oxygen content in prepared Cu-2%Ni alloy powder, good-quality joint between hard metal and steel is expected, if deoxidising atmosphere (vacuum) and good morphological properties of the powder are taken into consideration.

In the present article, the research work concerning the procedure of manufacturing these types of grinding tools is introduced, with a strong emphasis on the characteristics of the brazing agent used, the vacuum brazing procedure, as well as the resulting microstructural characteristics of the brazing joint between the cemented carbide particles and the structural steel base. Considering the relatively well investigated process of multiphase diffusion[4] during brazing with pure Cu, the aim of our work was also to find out if a similar phenomenon occurs in brazing with Cu-Ni alloy powder. The influence of a steel base chemical composition is also considered.

2. Experimental work

As a metal base for rough and sharp edged particles of the WC-Co composite, two different steels (soft low-carbon structural steel Č.0561 or DIN W.No.: 1.0570 with 0.2 mass % C and low-alloy hardening steel Č.4733, Ravne Steel Plant VCMo150 or DIN W.No.: 1.7228 with 0.5 % C, 1 % Cr and 0.2 % Mo) were selected. From the selected steels, round plates of standard grinding wheels dimensions (diameter approximately 115 mm and thickness 2 ÷ 6 mm) were made. For deposition, a mixture of metal powder (fraction 45 ÷ 75 μm of Cu-2 % Ni), binder and cemented carbide (ISO G10/G20 with 6 ÷ 10 % Co and nominal Vickers hardness 1500 HV) particles in size 1 ÷ 3 mm was prepared. After the deposition of the mixture on the steel base, the samples were vacuum brazed in IPSEN vacuum heat treatment furnace (type VTTC-324R).

Optimal brazing conditions were achieved in vacuum 10^{-3} mbars, in temperature range between 1100 and 1200° C, at heating rate ≈ 20° C/min. and at cooling rate ≈ 3° C/min. These brazing conditions ensure that the cemented carbide particles and the steel base remain in solid state during brazing, while the braze is melted. This ensures good wetting of cemented carbide particles and steel surface with the brazing agent.

The applied metal powder and the cemented carbide particles were examined by optical and scanning electron microscope. The apparent density and flowability of the prepared powders was determined by Hall's apparatus in accordance with MPIF standards[10] (Metal Powder Industries Federation Standards No.: 03 and 04). The oxygen content in metal powder was also determined. The chemical composition of selected steels was checked by X-ray fluorescence (ARL 3460 Metal Analyser). The hardness of individual components of grinding wheels was determined before and after brazing. Samples from manufactured grinding wheels (see **Fig. 1**) were then cut out for metalographic investigations and analysis with electron micro-probe analyzer (EPMA).

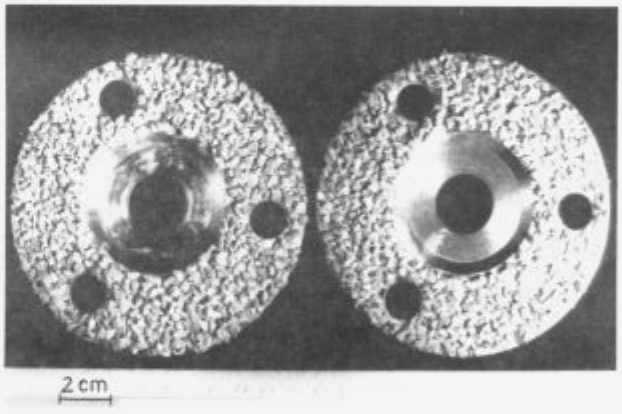

Figure 1: Macroscopic photo of grinding wheels manufactured at IMT Ljubljana
Slika 1: Makroskopski posnetek na IMT Ljubljana izdelanih brusnih plošč

3. Results and discussion

The water atomized Cu-2 % Ni powder prepared at IMT Ljubljana, which was used as the brazing agent in our experiments has mainly almost spherical particles (see **Fig. 2**). The powder particles are coated with a thin oxide film. Metalographic examinations also show internal porosity of some particles. The cellular solidification structure of powder particles (see **Fig. 3**) results from the high cooling rate (≈ $10^5 \div 10^7$ K/s) obtained during water atomization. The size of cells strongly depends on powder particle size because the cooling rate primarily depends on the particle size formed during atomization.

High apparent density and good flowability are the basic features of a high-quality brazing agents.

Because of regular powder particle shape, the prepared powder has a relatively high apparent density (≈4,4 g/cm^3) and good flowability (≈18 sec./50 g).

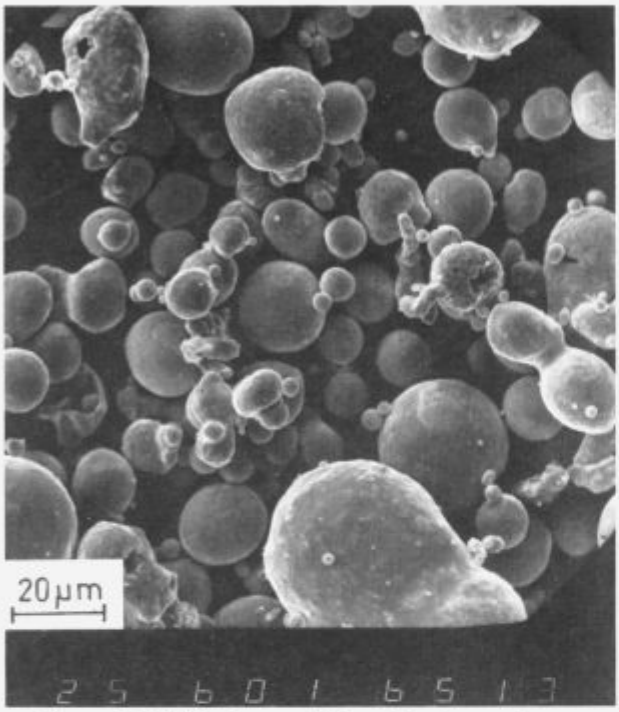

Figure 2: SEM micrograph of particle shape of water atomized Cu-2%Ni powder used as vacuum brazing agent
Slika 2: SEM posnetek delcev vodno atomiziranega prahu (spajke Cu-2%Ni) uporabljenega za vakuumsko trdo spajkanje karbidnih zrn z jekleno osnovo

As it has already been mentioned, the water atomized powders have a relatively high oxygen content (0.25 mass % of O_2 in prepared Cu-2%Ni alloy powder). This could be primarily attributed to particle surface oxidation during water atomization and surface adsorption of oxygen molecules during the handling with powder. In Cu based alloy-powders, oxygen solubility and oxides from slag[11] should also be taken into consideration. Individual contributions to the overall oxygen content of powder still have to be established in our future investigations. The brazing procedure is carried out in relatively high vacuum and therefore the high oxygen content of powder has little influence on the brazing quality. Because of the carbon content in the steel and in the cemented carbide, the reduction of oxygen with carbon is also possible. The Cu-Ni alloying system is one of complete solid solubility and therefore it can be concluded that the used braze is a substitutional solid solution.

Besides the braze, which is liquid at the brazing temperature, the diffusion processes (solid → liquid → solid) are influenced by the selected metal base (steel). Namely, because of the concentration gradients (and the driving force for diffusion is the gradient of the chemical potential), Fe and other alloying elements presented in the metal base diffuse across the braze at the interface braze/cemented carbide.

The diffusion of Fe is primarily influenced (suppressed) by the carbon content in steel[4], whereas the influence of other alloying elements (Cr, Mn, etc.) has not yet been analysed in detail.

In studying diffusion processes it has to be considered that mutual solubility of presented components is very small or practically equal to zero (solubility of braze in cemented carbide). Namely, the solubility of the main individual elements presented in the brazed components (Fe, Cr, Co, W) in braze (Cu) is relatively small. For example, Co solubility in Cu at brazing temperatures is ≈ 8 %, solubility of Cr is ≈ 0.65 % and Fe solubility is ≈ 5 %. But, W and C are practically insoluble in liquid Cu.

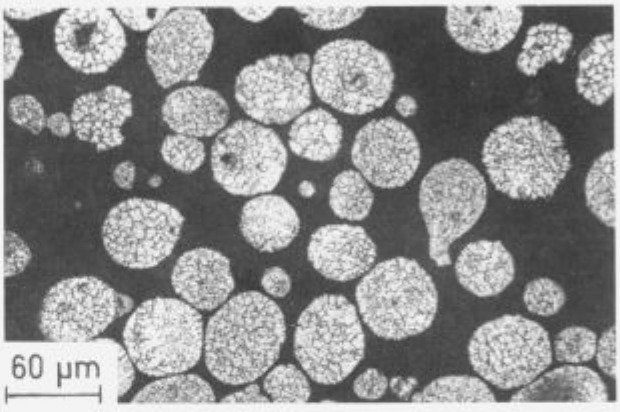

Figure 3: Optical micrograph of rapid solidified cellular microstructure of water atomized Cu-2%Ni powder particles with noticed internal porosity
Slika 3: Posnetek hitro strjene celične mikrostrukture delcev vodno atomiziranega prahu Cu-2%Ni z opazno notranjo poroznostjo

Cemented carbide particles were analysed with EPMA. Electron images show the expected sharp edged particles and the expected distribution of W and Co contents. In trace, Fe, Ni, Mn, Si and Cr are also present. The determination of qualitative and quantitative distribution of C is not possible with our EPMA.

3.1 Characteristics of cemented carbide particles/structural steel brazing joint

First, the brazing results analysis and a discussion of the brazing non-alloyed soft structural steel/cemented carbide with Cu-Ni braze will be presented. The selected steel has a fine grained ferrite-pearlite microstructure with approximately 15% of pearlite (see **Fig. 4**), low carbon content and Brinell hardness 205-215 HB. **Fig. 5** shows the cross section steel/braze/cemented carbide particle with elements distribution obtained with EPMA. It can clearly be seen that Fe diffused to the interfaces braze/cemented carbide particles, while W mostly remains in cemented carbide particles. Therefore, one can conclude that the diffusion of W is negligible, or rather, that it is limited to the diffusion to the interface cemented carbide/braze. Ni is found in braze. With Ni enriched regions are also interfaces steel/braze and braze/cemented carbide.

An increased amount of Co is noticed at the interface cemented carbide/braze and partially at the interface braze/steel. From this point of view it can be concluded that Co diffuses from the matrix of the cemented carbide particles to the interface cemented carbide/braze and across the braze to the interface braze/steel. The diffusion of Mn and Si is insignificant. On the basis of previous investigations[1,2,4], element

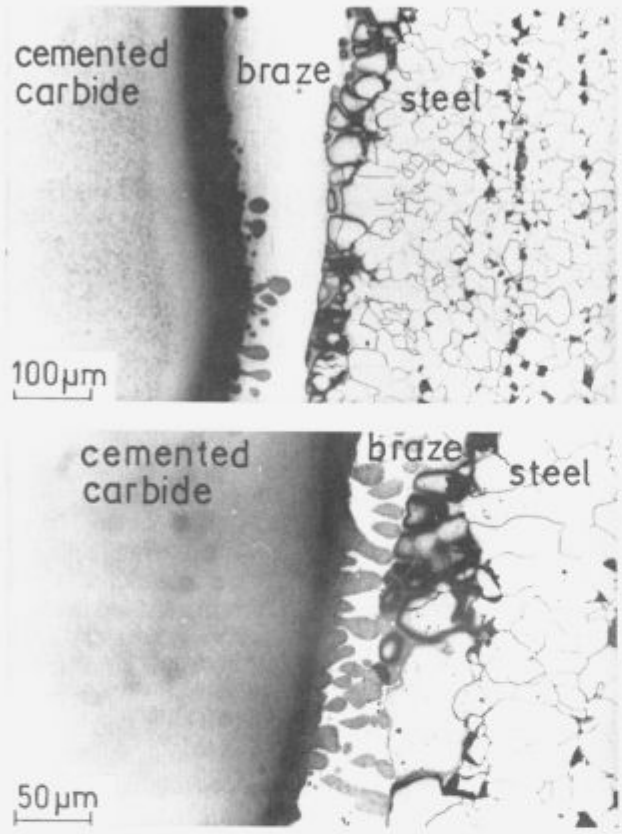

Figure 4: Microstructures of cemented carbide particle/structural steel joint of prepared grinding wheel
Slika 4: Mikrostruktura vakuumskega spoja zrn karbidne trdine s konstrukcijskim jeklom

distribution obtained with EPMA and metallographic examination (see **Fig. 4** and **5**) it can be concluded that at the interface cemented carbide/braze a thin layer (= 20 ÷ 40 µm) probably of an intermetallic compound enriched with Co and Fe was formed. Unfortunately, the determination of the C and O distribution is not possible by our EPMA. Therefore, data of other investigators have to be considered[4]. The diffusion of C from steel across the braze as well as by the decomposition of cemented carbide particles and then the diffusion of W and C to the interface cemented carbide/braze is possible.

Studies of the Co-Cu-Fe-W quaternary system at the brazing temperatures and their subsystems with C have shown that the formation of a number of very stable compounds is possible. In addition to µ phase $(Co,Fe)_7W_2(Co,Fe,W)_4$, the formation of cementite phases M_3 ($[Co,Fe,W]_3C$), M_6C and $M_{12}C$ that have large negative Gibbs' energies is also possible. Energetically the most stable phase is $M_{12}C$, but a spot analysis (WDX) of the Fe/Co-containing compound phase at the interface cemented carbide/braze showed[4] that at shorter brazing times especially phase M_3C is formed. The Gibbs' energy of this cementite phase is more than twice smaller than Gibbs' energy required for the formation of WC. Therefore it can be concluded that WC from cemented carbide particles during brazing is decomposed and released atoms of C and W diffuse across the Co matrix to the interface cemented carbide/braze.

C and Co reach Fe, which is present at interface, faster than W. Namely, the diffusion coefficient of C in Fe is very large because of its interstitial solubility and Co is the base of the solid solution of cemented carbide matrix. The diffusion of W is the slowest process, therefore it can be concluded that this process controls the formation of a compound layer and for very short brazing times energetically the most favourable process is the formation of a stable W-poor cementite phase.

Therefore in the first stage of brazing, C and Fe can diffuse from the steel across the braze to the interface braze/cemented carbide, because of their large concentration gradients. By the formation of cementite phase, the chemical potential of C is decreased and the conditions for WC decomposition, the diffusion of C and W to the interface cemented carbide/braze, as well as for the continuing growth and development of the compound layer are fulfilled. Some authors[4] explained the inferior strength of the vacuum brazed joint by the formation of a thin compound layer during brazing and appearance of microporosity behind this layer. The void formation during brazing with pure Cu, could be explained by the faster diffusion of Co from the cemented carbide matrix in comparison with the diffusion of other possible elements in the cemented

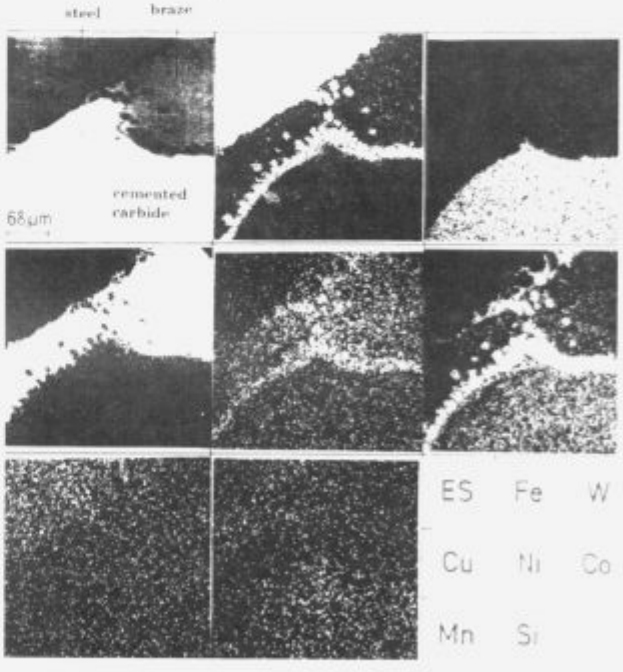

Figure 5: Elements distribution at the cemented carbide particle/structural steel joint of the prepared sample
Slika 5: Porazdelitev elementov v vzorcu izdelane brusne plošče na spoju zrno karbidne trdine/konstrukcijsko jeklo

carbide matrix (Kirkendall's effect). The metallographic examination of our samples (brazing joints) shows that microporosity is not present. On the basis of this, it can be concluded that the diffusion of Co is suppressed or, which is more probable, that Fe and especially Cu and Ni occupy the Co emptied sites. Namely, Ni, Fe and Co can form the system of a completely solid solution and therefore these elements can substitute for the Co in cemented carbide matrix and, as it was mentioned before, the micro-probe analysis of brazed samples really showed a region enriched by the Fe, Cu and Ni behind the formed compound layer.

At the interface steel/braze, the formation of a similar compound zone as observed at the interface braze/cemented carbide is not evident. The border zone steel/braze is enriched by Cu, Ni and Co (see **Fig. 5**). Co and Ni form a system of completely solid solubility with Fe, and solubility of Cu in γ Fe at brazing temperatures is = 7.5%. Therefore, from this point of view and from the morphology of the border zone (see **Fig. 4**) it can be concluded that an intercrystalline diffusion of Cu is occurred, the solution of the mentioned elements in Fe is carried out and a homogeneous solid solution in the system Fe-Co-Ni-Cu at the interface steel/braze is therefore formed. **Fig. 6** presents schematically a brazing joint with established diffusion directions of individual elements and formed border zones at the interface steel/braze and braze cemented carbide particles.

The grinding experiments with prepared grinding wheels from the soft low-carbon structural steel and

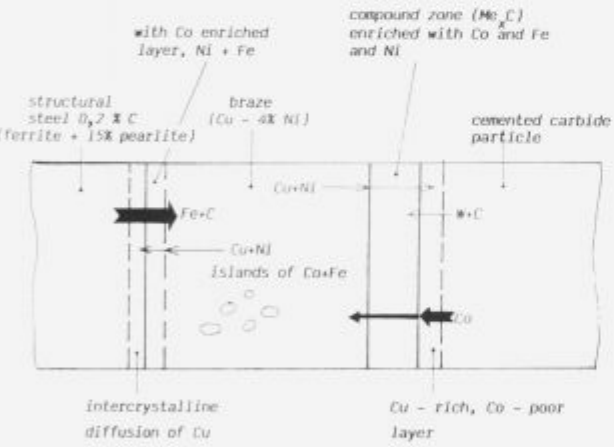

Figure 6: Schematic presentation of the brazing joint and the diffusion flows of the individual elements with generated border zones (sample of grinding wheel prepared by brazing of structural steel and cemented carbide particles)

Slika 6: Shematični prikaz vakuumskega spoja zrno karbidne trdine/konstrukcijsko jeklo z difuzijo posameznih elementov in nastalima mejnima conama

cemented carbide particles with Cu-Ni brazing agent showed that during the brazing a sufficiently strong diffusion bonded joint is formed. The average hardness of the steel base after brazing is 140 HV_1, of cemented carbide particles 1475 HV_1 and of the braze 100 $HV_{0.1}$.

3.2 Characteristics of cemented carbide particles/low-alloy hardening steel brazing joint

Now, the analysis of brazing experiments with the second selected steel will be presented. Here, in comparison with the first steel, a higher carbon content and a higher content of alloying elements (Cr, Mn, etc.) has to be considered. **Fig. 7** shows the cross section steel/braze/cemented carbide particle with element distribution obtained with EPMA. It can be clearly seen, that Fe diffuses to the interfaces braze/cemented carbide particles. W remains in cemented carbide particles. Therefore it can be concluded that the diffusion of W is negligible or more precisely that it is limited by the diffusion to the interface cemented carbide/braze.

Ni is mostly in the braze. With Ni enriched regions are also interfaces steel/braze and braze/cemented carbide. An increased amount of Co at the interface cemented carbide/braze as well as at the interface braze/steel is noticed. On the basis of that it can be concluded that Co diffuses from the matrix of cemented carbide particles to the interface cemented carbide/braze and across the braze to the interface braze/steel. The presence of Mn at the interface braze/cemented carbide is evident. Because of the presence of Cr in steel, the diffusion of Cr also occurs. The diffusion of Si is insignificant.

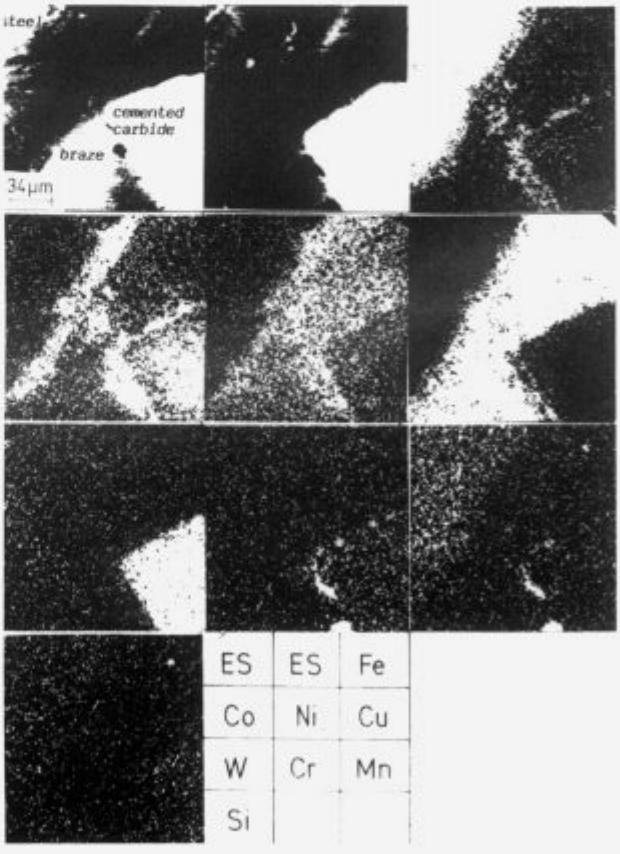

Figure 7: Elements distribution at the cemented carbide particle/low-alloy hardening steel joint of the produced grinding wheel sample

Slika 7: Porazdelitev elementov na spoju zrno karbidne trdine/jeklo za poboljšanje izdelanih brusnih plošč

On the basis of previous statements, element distribution obtained by EPMA and metallographic examination (see **Fig. 7** and **8**) it can be concluded that at the interface cemented carbide/braze, a thin layer (≈ 20 ÷ 30 μm), probably of an intermetallic compound enriched with Co and Fe, or what is more probable, concerning the diffusion of C, of the cementite phase Me_xC was formed. The thickness of the formed layer depends on the thickness of the braze and cemented carbide particles distance from the steel base, respectively, as well as on the brazing temperature and the soaking time at the brazing temperature.
In the layer of the braze, at certain places (islands), an increased content of Co and Fe can also be noticed. Because of intensive diffusion of Co out of cemented carbide particles, a diminished Co content behind the formed compound layer is observed. But at the same places, an increased content of Cu, Fe and Ni is noticed. Therefore it can be concluded that the diffusion of Ni, Fe and Cu proceeded in opposite direction. Besides Fe, Co, Ni and W (probably also C), Cr and Mn, were also found at the interface braze/cemented carbide. Therefore it can be stated that during the brazing of steel base and cemented carbide particles with Cu-Ni brazing agent (alloy-powder), a really very complex compound was formed. As it was mentioned above, some authors[4] have established that brazing joint between the steel plate and cemented carbide in this region is the weakest, because of the brittle nature of the compound layer formed during the brazing.

At the interface steel/braze seems to form no similar compound layer (as it was observed at the interface braze/cemented carbide). However, the noticeable increase of Co content is also observed, as well as the absence of W and the diminishment of Fe content because of its diffusion towards the cemented carbide. The border zone steel/braze is also enriched with Cu and Ni (see **Fig. 7**). Therefore, from that and from the morphology of the border zone (see **Fig. 8 a**) it can be concluded that as the intercrystalline diffusion of Cu proceeds, the solution of the mentioned elements in steel (Fe) is carried out and a homogeneous solid solution forms in the system Fe-Co-Ni-Cu at the interface steel/braze.

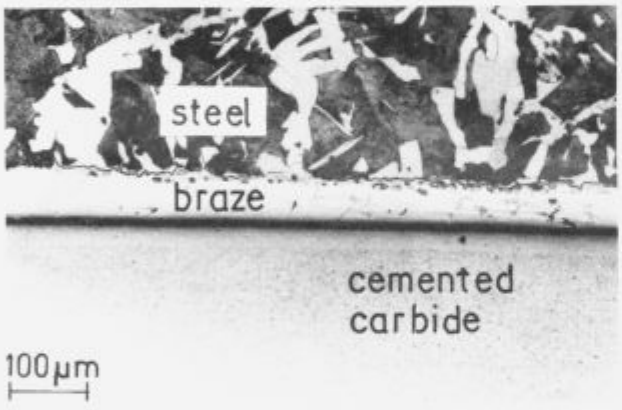

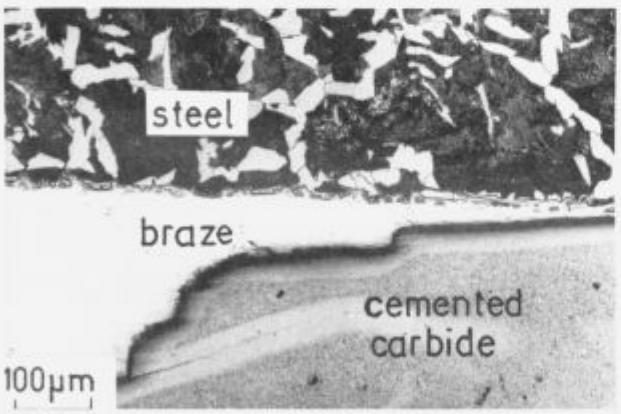

Figure 8: a) Microstructure of cemented carbide particle/low-alloy hardening steel joint of the grinding wheels produced at IMT Ljubljana and **b)** noticed damage (hair-shaped crack) of the cemented carbide particle
Slika 8: a) Mikrostruktura vakuumskega spoja zrno karbidne trdine/jeklo za poboljšanje vzorca brusne plošče izdelane na IMT Ljubljana in **b)** opazne poškodbe (lasne razpoke) karbidnih zrn

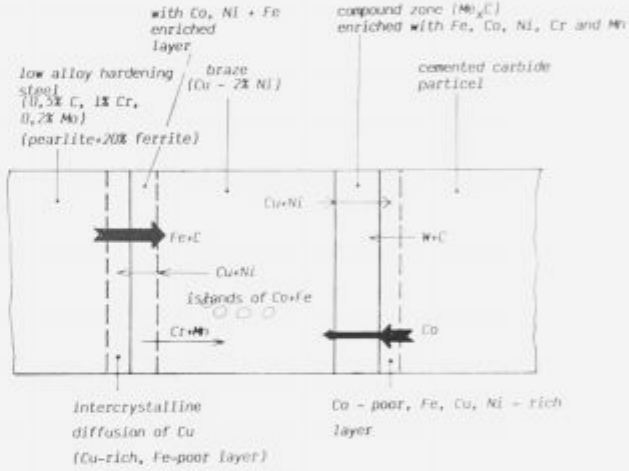

Figure 9: Schematic presentation of brazing joint and the diffusion flows of the individual elements with generated border zones (sample of grinding wheel prepared by brazing of low-alloy hardening steel and cemented carbide particles)
Slika 9: Shematični prikaz vakuumskega spoja karbidna trdina/jeklo za poboljšanje vzorca na IMT izdelane brusne plošče z difuzijo posameznih elementov in nastalima mejnima conama

Islands enriched with Fe and Co in the braze layer are observed, especially at some places, where the cemented carbide particles are very closely located to the steel base. Therefore it can be concluded that the most intensive diffusion of these two elements during brazing (in comparison with other active elements) occurs if the diffusion of interstitial C, which could not be analysed by our EPMA, is neglected.

Metallographic examinations also showed that some of the cemented carbide particles used were damaged (hair-shaped cracks). After brazing, around these cracks, a thin layer of cemented carbide with di-

minished Co content is observed. It can be concluded that during the brazing these damaged regions represent an active part for the diffusion of Co from cemented carbide to the interface cemented carbide/braze and across the braze to the interface braze/steel (see **Fig. 8 b**). **Fig. 9** presents schematically the brazing joint with established diffusion directions of individual elements and the formed border zones at the interface steel/braze and braze/cemented carbide particles.

The grinding experiments with prepared grinding wheels of low-alloy hardening steel and cemented carbide particles with Cu-2%Ni brazing agent showed that during the brazing a strong enough diffusion bonded joint is formed. The microstructure is ferritic-pearlitic with the prevailing content of pearlite and rare ferrite grains. The average hardness of the steel base after brazing is 200 HV_1, of cemented carbide particles 1980 HV_1 and of the braze 110 $HV_{0,1}$.

3.3 A comparison of both brazing joints

For the first brazing couple (structural steel/cemented carbide particles) only a marked Co and Fe rich compound layer at the interface cemented carbide/braze was observed. At the second brazing couple (low alloy hardening steel/cemented carbide particles), however, the marked enrichment with Co at both formed interfaces is observed. Here, the marked Co diminishment in the cemented carbide particle region close to the compound layer formed during brazing is also observed. Because of Cr presence in steel, the diffusion of Cr to the interface braze/cemented carbide occurred. The diffusion of Mn for the first brazing couple is insignificant, but it is evident for the second brazing couple. Therefore, on the basis of our investigations, it can be concluded that the low-alloy low-carbon structural steel for the brazing of cemented carbide particles with the steel base is a better option.

The most important parameters of brazing are the brazing temperature (including heating and cooling rate) and the soaking time at this temperature. Too high temperature and too long holding time of the brazing couple at this temperature enable the formation of a thicker layer of a hard and brittle compound phase at the interface braze/cemented carbide. It also causes the diminishment of the Co content at the cemented carbide border zone as well as formation of voids because of the Kirkendall effect and the resulting weakness of the brazing joint. The decomposition of WC because of C and W diffusion at interface cemented carbide/braze is also possible. Therefore lower temperatures (close to the melting point of the braze) and shorter soaking times at this temperature are more suitable for both selected steel bases. However, the brazing conditions have to be selected in such a manner that sufficient strength of the diffusion bonded joint is already formed.

4. Conclusions

The usability of Cu-2%Ni water atomized powder for the brazing of cemented carbide and steel base was investigated. On the basis of our investigations it can be concluded that water atomized Cu-2%Ni alloy-powder is suitable brazing agent. A vacuum brazing procedure for the manufacturing of grinding wheels containing cemented carbide particles was developed. The investigations show that for these types of grinding wheels, soft structural steel as a metal base seems to be the most convenient solution.

The aim of future experiments and investigations is to optimise the brazing procedure as well as to develop new shapes of grinding wheels. Future investigations should show which combination of selected materials (steel/braze/WC-C) will give a joint with the highest strength. We have in mind brazing experiments with different steels (structural steels, tool steels, etc.), brazes (pure Cu, Cu-Ni with different Ni contents, etc.) and different sorts of cemented carbide particles.

By metallographic examinations, analysis with EPMA and hardness measurements the brazing joints between structural as well as low-alloy hardening steel and cemented carbide particles using Cu-2%Ni brazing agent were partly evaluated. The diffusion joint is sufficiently strong and without noticeable defects. Its microstructural feature is a thin layer of intermetallic compound from the system Fe-Co(-W-Cr-Cu-Ni) or, more probably cementite phase M_xC type at the interface braze/cemented carbide formed during the brazing and intercrystalline diffusion of Cu at the interface braze/steel. However, only more detailed and systematical investigations with analysers (SEM/EDX, WDX, EAS) sensible for the light elements (O, C) distribution could fully explain the occurrence of multi phase diffusion and take into account all thermodynamic and kinetic aspects in order to answer what kind of compound is formed at the interface steel/braze and especially at the interface braze/cemented carbide during the brazing.

References

[1] D. Kmetič et al.: High temperature vacuum brazing with the simultaneous vacuum heat treatment, *Annual reports of IMT Ljubljana (slovenian language)*, IMT Report No.: 89-064, November 1991

[2] D. Kmetič et al.: Vacuum bonding of tool and structural steels in vacuum heat treatment furnace, *Annual reports of IMT Ljubljana (slovenian language)*, IMT Report No.: MI 87-032, November 1988

[3] E. Claire et al.: Part 3: Production of Metal Powders and Part 7: Powder Systems and Applications-Subsections: Cemented carbides and Metal Powders Used for Brazing and Soldering, *Metal Handbook, 9th edition*, Volume 7, Powder Metallurgy

[4] M. Stöck, K. Hack: Thermochemical Aspects of Multiphase Diffusion during Brazing of Hard Metal, *Z. Metallkd.* 84, 1993, 11, 759-766

[5] Commercial brochure: *DEGUSSA* (Lote, Lotpasten, Flussmittel), MH 58-4-889 B, Hanau, Germany
[6] Commercial catalogue: *MAHLER*, Brazing in Protective-gas and Vacuum Furnaces, Esslingen, Germany
[7] B. Šuštaršič, B. Breskvar, V. Leskovšek, A. Rodič: Microstructural characteristics of water atomized Cu-based powders for brazing, *Proceedings of 30th Symposium on Devices and Materials SD'94*, Zreče, Slovenia, 239-244
[8] J.J. Dunkley: The Production of Metal Powders by Water Atomization, *Powder Metallurgy International*, Vol. 10, No.1/78
[9] J.J. Dunkley, J.D. Palmer: Factors Affecting Particle Size of Atomized Metal Powders, *Powder Metallurgy International*, 1986, Vol. 29, No. 4
[10] MPIF: Standard Test Methods for Metal Powders and Powder Metallurgy Products, *Metal Powder Industries Federation*, Edition 1985/1986, Princeton, New Yersey
[11] J.J. Dunkley: The Factors Determining the Oxygen Content of Water Atomized 304L Stainless Steel Powder, *Reprint of Paper Presented at the National PM Conference*, Philadelphia, U.S.A., May 1981, Davy-Loewy R&D Centre

Kovine, zlitine, tehnologije / letnik 29 / 1995 / št. 3–4 / strani 413–416

Pulsed Plasma Nitriding of Stainless Steel

Nitriranje nerjavnega jekla v pulzirajoči plazmi

Torkar M.,[1] V. Leskovšek, IMT Ljubljana
B. Rjazancev, Department of Orthopaedics, Hospital Jesenice

A use could be found for pulsed-plasma nitrided AISI 316L stainless steel in a wide range of biomedical applications, e.g. femoral and biarticular heads of joint prostheses. Forged samples of steel were pulsed-plasma nitrided at a temperature of 540°C for 24 hours to increase the hardness of the surface. During nitriding, the hardness of the 70 µm thick layer uniformly increased to 958 HV 0.1. The hardness of the steel below the nitride layer remained unchanged, 210 HV 0.1. The thickness of the layer depended on the process parameters. The research showed that nitriding of stainless steel for medical implants in pulsed plasma is feasible.

Key words: stainless steel, pulsed plasma nitriding, biomedical applications

Nerjavno jeklo AISI 316L, nitrirano v pulzirajoči plazmi, bi bilo mogoče uporabiti za biomedicinske namene, npr. za femoralne in biartikularne glave kolčnih vsadkov. Kovani vzorci jekla so bili nitrirani v pulzirajoči plazmi 24 ur na temperaturi 540°C. Med nitriranjem je trdota 70 µm debele plasti enakomerno narasla do 958 HV 0.1. Trdota jekla pod nitrirano plastjo je ostala nespremenjena, 210 HV 0.1. Debelina nitrirane plasti je odvisna od parametrov procesa. Raziskava je pokazala, da je nitriranje medicinskih implantatov v pulzirajoči plazmi izvedljivo.

Ključne besede: nerjavno jeklo, nitriranje v pulzirajoči plazmi, uporaba v biomedicini

1. Introduction

An increase of the wear resistance and surface strength of different steels and alloys with nitride forming elements can be obtained by pulsed plasma nitriding[1]. Usually, also the corrosion resistance of the surface is increased, while the corrosion resistance of stainless steel is sometimes slightly diminished. Modern nitriding devices and technology, however, maintain or even increase the corrosion resistance[2].

Nitriding in pulsed plasma is beneficial due to the low temperature (between 350° C and 660° C) of the process and the possibility of influencing the composition of the nitrided layer (γ', ϵ, $\gamma'+\epsilon$, and diffusion layer)[3]. The low temperatures of the process maintain the mechanical properties of the material below the layer unchanged. The process is ecological friendly and nontoxic.

Gases in normal state are nonconductive for electrical current. This property is changed by high voltage or at low pressure when lightning or glow discharging appears, respectively. In both cases, the nonconductive gas is transformed to an ionized plasma with a sufficient electrical conductivity. Nitriding in pulsed plasma is based on glow discharging pulsed current in a low pressure chamber. Electrons are released on the cathodic surface of the sample, sputtering off the surface atoms, and nitrogen ions migrate into the specimen.

At a distance of some millimeters above the cathodic surface of the specimen, the ions accelerate and hit the surface with high kinetic energy. About 90 % of this energy is transformed to heat, which warms the surface up to the nitriding temperature. The heat is controlled by electric power, and no additional heating is required.

Nitrogen ions are highly reactive in the plasma, and iron nitrides start to form on the sputtered surface. Because of the low temperature, FeN molecules on the surface of the tool or sample decompose into lower nitrides. At the decomposition $FeN \rightarrow Fe_2N \rightarrow Fe3N \rightarrow Fe4N$, nitrogen is released. A part of the released nitrogen diffuses into the sample and the rest is returned into the plasma. The process

[1] Dr. Matjaž TORKAR
IMT, Lepi pot 11
61000 Ljubljana

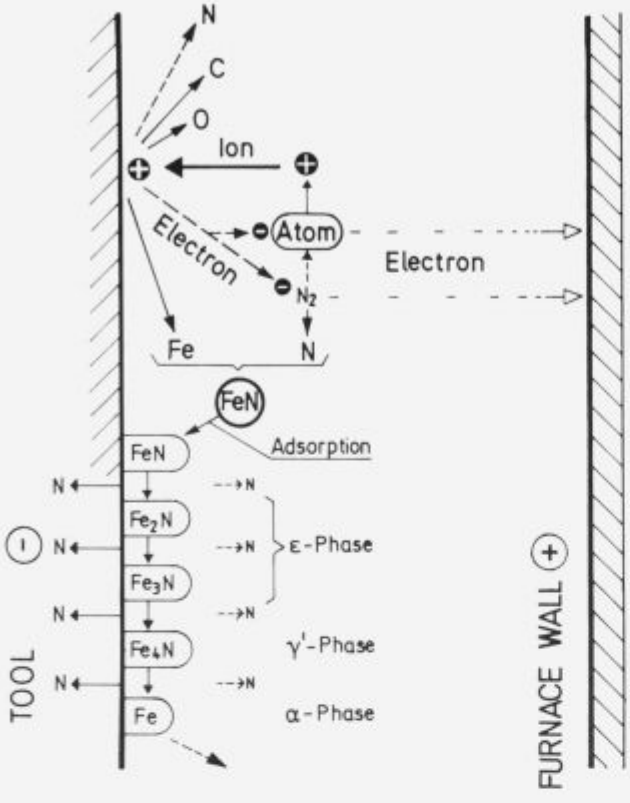

Figure 1:
Schematic presentation of the ion nitriding process

Slika 1:
Shematski prikaz postopka ionskega nitriranja

of ion nitriding is shown schematically in **Fig. 1**. In principle, all materials based on iron can be nitrided, since with glow discharging, ions of nitrogen are active enough to recombine on the surface. In some minutes of treatment, the nitride layer is formed and the steep gradient of concentration accelerates the diffusion of nitrogen into the specimen[4].

The objective of the present research was to check the nitriding of AISI 316L stainless steel in pulsed plasma.

2. Experimental work and results

2.1. Experimental procedure

The samples for nitriding were machined from the AISI 316L stainless steel bars with diameter of 30 mm and the composition of the steel was: 0.049 % C, 17.9 % Cr, 13.1 % Ni, 2.5 % Mo, 0.03 % Al and were pulsed-plasma nitrided at 540 °C for 24 h.

After nitriding, the samples were prepared for microstructure examination and hardness tests. The hardness was measured with a Vickers indenter, using a 100 g load and a 10 s load duration. The microstructure was examined, after etching with Marble's reagent, by optical microscopy, while the fracture surfaces of the nitride layer were examined by scanning electron microscopy (SEM).

2.2. Experimental results

In **Fig. 2 a** and **b**, the optical micrographs of unetched and etched nitrided layers are shown. The nitrided layer is light-gray in an unetched condition, and only inclusions are found by optical or scanning microscopy.

After etching in Marble's reagent, the nitride layer is darker and it looks homogeneous.

The optical micrographs **(Fig. 3 a and b)** of the transverse section through the base steel and nitride layer show Vickers imprints and a needle scratch, both of which confirm the increased hardness of the nitride layer. The needle scratch, easily visible in the base steel, disappeares when crossing the harder nitride layer. The increased hardness of the nitride layer is connected to the reduction of its fracture toughness and the appearance of a brittle fracture, whereas the fracture of the steel below the layer remains ductile. In **Fig. 4 a** the cracks in the nitride layer, formed at bending the nitrided surface to an angle 180° are shown. The fracture is brittle and the crack stops in the interface of the nitride layer-steel, because the base material has a higher fracture toughness. The topology and morphology of the nitrided surface with a bending crack is shown in **Fig. 4 b**. The nitride surface can be polished to a high brilliancy, which is important for medical use, as i.e. for femoral and biarticular heads of joint prostheses.

The modification of the surface morphology and topology may be beneficial for an improved biological performance or improved bone-bonding[5] at the uncemented modular stem or cement-bonding at the cemented stem.

The base steel shows after nitriding a ductile transgranular fracture **(Fig. 5)**.

Hardness measurements show an average and homogeneous hardness of 958 HV 0.1 in the layer **(Fig. 3 a)** and a hardness of 210 HV 0.1 in the base material. The usual hardness transition zone, found in nitrided steels, was not found. The results confirm that the process of ion nitriding is suitable for increasing of the relatively soft AISI 316L stainless steel surface. It is regarded as promising for increasing the wear resistance of such materials.

3. Conclusions

Ion nitriding of AISI 316L steel in pulsed plasma increases the surface hardness from 210 HV 0.1 to 958 HV 0.1, while the hardness of the base alloy is unchanged.

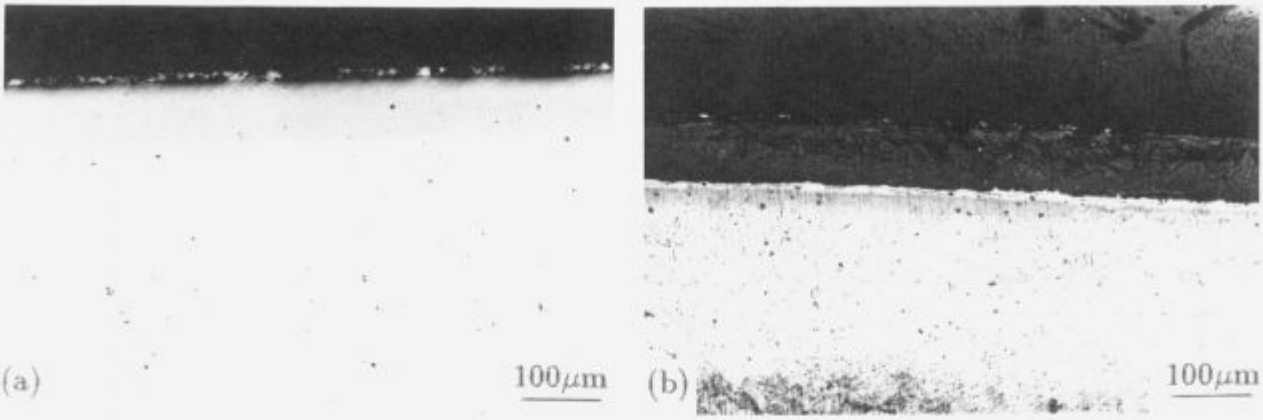

Figure 2 a and b: Optical micrograph of the nitrided layer after nitriding in pulsed plasma for 24 hours at 540° C, **(a)** - unetched, **(b)** - etched with Marble's reagent

Slika 2 a in b: Optični mikroposnetek nitriranega sloja po nitriranju v pulzirajoči plazmi, 24 ur na temperaturi 540° C, **(a)** - nejedkano, **(b)** - jedkano v Marble jedkalu

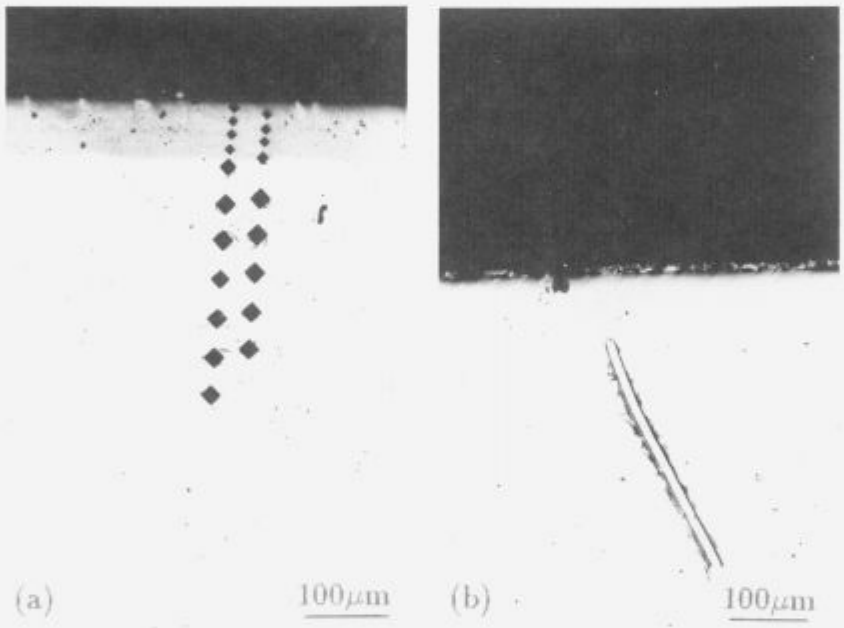

Figure 3 a and b: Optical micrograph of the nitride layer, **(a)**- Vickers indentions and **(b)**- a needle scratch

Slika 3 a in b: Optični mikroposnetek nitriranega sloja, **(a)**- odtisi merjenja trdote po Vickersu in **(b)**- raza preko nitriranega sloja, napravljena z iglo

The thickness of the layer after 24 hours of nitriding at 540° C is up to 70 μm.

The propagation of the crack opened in the nitride layer stopps at the interface nitrided layer-base steel due to higher ductility of the base steel. This indicates to a difference in fracture toughness between the nitrided layer and the matrix.

The modification of the surface morphology and topology may be beneficial for an improved surface bonding with bone or cement.

Acknowledgement

The authors are grateful to the Ministry of Science and Technology, Slovenia for supporting this work.

References

[1] H. Hornberg, Glimm-Nitrieren: ein Verfahren zum Nitrieren von Stahloberflächen mit Hilfe einer Glimmentladung, *Harterei Tech. Mit.*, 17, 1962, 2, 82.

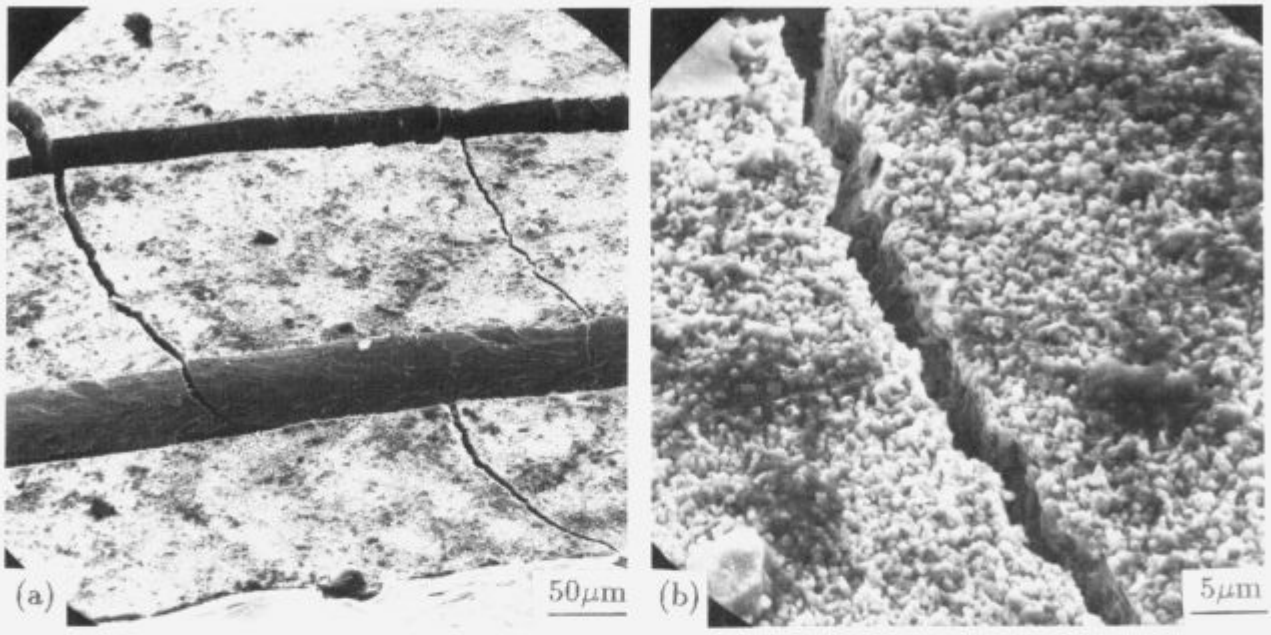

Figure 4 a and b: SEM micrographs. Nitrided surface with bending cracks **(a)**- bending angle 180° and **(b)**- detail of the surface

Slika 4 a in b: SEM posnetek nitrirane površine z razpokami, nastalimi pri upogibu, **(a)**- kot upogiba 180° in **(b)**- detajl površine

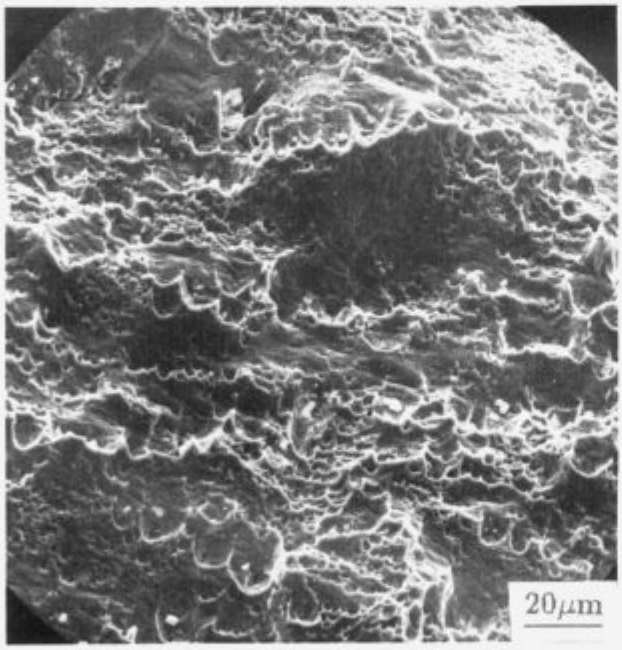

Figure 5: SEM micrograph. Ductile fracture of the base material

Slika 5: SEM posnetek žilavega preloma jekla pod nitriranim slojem

[2] R. Chaterjee-Fischer, Wärmebehandlung von Eisenwerkstoffen, *Expert Verlag, Sindelfingen*, 1986, 125

[3] M. Hempel, A. Kochendörfer and E. Hillnhagen: Gefügeveränderungen in α- eisen durch lonenbestrahlung, *Arch. Eisenhüttenw.*, 33, 1962, 6, 504

[4] H. Knüpell, K. Brotzmann and F. Eberhard, Nitrieren von Stahl in der Glimmentladung, *Stahl u. Eisen*, 78, 1958, 26, 1871

[5] C. P. A. T. Klein, J. G. C. Wolke, R. C. Vriesde, J. M. A. De Blieck-Hoger Vorst: Cortical bone ingrowth in grooved implants with calcium phosphate coatings: a gap model study, *J. Mater. Sci. Mater. Med.*, 5, 1994, 9&10, 569-574

Kovine, zlitine, tehnologije / letnik 29 / 1995 / št. 3–4 / strani 417–422

Hydrogen and Temper Embrittlement of Medium Strength Steel

Vodikova in popustna krhkost jekla srednje trdnosti

Ule B.,[1] V. Leskovšek, Institute of Metals and Technology, Ljubljana

The fracture ductility of high strength steel is strongly influenced by the presence of hydrogen, although hydrogen does not significantly affect the yield strength. The deterioration of fracture ductility is particularly evident in low strain rate tension tests, but less pronounced at conventional crosshead speeds. Microfractographic investigations of fracture surfaces of hydrogen charged high strength 5Cr-1Mo-0.3V steel from low strain rate tension test indicate that the growth and the coalescence of voids in the final stages of the fracture process are partly assisted by the decohesion of interfaces on which hydrogen is adsorbed. However, such phenomena are not observed in the experimental medium strength steel. Although a strong interaction between hydrogen and temper embrittlement was frequently observed in the alloyed steels[1,2] and though the magnitude of such effect was directly related to the degree of intergranular phosphorus enrichment[2], such synergy was not found in the experimental steel with post-martensitic microstructure.

Key words: high strength steel, medium strength steel, hydrogen and temper embrittlement, fracture ductility, low strain rate tension test

Na lomno duktilnost jekla z visoko trdnostjo močno vpliva v jeklu prisoten vodik, čeprav slednji nima znatnejšega učinka na napetost tečenja jekla. Poslabšanje lomne duktilnosti je zlasti očitno pri majhni hitrosti natezanja, medtem, ko je pri običajni hitrosti natezanja manj izrazito. Mikrofraktografske preiskave prelomnih površin nastalih pri počasnem natezanju vodičenega jekla 5Cr-1Mo-0.3V z visoko trdnostjo kažejo, da je rast in zlivanje por v končnih fazah procesa loma deloma podprta z dekohezijo medplastij, na katerih je adsorbiran vodik. Tega pojava nismo opazili pri preiskovanem jeklu srednje trdnosti, čeprav je bila pri legiranih jeklih često opažena močna interakcija med vodikovo in popustno krhkostjo[1,2] in čeprav je bila intenzivnost tega učinkovanja neposredno povezana s stopnjo interkristalne obogatitve s fosforjem[2] pa takšne sinergije nismo našli pri preiskovanem jeklu s postmartenzitno mikrostrukturo.

Ključne besede: jeklo visoke trdnosti, jeklo srednje trdnosti, vodikova in popustna krhkost, lomna duktilnost, upočasnjeno natezanje

1. Introduction

The adverse effect of hydrogen on mechanical properties has long been recognised in various metallic materials, especially in high strength steels. Hydrogen embrittlement of such steels often involves both a change in fracture mode and a reduction in ductility compared with the unhydrogenated condition[3]. It has also been established that the kinetics of hydrogen embrittlement depends on the strain rate[4-6]. However, at constant static load, the failure of high strength hydrogen charged steels, known as delayed failure, frequently occurs. This is caused by stress induced segregation of hydrogen and is characterised by the nucleation of a microcrack which then grows until it reaches a critical size, resulting in an abrupt failure. The incubation period, and the time to failure, are prolonged with a decrease in load until, at a sufficiently low load, delayed failure does not occur. Therefore, a threshold stress intensity factor K_{th} can be introduced which is considerably lower than the critical stress intensity factor or fracture toughness K_{Ic} of the uncharged steel.

Our preliminary investigations confirm that low concentrations of hydrogen (< 1 ppm by weight) in

[1] Dr. Boris ULE
IMT, Lepi pot 11
61000 Ljubljana

high strength steel have no substantial influence on its fracture toughness measured at conventional strain rate (1 mm min^{-1}). However, the low strain rate (0.1 mm min^{-1}) of hydrogen charged high strength steel decreases the fracture ductility, which indicates the existence of the threshold stress intensity factor at semi-static testing conditions[6].

Because the interaction between hydrogen and temper embrittlement was frequently observed in low and medium alloyed steels[1,2], the synergism between both embrittlements was investigated in a 5Cr-1Mo-0.3V steel with post-martensitic microstructure. The aim of the present work is therefore not only to demonstrate the applicability of low strain rate tension test in order to study the hydrogen embrittlement phenomena in high strength steel, but also to study the possible interaction between hydrogen and temper embrittlement in medium strength steel.

2. Experimental

A secondary hardening steel containing 0.38 C, 0.99 Si, 0.38 Mn, 0.012 P, 0.01 S, 5.19 Cr, 1.17 Mo, and 0.23 V (all wt-%) was used. Cylindrical tensile specimens with 10 mm dia. were machined from a forged rod after being homogeneously annealed and normalised. Some specimens were austenised at 980°C for 30 minutes in a vacuum furnace, quenched in a flow of gaseous nitrogen at a pressure of 0.5 MPa, and then tempered at temperatures of 620, 640 or 670°C. Three separate classes of yield stress, 1220, 1020 and 900 MPa respectively, were achieved.

The remaining specimens were quenched under the same conditions, then tempered twice for 2 hours at 710°C with intermediate undercooling (yield stress: 668 - 679 MPa, Charpy V-notch impact energy: 72 J), whereas some of these specimens were additionally tempered for 24 hours at 570°C, i.e. in the temperature range of reversible temper embrittlement[7,8] (yield stress: 648 - 665 MPa, Charpy V-notch impact energy: 37 J). In such cases, the experimental steel had a post-martensitic microstructure.

The cathodic charging of tensile specimens was performed for 1 h in 1 N sulphuric acid at a current density of 0.3 mA cm^{-2}. The concentration of hydrogen in some specimens (bulk concentrations) was determined using a high temperature (1050°C) vacuum extraction technique with gas chromatographic analysis. Tension tests were performed after the hydrogen charging of specimens had been completed and the specimens had been exposed to air for 24 hours. This enabled the concentrations of hydrogen to approach the residual value of approximately 0.8 ppm by weight which remained almost time independent.

The tension tests were performed at a conventional strain rate, i.e. at a crosshead speed of 1 mn min^{-1}, and at a lower strain rate, i.e. at a crosshead speed of 0.1 mm min^{-1}.

The fracture surfaces of the tensile specimens were examined in a scanning electron microscope (SEM).

3. Results

3.1 Tensile Properties

The results obtained from different strain rate tension tests for both uncharged and hydrogen-charged steel are pointed out in **Table I** and **II**. The results in **Table I** refer to the specimens which were quenched and tempered in a temperature range from 670 to 620°C with a class of yield stress of approx. 900 MPa, 1020 MPa and 1220 MPa, respectively.

Table I: Mechanical properties of uncharged and hydrogen charged steel, quenched and tempered up to high yield stresses.

Tabela I: Mehanske lastnosti nevodičenega in vodičenega jekla, ki je bilo kaljeno in popuščano na visoko napetost tečenja

Crosshead speed 1 mm min^{-1}			Crosshead speed 0.1 mm min^{-1}		
Yield stress MPa	Uniform elongation %	Reduction of area %	Yield stress MPa	Uniform elongation %	Reduction of area %
Uncharged steel					
924	8.7	52	910	8.5	51
1010	7.4	51.3	1027	6.5	50.3
1270	6.4	50	1214	6.2	50.3
Hydrogen-charged steel					
885	8.4	50.3	899	8.1	47.7
1082	7.2	49.3	1078	6.5	42.7
1209	6.1	47.3	1226	6.0	27.3

The decrease of the crosshead speed at tension had no influence on the mechanical properties of the uncharged steel, whereas it essentially influenced the reduction of area in the hydrogen charged steel (approx. 0.8 ppm hydrogen). The loss of ductility was more pronounced in steel with a higher yield stress.

The results in **Table II** refer to the steel with a post-martensitic microstructure, i.e. specimens which were quenched and tempered twice at 710°C with intermediate undercooling, and specimens which

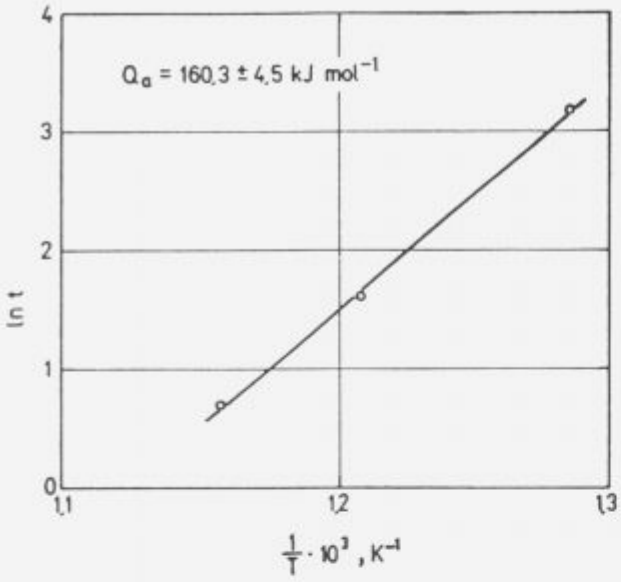

Figure 1: Evaluation of the activation energy of segregation of phosphorus according to Arrhenius equation (from Ref. 7)

Slika 1: Izvrednotenje aktivacijske energije za segregiranje fosforja z uporabo Arrheniusove enačbe (Ref. 7)

were further, additionally, tempered for 24 hours at 570°C, both with a class of yield stress of approx. 660 MPa. A weak reversible temper embrittlement of experimental steel, having a high tempered post-martensitic microstructure, was produced with additional tempering as confirmed by our preliminary investigations of the time-temperature relationship of the Charpy impact energy reduction resulting from such tempering[7]. An activation energy of about 160 kJ mol^{-1}, which is very close to that for bulk diffusion of phosphorus in ferrite, was derived from the slope of a log-log plot of time versus reciprocal tempering temperature **(Fig. 1)**.

Indeed, it has already been confirmed, using Auger spectroscopy, that in particular phosphorus segregates in this type of steel. Romhanyi and coworkers[9] found up to 6 % P and 1 % S at grain boundaries, and a strong carbon peak with carbide structure is also remarkable in Auger spectra of such steel, austenitized at 1100°C, quenched and tempered at 600°C **(Fig. 2)**. However, the segregations in our experimental steel, quenched from much lower temperature, was not so intense, and the embrittlement phenomena could be detected only by impact testing and not at all at semi-static tensile tests.

The results from both **Tables** are also shown in Diagram **(Fig. 3)**, where the tendency for hydrogen embrittlement is formulated in accordance with Morimoto and Ashida[10]:

$$\text{Degree of embrittlement} = \frac{R.A._{.1} - R.A._{.0.1}}{R.A._{.1}} \times 100\% \quad (1)$$

where $R.A._{.1}$ is the reduction of area at conventional strain rate tensile test, i.e. at a crosshead speed of 1 mm min^{-1} and $R.A._{.0.1}$ is the reduction of area at low strain rate tensile test, i.e. at a crosshead speed of 0.1 mm min^{-1}.

Table II: Mechanical properties of uncharged and hydrogen charged steel quenched and tempered twice at 710°C and of the same steel, additionally tempered for 24 hours at 570°C

Tabela II: Mehanske lastnosti nevodičenega in vodičenega jekla, ki je bilo kaljeno in dvakrat popuščano pri 710°C ter istega jekla, ki je bilo dodatno popuščano 24 ur pri 570°C

Crosshead speed 1 mm min^{-1}			Crosshead speed 0.1 mm min^{-1}		
Yield stress MPa	Uniform elongation %	Reduction of area %	Yield stress MPa	Uniform elongation %	Reduction of area %
Quenched and tempered twice at 710°C(Charpy V-notch energy:72 J)					
Uncharged steel					
679	12.4	55	668	11.8	55.7
Hydrogen-charged steel					
668	11.2	45	661	10.3	43.1
Quenched and tempered twice at 710°C further, additionally, tempered for 24 hours at 570°C (Charpy V-notch energy: 37 J)					
Uncharged steel					
665	11.1	51.7	664	11.7	51.7
Hydrogen-charged steel					
648	11.1	52.5	640	10.9	53

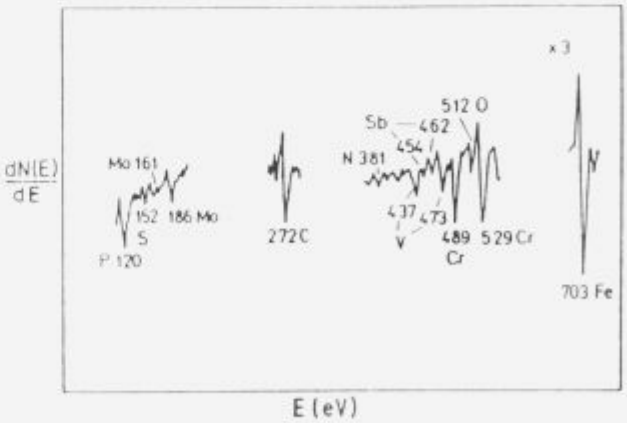

Figure 2: Auger spectrum of the intergranular surface of steel with 5 % Cr, austenitized at 1100°C, quenched and tempered at 600°C (from Ref. 9)

Slika 2: Augerjev spekter z intergranularne površine jekla s 5% kroma, austenitizirano pri 1000°C, kaljeno in popuščano pri 800°C (Ref. 9)

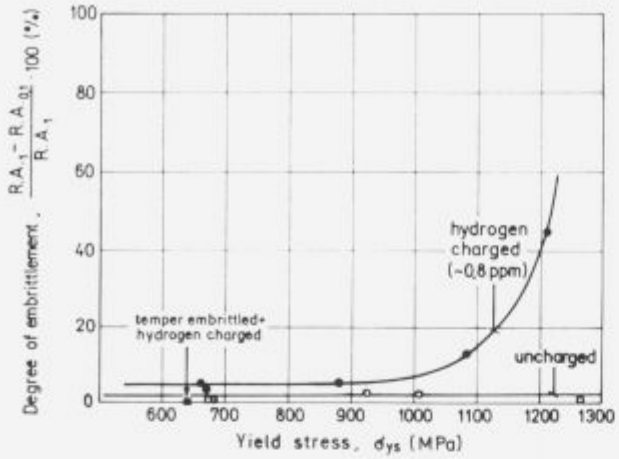

Figure 3: Degree of embrittlement of hydrogen charged steel as function of yield stress

Slika 3: Stopnja krhkosti vodičenega jekla v odvisnosti od napetosti tečenja

3.2 Fractography

The micromorphology of the typical fracture surface of hydrogen charged low-strain rate tensile specimen with yield stress of 1226 MPa, is shown in **Fig. 4** and **5**. It can be concluded that the hydrogen-induced fracture is locally ductile, tearing type of fracture with some quasicleavage details on the periphery of larger and deeper tunnel-type dimples.

The fracture surface of hydrogen charged high strength specimens obtained at conventional strain rate test and the fracture surface of hydrogen charged low- and conventional-strain rate test specimens of medium strength, i.e. the fracture surface of hydrogen charged steel, either quenched and tempered twice at 710 °C or of the same steel additionally tempered for 24 hours at 570 °C, are totally ductile **(Fig. 6)**. Of course, the fracture surface of

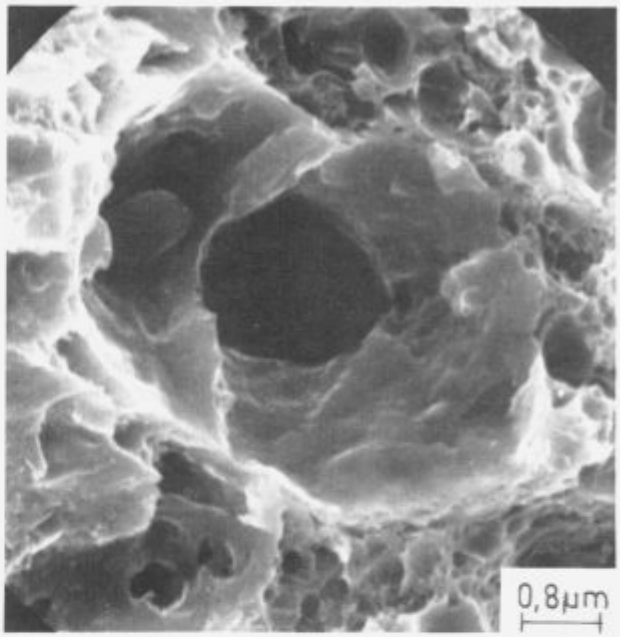

Figure 5: Detail from Fig. 4 (SEM)

Slika 5: Detail iz slike 4 (SEM)

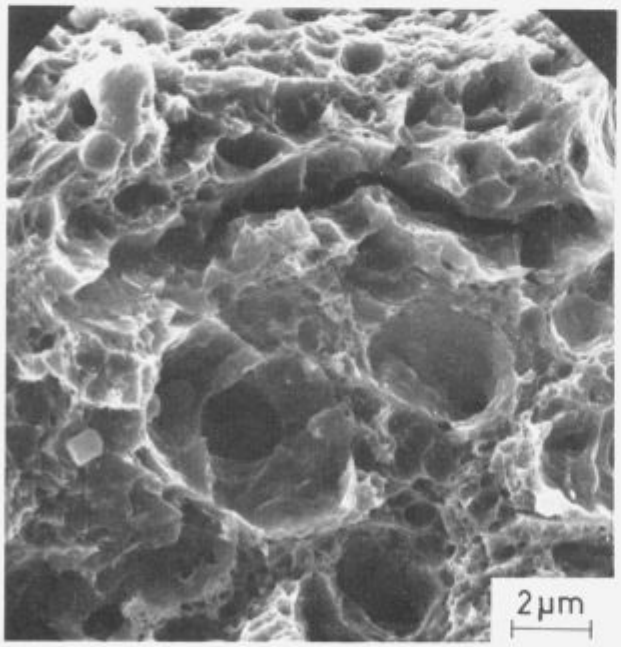

Figure 4: Fracture surface of hydrogen charged low-strain rate tensile specimen with yield stress of 1226 MPa (SEM)

Slika 4: Prelomna površina vodičenega in počasi natezanega preizkušanca z napetostjo tečenja 1226 MPa (SEM)

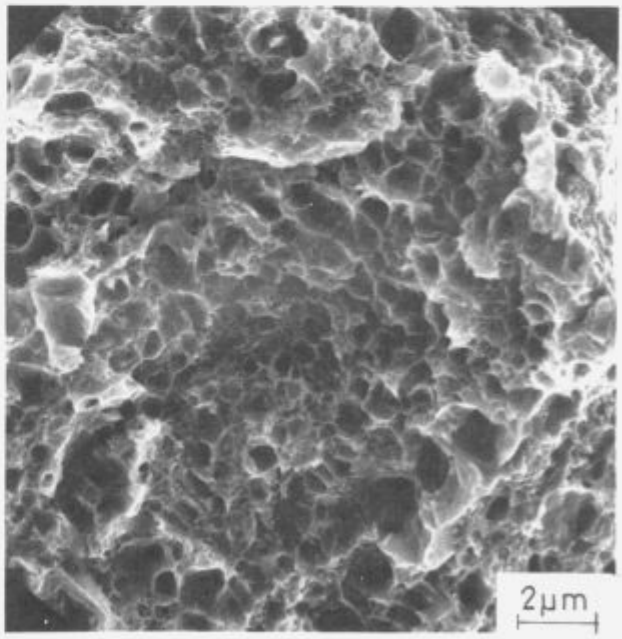

Figure 6: Fracture surface of hydrogen charged low-strain rate tensile specimen with yield stress of 640 MPa (additionally tempered for 24 hours at 570 °C) (SEM)

Slika 6: Prelomna površina vodičenega in počasi natezanega preizkušanca z napetostjo tečenja 640 MPa (dodatno popuščano 24 ur pri temperaturi 570 °C (SEM)

additionally tempered impact specimens as for instance Charpy V-notch specimens - even uncharged - are of mixed mode. After an additional tempering at 570 °C for 24 hours, the crack propagation path changes and sporadic intergranular fracture along preaustenite grain boundaries, and quasicleavage fracture details, and single ductile tearings can be regularly observed[7].

4. Discussion

Low concentration of hydrogen in high strength steel have no significant influence on the mobility of the dislocations in earlier stages of the tensile deformation process. Hydrogen has almost no effect on

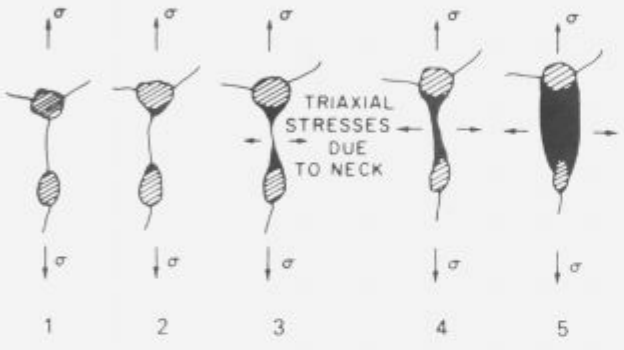

Figure 7: Schematic representation of microvoid formation, growth, and coalescence along grain boundaries in which hydrogen is adsorbed (from Ref. 13)

Slika 7: Shematski prikaz tvorbe mikropor, njihove rasti in zlivanja vzdolž meja zrn, na katerih je adsorbiran vodik (Ref. 13)

the yield stress or on the uniform elongation of steel, and it only affects the reduction of area. However, the reduction of area decreases only if the strain rate is low enough to enable the Cottrell atmosphere of the hydrogen atoms pinned on the dislocations to penetrate deep into the plastic zone of the tensile specimens. Since the size *l* of the plastic zone of a hydrogen charged specimen is approximately half the diameter of the neck ($l = 3$ mm) at fracture, and the crosshead speed v is 1.6×10^{-3} mm s^{-1} (0.1 mm min^{-1}), a value of strain rate $\dot{\varepsilon} = v/l = 5.3 \times 10^{-4}\ s^{-1}$ is obtained. In earlier literature[11] higher $\dot{\varepsilon}$ values are quoted for stainless steel. However, the investigations performed by Nakano *et al.*[12] on hydrogen charged steel with yield stress of 500 MPa using low strain rate measurements show that at sufficient concentration of hydrogen in steel the reduction of area asymptotically approaches the lower value even at a critical strain rate of $\dot{\varepsilon} = 10^{-4}\ s^{-1}$, which is of the same order of magnitude as in the present investigations.

Microfractographic examinations show that hydrogen charged low strain rate tensile specimens exhibited some interfacial separation on the fracture surface. The growth and the coalescence of microvoids along the grain boundary, schematically shown in **Fig. 7**, are accelerated by separating internal interfaces where hydrogen is adsorbed[13,14].

Microvoid coalescence and the separation of internal interfaces due to adsorbed hydrogen become operative when the triaxial stress state in the narrow neck of the tensile specimen is formed (**Fig. 7**, sequences 3 to 5), resulting in the "condensation" of the last stage of plastic deformation in the low strain rate tension testing of high strength hydrogen charged steel. However, such phenomena are not observed in medium strength steel. Although a strong interaction between hydrogen and temper embrittlement was frequently observed in such alloyed steels[1,2] and though the magnitude of such effect was directly related to the degree of intergranular phosphorus enrichment[2], such synergy was not found in the experimental steel with post-martensitic microstructure. In studying the influence of bulk and grain boundary phosphorus content on hydrogen induced cracking in low strength steel, Dayal and Grabke[15] also found that the effect of phosphorus is related to the bulk content and not to the grain boundary concentration. Obviously, in the case of the experimental steel with post-martensitic microstructure, the influence of hydrogen decreases and becomes more complicated due to some particular effect of the microstructure. In agreement with Charbonnier and Pressouyre[16] these results show that the nearer is the actual microstructural state to the state of the thermodynamical equilibrium, the less susceptible is the steel to hydrogen embrittlement.

5. Conclusions

The relevance of the low-strain rate tension test to establish the hydrogen embrittlement susceptibility of both high and medium strength steel is demonstrated. The applicable **formula (1)** for the estimation of such susceptibility[10], based on the reduction of area measurements at the low and the conventional strain rate tensile test, is also successfully adopted. The synergism between hydrogen and temper embrittlement was not found in the experimental, additionally tempered steel with post-martensitic microstructure. On the contrary, such steel is less susceptible to the influence of hydrogen, due to some particular effects of the microstructure which is close to the thermodynamical equilibrium.

References

[1] C. A. Hippsley and N. P. Haworth: *Mater. Sci. Tech.*, 4, 1988, 791-802

[2] C. A. Hippsley: *Mater. Sci. Tech.*, 3, 1987, 912-922

[3] I. M. Bernstein and A. W. Thompson: *Int. Metall. Rev.*, 21, 1976, 269
[4] J. K.Tien, A. W. Thompson, I. M. Bernstein and R. J. Richards: *Metall. Trans.*, 7A, 1976, 821
[5] M. Hashimoto and R. Latanision: *Metall. Trans.*, 19A, 1988, 2799
[6] B. Ule, F. Vodopivec, L. Vehovar, J. Žvokelj and L. Kosec: *Mater. Sci. Tech.*, 9, 1993, 1009-1013
[7] B. Ule, F. Vodopivec, M. Pristavec and F. Grešovnik: *Mater. Sci. Tech.*, 6, 1990, 1181-1185
[8] J. Janovec, P. Ševc and M. Koutnik: *Kov. Zlit. Teh.*, 29, 1995, 40
[9] K. Romhanyi, Zs. Szasz Csih, G. Gergely and M. Menyhard: *Kristall Tech.*, 15, 1980, 471-477
[10] H. Morimoto and Y. Ashida: *Transactions ISIJ*, 23, 1983, B-325
[11] M. B. Whiteman and A. R. Troiano: *Corrosion*, 21, 1965, 53-56
[12] K. Nakano, M. Kanao and T. Aoki: *Trans. Nat. Res. Inst. Met. (Jpn)*, 29, 1987, 34-43
[13] H. Cialone and R. J. Asaro: *Metall. Trans.*, 10A, 1979, 367-375
[14] H. Cialone and R. J. Asaro: *Metall. Trans.*, 12A, 1981, 1373
[15] R. K. Dayal and H. J. Grabke: *Steel Research*, 58, 1987, 179-185
[16] J. C.Charbonnier and G. M. Pressouyre: Residual hydrogen in steels, *4th International Conference "Residuals and Trace Elements in Iron and Steel"*, Portorož, Yugoslavia, October 1985, Proceedings, pp. 81-103

Kovine, zlitine, tehnologije / letnik 29 / 1995 / št. 3–4 / strani 423–426

A New Concept of Quality Evaluation of High Energy Electron Beam Used in Welding

Nov način ovrednotenja visoko energijskega curka elektronov v varilni tehniki

Wójcicki S.,[1] IVT, Warsaw

The proposition of a new technological parameter, so called "coefficient of electron beam energy consumption", fot the mathematical description of the quality of electron beam used in welding technology is presented. Some features of this parameter are shown.

Key words: electron beam welding, coeficient of energy consumption

Podan je predlog novega tehnološkega parametra imenovanega "koeficient porabe energije elektronskega curka" za matematični opis kvalitete elektronskega curka, ki se uporablja v varilni tehniki. Prikazane so nekatere značilnosti tega parametra.

Ključne besede: varjenje, elektronski curek, poraba energije

1. Introduction

The high energy electron beam (EB) **(Fig. 1)** is usually characterized by perveance and by means of three groups parameters:

- geometric: the envelop form, crossover size - $2r_c$, aperture angle - 2α, diameter of the focus spot - $2r_s$;
- energetical: integral power, energy density in the planes of crossover and focused spot, brightness, dimensions of the active zone[1,2];
- structural: electron density distribution in different EB cross sections, phase diagrams, emittance.

The evaluations of these parameters by measurements or computer calculation are difficult in practical systems. In first case, a special apparatus is required and moreover, the obtained data are deformed by measurement error. In the other case, it is impossible to simulate all factors and phenomena, like ion focusing, aberrations of electron gun etc., that have a big influence on the parameters of EB. Consequently, the calculated parameters of EB are loaded with considerable errors also. The anticipation of the technological effects, that could be obtained by using a particular EB is difficult because of unknowledge of real parameters of EB. For example, in EB welding technology it is known[1,2,4] that the relationship between the depth of welds h and parameters of EB is given by the empirical formula:

$$h = M \cdot \frac{U^{\nu} \cdot I^{\beta}}{V^{\gamma}} \qquad (1)$$

where U - accelerating voltage, I - EB current, v - speed of welding, M - constant dependent on the thermal properties of welded materials, and α, β, γ - experimental coefficients representing the features of EB. Usualy $\alpha \approx 0{,}3 \div 1{,}3$, $\beta \approx 0{,}7 \div 1{,}0$, $\gamma = 0{,}3 \div 1{,}0$.

Becasuse the value of α, β, γ coefficients vary in a wide range there is no other way to present technological posibilities of EB /and their technological quality/ than to examine experimental welds and to compare their cross sections - as it is shown in **Fig. 2**[3] - or drawing up the plots showing relationship between depth of welds and EB parameters and others parameters of welding. The typical diagram h = f(v) is shown on Fig. 3.

2. Coefficient of electron beam energy consumption

The aim of this work is the presentation of a new idea of quantitative evaluation of the high energy EB quality. This idea is based on the mathematical description of technological effects that EB causes in the materials. In the case of an EB welding technology, the most important parameter is the possibility of obtaining deep and narrow welds by applying the smallest possible amount of EB energy during the operation.

From this point of view, we propose to introduce for description of the EB, the so called *"coefficient (K) of EB energy consumption"* defined as:

[1] Dr. Sc. S. WÓJCICKI
Institute of Vacuum Technology
Długa Street 44/50
00-241 Warsaw, Poland

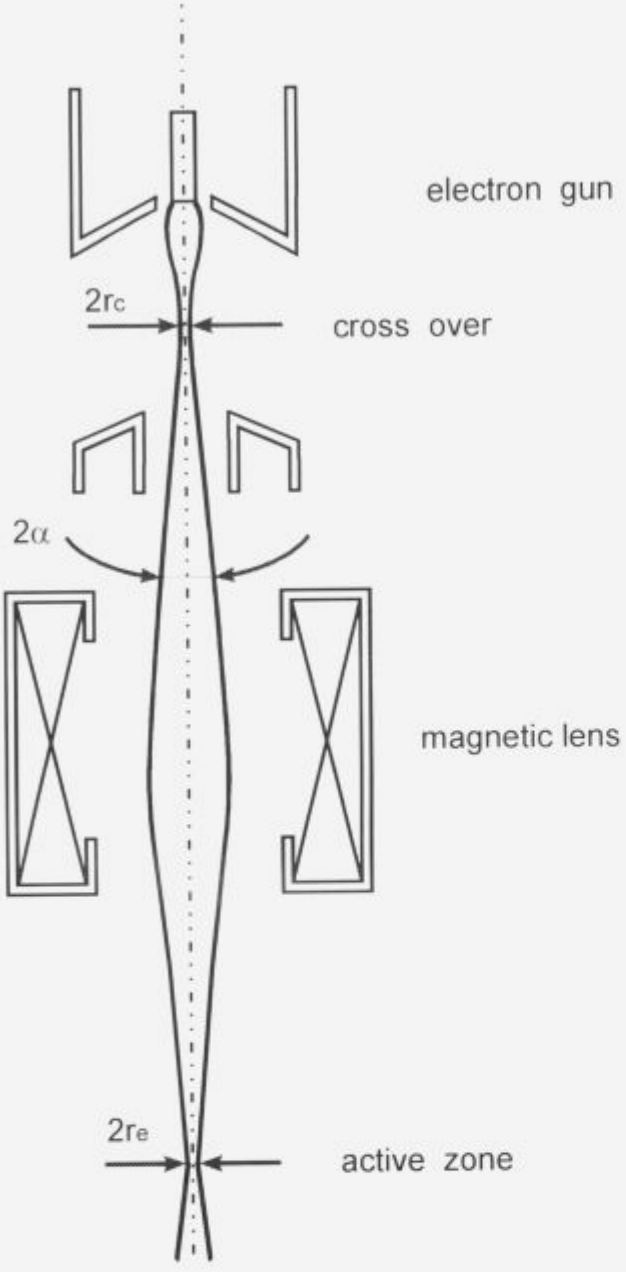

Figure 1: Same of the geometric parameters of EB: crossover diameter - $2r_c$, aperture angle - 2α, spot diameter - $2r_e$

$$K = \frac{U \cdot I}{v \cdot h} \left[\frac{J}{mm^2}\right] \quad (2)$$

where U - accelerating voltage, I - EB current, v - velocity of welding, h - depth of weld.

The physical interpretation of this technological parameter of EB is very simple. It is the quantity of energy which is indispensable to create a weld with unit depth on unit length of weld.

EB with lower coefficient of energy consumption K are better than those which need more energy to make the welds with the same depth. For example, coefficient K for first EB (Fig. 2) is equal:

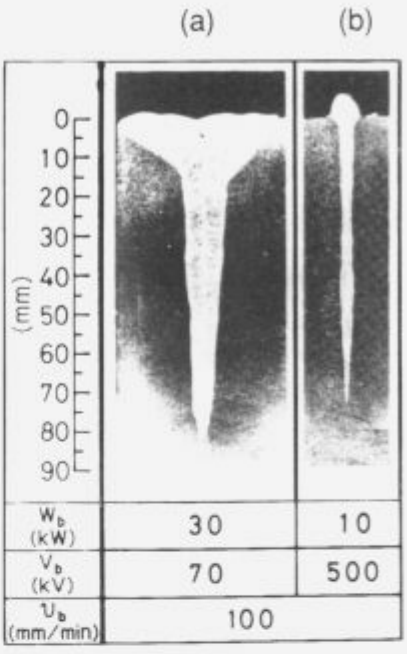

Figure 2: Comparison of welds made in JWI[1] by EB with different coefficient of energy consumption $K_{Fe\,1.33}$:
a) accelerated voltage V_b = 70 kV, beam power W_b = 30 kW, welding velocity v = 1,33 mm/s, depth of weld h = 80 mm, $K_{Fe\,1.33}$ = 221 J/mm²;
b) V_b = 500 kV, W_b = 10 kW, v = 1,33 mm/s, h = 75 mm, $K_{Fe\,1.33}$ = 100 J/mm²

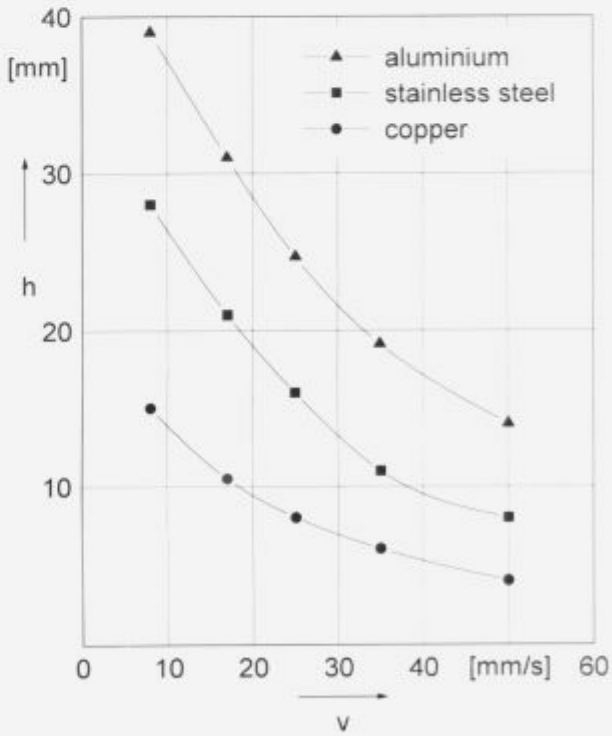

Figure 3: The typical relationship between weld depth h and the velocity of welding v for aluminium, stainless steel and copper. Electron beam power P = 8 kW

HIGH AND ULTRA-HIGH VACUUM COMPONENTS

416 PAGES 38 CATEGORIES
10 SECTIONS 4 CURRENCIES
2 INDEXES ...

1 CATALOGUE

CABURN MDC

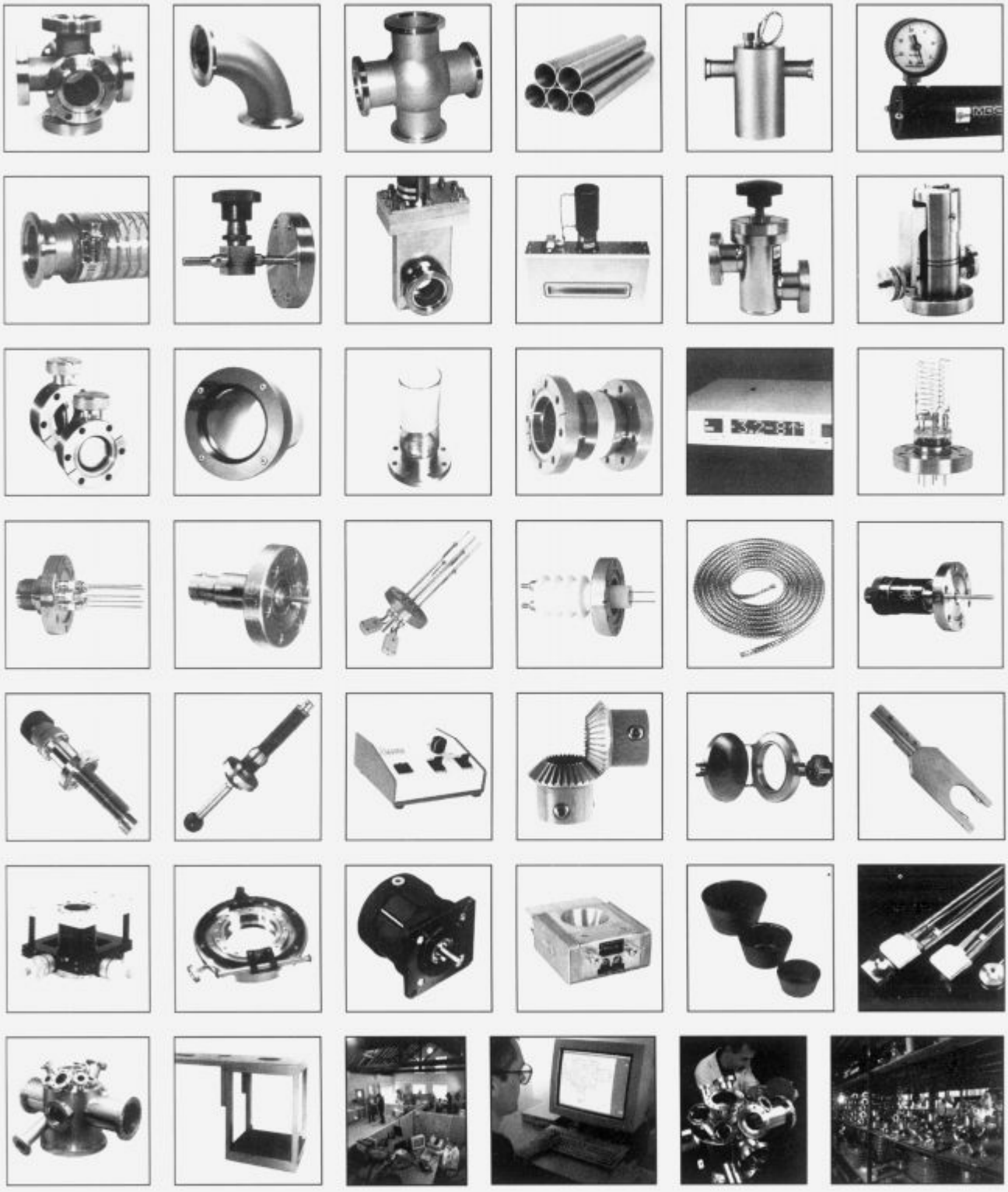

Head Office

Caburn-MDC Limited
The Old Dairy, The Street,
Glynde, East Sussex
BN8 6SJ United Kingdom

Tel: +44 (0)273 858585
Fax: +44 (0)273 858561

Berlin

Caburn-MDC
Ostendstrasse 1
D-12459 Berlin
Germany

Tel: +49 (0) 30 6953 9840
Fax: +49 (0) 30 635 3786

Lyon

Caburn-MDC S.A.R.L.
Novacité-Alpha
B.P. 2131
F-69603 Villeurbanne Cedex
France

Tel: (+33) 78 94 56 30
Fax: (+33) 72 44 34 85

Torino

Caburn-MDC
(Alberto Rava)
Str. Molinetti 41, Il Molino
10098 Rivoli, Torino
Italy

Tel: +39 (0) 11 95 85 134
Fax: +39 (0) 11 95 66 515